INVESTIGATION OF HEMORHEOLOGIC EFFECTS OF FLOW DIVERTING STENT IMPLANTATION IN CEREBRAL ANEURYSMS

by
Osman Ergin

Submitted to Graduate School of Natural and Applied Sciences
in Partial Fulfillment of the Requirements
for the Degree of Master of Science in
Mechanical Engineering

Yeditepe University
2023

INVESTIGATION OF HEMORHEOLOGIC EFFECTS OF FLOW DIVERTING STENT IMPLANTATION IN CEREBRAL ANEURYSMS

APPROVED BY:

Assoc. Prof. Dr. Ali Bahadır Olcay ……
(Thesis Supervisor)
(Yeditepe University)

Prof. Dr. İsmail Oran
(Thesis Co-Supervisor)
(Ege University)

Prof. Dr. Emre Alpman ...……
(Marmara University)

Assist. Prof. Dr. Ali Fethi Okyar ...……
(Yeditepe University)

DATE OF APPROVAL: ..../..../2023

I hereby declare that this thesis is my own work and that all information in this thesis has been obtained and presented in accordance with academic rules and ethical conduct. I have fully cited and referenced all material and results as required by these rules and conduct, and this thesis study does not contain any plagiarism. If any material used in the thesis requires copyright, the necessary permissions have been obtained. No material from this thesis has been used for the award of another degree.

I accept all kinds of legal liability that may arise in case contrary to these situations.

Name, Last name Osman Ergin

Signature …..…….……..

ACKNOWLEDGEMENTS

It is my pleasure to acknowledge the incredible aid and motivating presence of my professor Assoc. Prof. Ali Bahadır Olcay throughout all the work that I put into this thesis. The unique way of his approach to each obstacle in every step of the way has given me the will to pursue remarkable multidisciplinary fields of engineering which broadened my vision immensely. I thank him for making me fall in love with science even more and teaching me the importance of perseverance. I would like to thank Prof. Dr. İsmail Oran for believing in me, giving me the chance to work on this topic and his eye-opening guidance in this unique field.

I would like to thank my lab mate Görkem Güçlü for his guidance and my lab- and classmates Can Ünsal, Batı Altındağ and Furkan Tercanlı for always being motivating, kind and helpful.

Last and most importantly, I am forever grateful to every member of my family İlhan, Sunay, Çağlar, Neslihan, Pablo, Ceren and Hannah for being the best family a person can ever ask for. Their continuous support at every phase of my life has always been crucial for me to become a better person. I will pursue greatness in the virtues that I have learned from them.

ABSTRACT

INVESTIGATION OF HEMORHEOLOGIC EFFECTS OF FLOW DIVERTING STENT IMPLANTATION IN CEREBRAL ANEURYSMS

Flow diverter stents (FDS) are one of the most effective methods in treating cerebral aneurysms to prevent rupture and therefore cerebral hemorrhage that can cause deteriorating or fatal incidents for the patients. Implanting an external medium to the human body causes inevitable hemodynamic changes. Even though the FDS method is quite an efficient treatment method, there are some studies which point out complications of delayed hemorrhage following FDS treatment within 30 days. These complications were found to be occurring in patients with inherited and acquired von Willebrand Disease (vWD). The von Willebrand factor (vWF) activity gets reduced as a result of supraphysiological forces acting on the blood flow leading to an excessive increase in shear stress and shear strain rate. The threshold shear stress and shear strain rate values are known to be as 10 Pascal (Pa) and 5000 s^{-1}, respectively. The objective of this thesis is to prove the implantation of a FDS leading to a pathological increase in shear stress and shear strain rate through numerical simulations. As FDS treatment is a once in a lifetime surgery, conducting virtual surgeries and simulations are of impeccable importance. The majority of the cerebral aneurysms occur on internal carotid artery (ICA) and middle cerebral artery (MCA). Six patients with three ICA and MCA aneurysms each were chosen. Digital subtraction angiography (DSA) images were processed through various methods to prepare patient specific cases. Before treatment cases were prepared for each patient and virtual stent implantation was conducted on each model, where every patient had received both 48 and 64 wire FDS treatments in separate cases. Conclusively, 18 simulations were solved with each patient having three simulations. Blood was modeled as a non-Newtonian fluid, patient specific Womersley velocity profile was generated and inserted for each patient as boundary conditions. The dramatic increase in both shear stress and shear strain rate values were observed with the numerical simulations of post FDS implantations. Shear stress and shear strain rate values were above 10 Pa and 5000 s^{-1} for all patients after treatment. Supplementary parameters pointed out indications of FDS effect on delayed parenchymal microhemorrhages after inspecting distal of every patient artery through oscillatory shear index (OSI) and time-averaged wall shear stress (TAWSS).

ÖZET

BEYİN ANEVRİZMALARINA YERLEŞTİRİLEN AKIM DEĞİŞTİRİCİ STENTİN HEMOREOLOJİK ETKİLERİNİN İNCELENMESİ

Akım çevirici stentler (FDS), beyin anevrizmalarının tedavisinde hastalarda hayat kalitesini düşüren veya ölümcül olaylara neden olabilen yırtılma ve yırtılmanın bir sonucu olarak beyin kanamalarını önlemede kullanılan en etkili yöntemlerden biridir. İnsan vücuduna dışarıdan bir cisim yerleştirmek, kaçınılmaz hemodinamik değişikliklere neden olur. FDS oldukça etkili bir tedavi yöntemi olsa da, tedavi sonrası 30 gün içinde gecikmiş kanamalı komplikasyonlara işaret eden araştırmalar mevcuttur. Bu komplikasyonların kalıtsal ve edinilmiş von Willebrand hastalığı olan hastalarda ortaya çıkabilmektedir. Von Willebrand faktörü (vWF) aktivitesinin azalması, kan akışına etki eden suprafizyolojik kuvvetlerin kayma geriliminde ve kayma gerinimi hızında aşırı bir artışa yol açmasının bir sonucu olarak ortaya çıkar. Eşik kayma gerilimi ve kayma gerinim hızı değerleri sırasıyla 10 Pascal (Pa) ve 5000 s^{-1} olarak bilinmektedir. Bu tezin amacı, bir FDS implantasyonunun kayma gerilimi ve kayma gerinim hızında patolojik bir artışa yol açtığını sayısal simülasyonlarla belirleyebilmektir. FDS tedavisi ömür boyu bir kez yapılan bir ameliyat olduğundan, sanal ameliyatlar ve simülasyonlar gerçekleştirmek kusursuz bir öneme sahiptir. Serebral anevrizmaların çoğu, internal karotid arter (ICA) ve orta serebral arterde (MCA) meydana gelir. Bu tez, üç ICA ve üç MCA anevrizma hastası olmak üzere toplam altı hastayı içermektedir. Sayısal çıkarımlı anjiyografi (DSA) görüntüleri çeşitli yöntemlerle işlenerek her hasta için kendilerine özel vakalar hazırlanır. Başlangıçta her hasta için bir tedavi öncesi vakası hazırlanır ve daha sonra her hastanın ayrı vakalarda 48 ve 64 telli FDS tedavisi aldığı her model üzerinde sanal FDS yerleştirme gerçekleştirilir. Sonuç olarak, her hasta üç simülasyona sahip olacak şekilde 18 simülasyon çözülmüştür. Kan, Newtonyen olmayan bir akışkan olarak modellenmiş, hastaya özel Womersley hız profili oluşturulmuş ve bunlar her hasta için sınır koşulları olarak eklenmiştir. FDS implantasyonunun ardından hem kayma gerilimi hem de kayma gerinim hızı değerlerinde çarpıcı artış sayısal simülasyonlar ile gözlemlenmiştir. Tedavi sonrası tüm hastalarda kayma gerilmesi ve gerinim hızı değerleri 10 Pa ve 5000 s^{-1}'in üzerindedir. Ek parametreler, her hasta arterinin distali incelendikten sonra gecikmiş parankimal mikro kanamalar üzerinde FDS etkisinin göstergelerine işaret eder. Her hasta arterinin distalinin osilatör kayma indeksi (OSI) ve zaman ortalamalı duvar kayma gerilimi (TAWSS) gibi ilave parametreler aracılığıyla incelenmesi sonrası gecikmiş parankimal mikro kanamalar üzerinde FDS etkisinin göstergelerine işaret etmektedir.

TABLE OF CONTENTS

LIST OF FIGURES

LIST OF TABLES

LIST OF SYMBOLS/ABBREVIATIONS

2D	Two dimensional
3D	Three dimensional
AvWD	Acquired von Willebrand disease
CAD	Computer-aided design
CFD	Computational fluid dynamics
CFX	Computational fluid dynamics software by ANSYS
CT	Computed tomography angiography
DSA	Digital subtraction angiography
μ	Dynamic viscosity
EMSA	Effective metal surface area
FDS	Flow diverter stent
HBR	Heartbeat rate
ICA	Internal carotid artery
LICA	Left internal carotid artery
LMCA	Left middle cerebral artery
LVAD	Left ventricular assist devices
M	Million
MCA	Middle cerebral artery
MRA	Magnetic resonance angiography
NSI	No stent implantation
TAWSS	Time-averaged wall shear stress
OSI	Oscillatory shear index
RICA	Right internal carotid artery
RMCA	Right middle cerebral artery
VFR	Volumetric flow rate
vWD	von Willebrand disease
vWF	von Willebrand factor
WSS	Wall shear stress

1. INTRODUCTION

Cerebral aneurysms play a major role in cerebral hemorrhages, impacting the life of the patients and even resulting in fatal consequences with a not to be underestimated rate in the world [1–7]. The prognosis of cerebral aneurysms are not simple, and they most frequently occur in the ICA and MCA, in order. These arteries, especially ICA, are two of the main arteries in feeding the brain. Cerebral aneurysm formation can lead to symptoms which can cause severe pain and discomfort to the patient. The life threatening phase gets initiated by the rupture of the aneurysm which leads to cerebral hemorrhage with the result of leaving the person disabled or dead. In this thesis three ICA sidewall and three MCA bifurcation aneurysm patients are chosen to investigate both hemodynamics at the aneurysm region and effect of forces on blood flow at the struts of the FDSs.

The occurrence of cerebral aneurysms can be caused by several different circumstances for the patient. Certain inherited diseases, age, lifestyle, eating habits and smoking leading to high blood pressure can all be a cause of cerebral aneurysm generation [8]. Gender also plays a huge role not only in aneurysm forming but also the characteristics of the blood flow [9,10]. Females have higher occurrence rates of intracranial aneurysm forming [11,12]. One of the main reasons for this is the different morphologies for the arteries between men and women where smaller artery diameters and geometry of bifurcation results in higher stresses on the blood flow. With post-menopause phase the estrogen levels in the women body start to reduce which is an essential hormone in protecting the artery health [13,14]. In the very physical scope, an aneurysm forms on an artery due to the existence of a fragile zone on the artery itself. This fragility might occur due to several reasons such as turbulence in the blood flow, vortex generation, magnitude and directional deviations of the wall shear stress (WSS) parameter. Those physical circumstances most likely lead to the weakening of the artery wall, forming and enlarging aneurysm and conclusively cause rupture [15].

Cerebral aneurysms show four different shape formation. These are called saccular, fusiform, mycotic and dissecting aneurysms. A substantial number of cerebral aneurysms are in the form of saccular aneurysms. Hence, all six patients available in this study have saccular aneurysms [16,17]. Diagnosis of cerebral aneurysms are challenging, where eighty five percent of them form and exist without any symptoms. Due to a direct symptom of the aneurysm or seldomly to be identified during a coincidentally undertaken scan, cerebral

aneurysms are diagnosed through computed tomography angiography (CTA) and Magnetic resonance angiography (MRA) [18].

More than a decade, FDS's are seen as one of the most favorited treatment methods of intracranial aneurysms [19–23]. Compared to other available treatment methods alone, FDS implantation is considered to be a less complex and a highly safe treatment approach [24–27]. Considerably high efficiency and prevention of large-scale skull opening surgeries make FDS a suitable choice in treating patients. Especially in wide necked cerebral aneurysms, FDS implantation is an option being widely chosen with or without coiling treatment method [28–30]. Some studies show results of deploying multiple stents to a single aneurysm geometry, where multiple stent cases lead to no significant hemodynamic change on the blood flow [31,32]. The main importance of an FDS treatment is hoped to be non-invasive placing of it into the artery and diverting the blood flow away from the aneurysm sac [33]. In achieving this, it is with great importance to choose the correct FDS type which will suit the patient specific characteristics of the parent artery [34]. In doing so, the efficiency in diverting the blood flow would increase and therefore the feeding of the aneurysm with blood would reduce which is hoped to lead to stagnation, increase in viscosity in the aneurysm sac, the prevention of rupture and the reduction in size of the aneurysm with regards to the work of macrophages [35–37]. Critical parameters in selecting the most suitable FDS for the patient are porosity value, wire thickness, FDS diameter and working length of the FDS. Depending on the morphology of the patient aneurysm, the chosen FDS could have a different porosity value when implanted in the artery than the catalogue porosity values. This example could occur due to the location of the aneurysm in which it exists on the curved region on the artery rather than the linear region. A bent FDS would have two different sides where compressed part has smaller porosity compared to the part which is under tension. Therefore, it is also a necessity to inspect the porosity or effective metal surface area (EMSA) values of the implanted FDS not only in the linear shape but in the state which it is existing in the artery. EMSA is a frequently used parameter in FDS studies[38–40].

Clinical trials with the recent version of FDS's show successful obstruction figures of 62.8 percent [41]. There are also various studies inspecting hemodynamics through Computational Fluid Dynamics (CFD) [42–45]. These type of studies show positive results, however this does not imply that FDS treatment method is purely safe. So far, the studies

mostly investigate the advantages of FDS treatment such as occlusion rate and diverting the flow away from the aneurysm sac. However, there are also a considerable amount of death rate exceeding eight percent in similar studies [46]. This proves the necessity to inspect and understand the direct and indirect effects of the FDS influence on the hemodynamics, change in blood characteristics and even causing or cannot preventing rupture during the treatment of intracranial aneurysms.

Further consideration of the aforementioned description about FDS implantation being non-invasive is needed. Addition of an external medium could most likely affect the hemodynamics and the human body has to adapt to it. This effect on hemodynamics and the procedure of adaptation to FDS may most possibly change the physical and chemical structure within the artery and the aneurysm. Those were the words which initiated the heart and soul of this thesis. It was found with a clinical research that there are strong points to a relation between FDS and vWD and that delayed intracranial hemorrhage following FDS treatment might be related with type 2A Acquired vWD (AvWD) [47]. Implantation of a foreign body within the artery causes delayed aneurysm rupture within thirty days of receiving the treatment.

Bleeding of a blood vessel due to an injury is clotted as a healthy human body reaction. vWF protein available in the blood leads the thrombocytes to cluster and stick with each other. With the diminishing number of vWF multimers, clotting capability for the human body decreases as well and this leads to vWD [48–52]. Considering inherited bleeding diseases, VWD is widely accepted to be one of the main underlying situation [53]. The occurrence of vWD is one for every ten thousand person. That concludes to a minimum of 800.000 people living in the world which might be in the risk group of getting FDS treatment if needed [54]. For the first time, vWD was inspected and named after Professor Erik von Willebrand where he was investigating and trying to find a relation of family members with possibly inherited bleeding disorder [55]. Important characteristics of vWD are extended bleeding time (BT), low number of vWF overall, absence of large vWF multimers and greatly decreased vWF activity due to increased breakdown of the proteins in the A2 domain of vWF [56]. For vWF multimers to be effective in clotting the blood, it has to be available as a large multimer. Bleeding may occur in a case where the size and/or activity of vWF multimers are reduced by a direct, an indirect or an external effecting mechanism/body. There are two different groups residing under vWD which are the results from either congenitally mutated vWF or

acquired deformation of the vWF. The acquired deformation leads the vWF multimers into a fragile state where they undergo proteolysis in the blood plasma [57,58].

VWF is a multimer existing in the blood. This multimer helps platelet binding during a vascular damage occurrence. Being the longest protein in the body, vWF monomer is made up of three important domains. As explained above, the middle domain A2 gets broken down. vWF is severed by an enzyme called ADAMTS- 13 which is found in the blood circulation [59–61]. Globally within the circulation, vWF multimer exists inactively in a folded shape. The activation of the vWF multimer occurs due to the exertion of supraphysiologic shear stress and shear strain rate. An external body existing in the cerebral arteries disturbs the blood and its flow. This disturbance is thought to be leading to an unrestrained increase in shear forces. Being exposed to excessive shear forces leads to the elongation of the vWF multimer which is transforming into an active form [62,63]. This excessive shear exposition happening with each heartbeat, causes the severing of the vWF multimer and tearing it into smaller pieces by the effect of ADAMTS-13 enzyme, thus creates a situation where vWF activity being reduced in the blood [64,65].

Implantation of endovascular tools such as left ventricular assist devices (LVAD) generate high shear values in the blood, lead to type 2A acquired vWD (AvWD) [66]. Several CFD studies show that FDS existence produce high shear in blood due to strut widths of approximately 200µm [43]. The vWD is occurring due to the reduced activity in vWF. From a similar study it was found that in distinguishing patients with reduced vWF activity, parameters of aneurysm volume and morphological index are used. FDS implantation may reduce vWF activity in a saccular aneurysm which is larger than 8 mm in any of the dimension [47]. Reduction in vWF activity and cerebral hemorrhage occurrences post FDS treatment are found to be two most important functions of shear-inducing external body implantation caused type 2A AvWD [67–70].

The two most significant complications leading to hemorrhages following FDS treatment are the late rupture of the aneurysm, which mostly occurs in the first thirty days, and the bleeding of the brain parenchyma. Therefore, it is of the utmost importance to investigate the mechanical disturbance of the FDS implantation on blood flow. It is shown by studies that MRI results following FDS treatment display aneurysm wall injuries caused by intrasaccular thrombus generation [71]. Thrombi aggregation within aneurysm domain consequently leads to a late aneurysm rupture following FDS treatment [72]. Studies show

the less enlightened complication of late brain parenchyma bleedings occurring after FDS treatment take place as microhemorrhages and ischemic lesions. Those lesions and microhemorrhages are obtained through diffusion-weighted imaging (DWI) and MRI, respectively [73]. Reduced activity of vWF after FDS implantation transforms the brain into a hemorrhagic phase where in the distal of intracranial artery bleeding could occur due to the platelet aggregation continuation [74].

The disturbance occurring in the blood flow due to an external body implantation, an FDS for intracranial aneurysm treatment in this case, changes the physical parameters existing for a physiological flow. The existence of FDS in the region of the intracranial aneurysm neck causes differences in the blood flow. Inflow and outflow starts to happen while the blood flow is entering the aneurysm sac through the struts of the FDS. Flow separation, change in velocity and viscosity also inevitably get accompanied with a supraphysiological increase in shear stress and shear strain rate. Pathological flow starts to occur from the threshold values of 10 Pa and 5000 s^{-1} for shear stress and shear strain rate, respectively [75]. The unfolding of the vWF starts to occur from those threshold values which turns the vWF to be elongated and activated. Once the vWF multimer gets elongated and removed from its globular form, it gets cleaved by ADAMTS- 13 enzyme on its A2 domain. With this vWF activity gets reduced as it has to exist in large size and amount within the blood. That leads to the dysfunction of the vWF in clustering thrombocytes when hemorrhage occurs. Before FDS treatment it should be remembered that an aneurysm existence already may lead to pathological blood flow for giant aneurysms. This should be investigated as well by running simulations of the non-treated patient models initially. This way the effect of the supraphysiological forces can be clearly distinguished for the shear values in the blood.

Investigating shear stress and shear strain rate on the fluid is crucial in understanding the FDS affecting hemodynamics. As mentioned earlier, there are two complication types following FDS implantation: delayed aneurysm hemorrhage and delayed parenchyma microhemorrhages due to AvWD. Delayed parenchyma hemorrhage can be understood by investigating deeper into what are taking place on the distal artery wall following FDS treatment. It may be very likely that certain regions are more likely to already have higher shear forces on both proximal and distal part of the artery even before treatment. Therefore, it is pivotal to calculate stresses and strains occurring on the walls of the artery and the aneurysm for both pre- and post-FDS treatment cases. Time-averaged wall shear stress

(TAWSS) and oscillatory shear index (OSI) are functional in understanding the WSS values and directional change in WSS for the whole cycle, respectively. OSI has the upper boundary of 0.5 which stands for the direction of the WSS vector having the complete opposite direction [76]. In several researches the strength in using TAWSS and OSI for intracranial aneurysm fluid flow simulations are shown [77–81]. Rupture of the aneurysm is linked with high values of OSI parameter [82]. In another study high OSI and low WSS in the same region are associated with aneurysm rupture [77,83]. It may be proven useful to investigate TAWSS and OSI values for the distal of the artery to potentially observe and determine if the walls of the artery are deteriorating following FDS implantation. This may help in understanding the complication of delayed parenchymal hemorrhages occurring following FDS treatment within thirty days of implantation where a link to vWD and FDS treatment can be made once more for the hemorrhagic complication types.

In this thesis, 48 and 64 wire FDS types implanted separately in order to inspect whether they would have any different influences on hemodynamics. The number of wires chosen in such a way that they would represent the most common FDS models available in the market where their EMSA values are depicted as thirty five for both. Having the opportunity to do a comparison between without FDS, 48 wire and 64 wire FDS may indicate not only shear inducing effect of FDS implantation but also if there can be a better option from the two FDS types chosen in this study. In a geometry where FDS implantation did not happen yet, it should be not forgotten that due to the existence of the aneurysm on an artery the flow there already happens pathologically. With this in mind, it could be a possibility where for certain patients before FDS treatment the shear values be in the vicinity of threshold values at certain location in the domain. However, the results from the CFD simulations may show the clear supraphysiological forces being exerted within the blood flow. The morphology of each patient makes the circumstances unique for themselves. Therefore, the importance in this method relies on comparing the before and after FDS treatment models for the same patient. There are going to be geometrical differences between 48 and 64 wire FDS types when they get implanted to the same patient. This is due to keeping the porosity at the same value but having different wire numbers. FDS struts at the neck region of the aneurysm will have different shapes with different angles at each corner on the struts. FDS struts with smaller openings could lead to higher shear forces as the fluid velocity would decrease. This is a typical behaviour in non-Newtonian fluids which show shear thinning characteristic [84–

86]. Therefore, investigating the difference between 48 and 64 wire FDS which are implanted on the same patient can be considered while inspecting the shear stress and shear strain rate values results which will be obtained from the simulations. This investigation may be highly useful in deciding why a FDS with certain wire number or wire thickness can be beneficial in keeping the shear forces relatively smaller.

Implantation of FDS is done by a catheter system where the FDS is deployed at the desired location by the surgeon. All FDS catalogues include several parameters such as porosity or EMSA, work and total length, implant and targeted artery diameter values. Most critically, porosity or EMSA values specified in the catalogs stand for the reference shape of linear tubes without any angles existing due to the patient artery geometry which is not straight. Depending on the location where an intracranial aneurysm takes form on the artery, the EMSA values can dramatically differ than the catalog values. In an instance, an aneurysm existing on the concave arc of the artery would have higher EMSA and lower porosity compared to an aneurysm being on the convex arc of the artery with the same diameter and neck diameter. FDS implanted in an angled artery also has difference in the strut shapes where blood flow passing through the FDS. Blood flow passing through relatively smaller and less porous FDS domain at the aneurysm neck. The region which the blood flows through the FDS struts turns into an inflow jet. This highly dynamic phenomenon causes the blood flow to have a dramatic increase in velocity while passing through towards to aneurysm sac and later exiting from the outflow region on the FDS at the aneurysm neck. Inflow and outflow regions on the FDS domain as shown in Figure 1.1 helps in understanding where blood enters and exits the blood flow with considerably higher velocities. Inflow stands for blood flow leaving FDS and entering into aneurysm where outflow implies blood flow leaving aneurysm and passing through FDS and entering into the main artery. Supraphysiologic forces occur at that very moment due to stent struts where shear stress and shear strain rate values expected to be increased way over physiological thresholds [87].

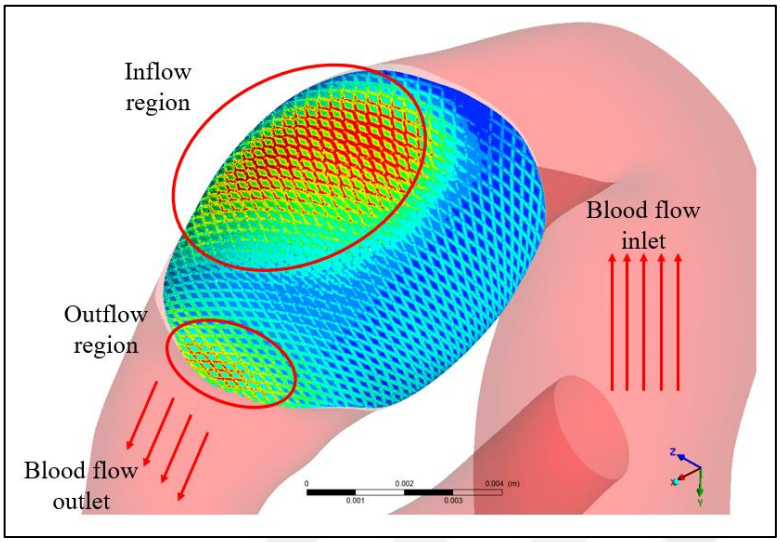

Figure 1.1. Inflow and outflow zones on FDS where blood flow enters and exits the aneurysm sac with large velocity values

Patient specific, real-life clinical images are used in this study. With this, it is aimed to achieve such circumstances in domains and conditions where simulation results presenting highly accurate data for a highly realistic set of domains. The importance of showing the effectiveness and complications generated by FDS implantation is paramount considering the fact that FDS treatment cannot be reversed, and it has to stay with the patient life-long. Therefore, many studies investigate the advantages of FDS treatment and how it helps save lives and prevents life quality diminishing incidents' reduction in occurrence, this is not entirely correct and the negative results of this external body implementation to a cerebral artery has to be investigated by in-depth mathematical, physical and clinical approaches together. This is such a dire situation where delayed intracranial hemorrhages or delayed brain parenchymal bleedings occur due to the FDS treatment within a month after it is deployed but on the other hand the aneurysm left untreated can rupture and cause no less harmful than the complications might still take place. Therefore, shining a light to this complex and unstable aneurysm morphology to help in any way it is possible in pointing out also any inefficiencies and problems occurring is of great significance.

Virtual FDS implantation can be conducted with the help of computer aided design (CAD) software such as Spaceclaim 2021 as in this study. Following that, generating a fluid domain and running fluid flow simulations are possible through CFD software. In this thesis work, CFX module from ANSYS is chosen to define the 3D geometry, mesh it, define boundary

conditions, solve the simulations and retrieve the results from those simulations. This study aims to be distinctive in creating highly realistic patient specific circumstances for the simulations. This starts with the implementation of patient specific geometry. That can be accomplished through MRI, CT or DSA images of real patients to be processed through several software and eventually obtain three-dimensional patient specific cerebral artery and aneurysm geometry. Virtual stent implantation with a chosen FDS which is identical to the actual FDS gives the flexibility to see various effects of different FDS choices on the same patient. Inspecting similar studies can point out the importance of defining crucial parameters properly such as the fluid characteristics, velocity profiles and pressure inputs or outputs [88–93]. Certain clinical data as heartbeat rate (HBR) and blood pressure measurements can serve key importance in defining boundary conditions.

The CFD approach is an efficient way to obtain and comment on important parameters. The nature of immediate change in blood flow characteristics following a FDS implantation makes this type of investigation possible. Such as reality, in many studies with CFD investigations it is observed that immediately after the treatment the blood flow changes for the first couple of cardiac cycles already. CFD makes it possible to have a deep dive in the hemodynamics of a patient before and after FDS treatment. Creating a patient specific model and cases with the most realistic circumstances rely heavily on defining the fluid type, velocity profile and constructing the remaining boundary conditions physically and mathematically accurate. Because shear stress and shear strain rate are two of the most important parameters to investigate, the blood should be defined with the Bird-Carreau model as a non-Newtonian fluid [94,95]. The relation between shear related investigations and modelling the blood as non-Newtonian is the shear-thinning characteristic of the blood defined by Bird-Carreau model. Another highly important condition to create the most realistic model is implementing a velocity profile which matches the blood flow quite well. For this reason, Womersley velocity profile is chosen for this thesis.

Main objective of this thesis is to inspect the relation between FDS implantation in treating cerebral aneurysms and reduced vWF activity caused by the shear inducing repercussion of the FDS treatment. Six different patients are chosen with aneurysms residing on ICA and MCA. The study initiated with the goal of proving the triggering of the shear stress and shear strain rate excessiveness following FDS treatment. Patient specific geometries are constructed, virtual FDS surgery is conducted and three cardiac cycles long CFD simulations

are solved and inspected. Various plots for each time step are constructed and numerous shear related contours for every peak systole and diastole of a cardiac cycle are generated while presenting the simulation results. Complementary investigations are also done with several other parameters with the motivation to understand complications of delayed hemorrhages following FDS treatment. Calculating shear stresses on aneurysm or artery wall can give further insight into comprehending rupture prone regions and can be harmonious with the hemorrhages caused by type 2A AvWD following FDS treatment for giant aneurysms. Not only instantaneous activation of vWF multimers through shear stress and shear strain rate exceeding over physiological threshold values are investigated, but also volumetric percentage of blood which contains activated vWF multimers are calculated. One of the novelty of this research lies in understanding if and to what extent FDS treatment may lead to complications of delayed hemorrhages following its deployment. Obtained results and driven conclusions from this thesis may heighten the awareness in choosing a treatment method for cerebral aneurysms where ICA and MCA aneurysms in this study represent a majority for the location of cerebral aneurysm occurrences with a 52 percent occurrence rate combined with together [18]. The risks of FDS treatment can be laid out in-depth for clinical use through the results obtained in this thesis which has the intention to show those risks with clear indications.

2. MATERIALS AND METHODS

The main objective in this study is to create a real-life scenario of the blood flow occurring through the cerebral arteries and aneurysms of each patient in the most realistic way possible. To reach this objective, patient specific geometries are generated. FDS with 48 and 64 wires are modelled and virtually implanted into the patient specific geometry. To simulate the blood flow in a patient specific way, Womersley velocity profiles are created to be implemented in generating blood flow. Bird-Carreau blood type is introduced to be able to model the blood as a non-Newtonian fluid due to its shear-thinning characteristic. Volumetric flow rate (VFR) is also specified for each patient according to patients' gender and age as well as their aneurysm location. Parameters like some important ones as wall shear stress, shear strain rate, TAWSS, OSI and dynamic viscosity are defined in the transient results in order to obtain and write the data at each time-step. Following the setup construction, simulations are solved by using ANSYS CFX-Solver.

2.1. MODELLING PATIENT SPECIFIC GEOMETRIES

The construction of the patient specific geometries is made possible with the digital subtraction angiography (DSA) data provided by the Ege University Medical School, Department of Radiology, İzmir, Turkey. These data consist of DICOM images of the patients' which are taken before FDS implantation. Therefore, the DICOM images do not contain anything but the artery and aneurysm themselves. With the goal to convert those DICOM images of six patients, several steps are applied to convert these two-dimensional images into three-dimensional surfaces and then solid parts.

Initially the DSA images are extracted as three-dimensional surface geometries by the use of Slicer 4.10.2 [96]. Following the execution DSA image processing that generated surface geometries further smoothening is required to construct proper mesh elements further down the CFD road. This is a crucial step which is taken to eliminate any geometrical issues existing on the surface which may lead to errors in the Mesh section of the fluid domain construction. Following the smoothening, which is done with the help of Meshmixer software (Autodesk Inc., USA), the geometries are imported to the Spaceclaim module from

ANSYS 19.2. After obtaining the patient specific geometry, 48 and 64 wire FDSs are modelled. Implantation of the FDS is achieved with Spaceclaim.

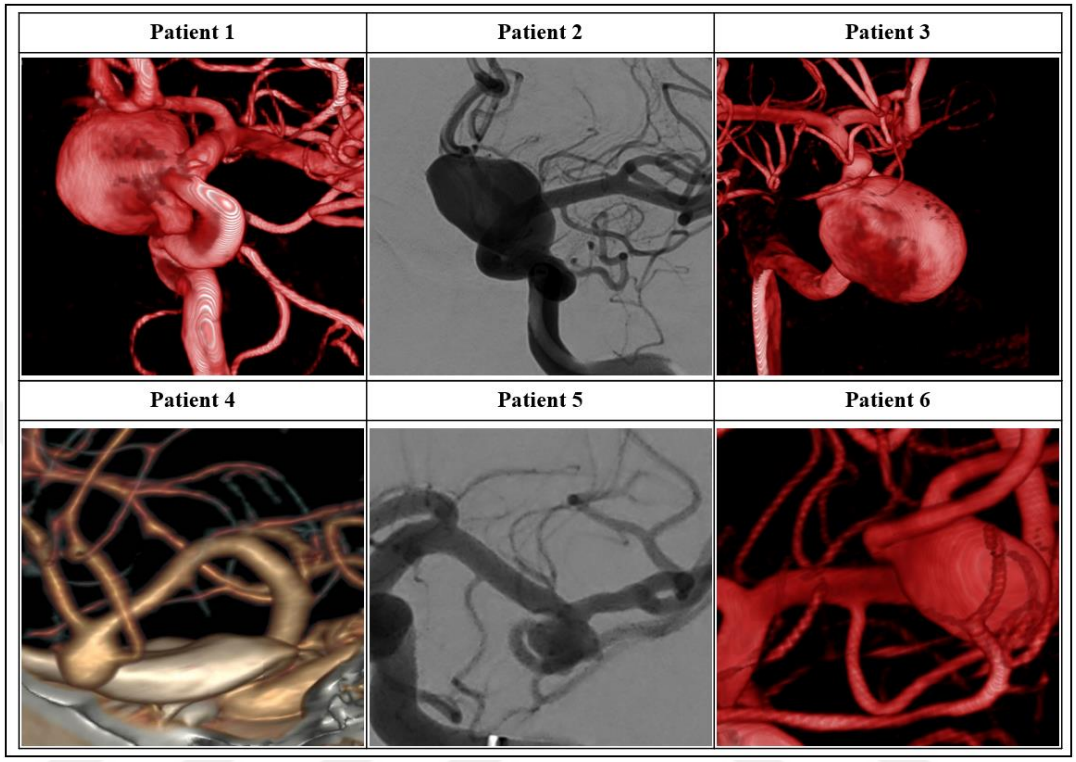

Figure 2.1. Clinical patient specific images taken before the implantations of FDS

DSA images of all six patients are shown in Figure 2.1 where aneurysms of three ICA and three MCA patients are visible. Each patient is female and from patient 1 to patient 6 they have various ages from late twenties to early sixties. Each patient's FDS is modelled accordingly with their morphological dimensions which means each patient has FDSs with different diameters.

Table 2.1. Age, average artery diameter and aneurysm height for each patient

Patient #	Age	Gender	Average Artery Diameter (mm)	Aneurysm Height (mm)	Aneurysm Neck Diameter (mm)
Patient 1	56	Female	4.12	19.6	8.40
Patient 2	64	Female	4.29	18.6	8.46
Patient 3	39	Female	3.98	17.9	8.07
Patient 4	60	Female	3.31	5.51	4.92
Patient 5	54	Female	2.72	4.68	3.98
Patient 6	29	Female	3.63	5.92	6.63

vWF is activated and later on reduced in activity due to several morphological parameters [97]. All ICA patients in this research have aneurysm height of 8 mm or above and large neck sizes which makes them suitable for the investigation of vWF activation due to supraphysiological shear stress and shear strain rate values.

First three patients show a vertical course where the blood flows from bottom to top for the planes shown in Figure 2.1. For patients 1 and 2 anatomically, aneurysms are located at the left internal carotid artery (LICA) and patient 3's aneurysm is located at the right internal carotid artery (RICA). The last three patients, MCA patients, show a horizontal course of blood flow. Anatomically the aneurysm is located at the right middle cerebral artery (RMCA) for patient 1 and for patients 2 and 3 aneurysms are located at the left middle cerebral artery (LMCA). Cerebral arteries exist in the brain in a symmetrical structure as they are mirrored for the right and left sides [97,98]. As generating the closest real-life scenario being the objective, the first crucial requirement of having an identical artery and aneurysm geometry of the patient is done using the methods and software mentioned.

2.2. FLOW DIVERTER STENT SPECIFICATIONS AND IMPLEMENTATION

After generating the patient specific aneurysm geometries, FDS must be modelled. One of the crucial phases in this thesis work is to structure FDS models in a realistic way. Certain parameters must be known in order to achieve the correct model of FDS. Parameters dictated by the patient are artery diameter and neck area. The ones depending on FDS brands and

models are wire thickness, wire numbers, porosity, work length, pattern of varying wire thicknesses are some parameters to be known. Having the values for each of those parameters, FDS modelling can be done. Porosity is one of the most important parameters to set right as it will have the most influence in diverting the flow by not allowing a certain volume of blood. However, the porosity of the FDS catalogues provided by the producing companies presents only the porosity value when FDS preserves its linear and tubular shape (i.e., prior to placement) contrary to the reality where an FDS can undergo bending or bulging (i.e., after placement into the aneurysm carrying artery). This difference can arise due to the exact location of the aneurysm on the artery, the angle which the artery has making the FDS have the same shape and discrepancy between artery diameter and FDS's work diameter.

Two different FDS types are used in this study. Each FDS has the same porosity and wire thickness values where the difference is relying mainly on one FDS being made of 48 wires and the other 64 wires. In this sense, while investigating whether FDS treatment has effects on altering blood flow a comparison between two different FDS types can be made in a possible scenario which one gives better results for the patients. For each patient the artery diameters are different and therefore different FDS diameters can be used for each patient. These diameter differences do not result in any change in the sense of effectiveness of the FDS for the patients, as the porosity of each FDS is set to be the same at their own work diameters.

Table 2.2. Values of FDS parameters

FDS Type	Wire Thickness	Porosity (%)	Number of Wires
48 Wire	30 µm	65	48
64 Wire	30 µm	65	64

The construction of each FDS for each patient is done using SpaceClaim through ANSYS 19.2 Academic. Initially each FDS modelled fully in their actual work length. Later, having each FDS at their correct alignment, FDS wires existing at the aneurysm neck area are kept and the rest got removed from the geometry. The main reason behind this procedure is to avoid having unnecessary mesh elements during meshing. This is possible to do as the effective area of the FDS is where the aneurysm neck is. Having less mesh elements after

this step lowers the mesh element number and therefore keeps the computational time at reasonable levels during the solution of the simulations. Having reasonably lower computational time during the solution is desired as there are eighteen simulations to be solved in total.

Virtually implanting FDS to each patient specific geometry gives the opportunity to investigate and to understand the hemodynamics and the effects which are leading to vWF activation. Another important aspect of virtually implanting the FDS to the patients, make it possible to observe the differences occurring in FDS shape due to the variations in artery morphology for each patient. Some patients have their aneurysm at a sharp curve which causes a big difference in actual EMSA value. This may be one of the reasons to have different efficiency in FDS treatment to alter the blood flow however the outcome might be an unsuccessful result.

2.3. MESH MODEL

Following the virtual stent placement, preparation for the simulation starts with meshing the geometry. Here creating a proper fluid domain is initiated. Meshing is a crucial step in this study for various reasons. A correctly meshed geometry is the first step in getting correct results at the end of the simulation and will prevent unnecessary computational time. Having a mesh independent geometry is required to reduce the level of error in a simulation. Mesh independency is further explained later in this section.

All six patients have three separate simulations, making up a total of eighteen simulations. Each patient has a before treatment model which does not include the implanted FDS. The other two simulations for each patient are done with 48 wire and 64 wire FDS implantation. Before treatment geometries require a much smaller number of elements as they do not contain an implanted FDS, as explained earlier briefly. All six patients have a number of elements in the vicinity of 1M. As expected, ICA patients have a greater number of elements than MCA patients as they have larger artery diameters and much larger aneurysms. 48 and 64 wire models have substantially higher number of elements. The main reason behind this is that the volume and surface area of FDS wires are considerably smaller than artery and aneurysm dimensions. This requires a finer mesh construction. FDS is located at the neck region of aneurysm for each patient, which makes the FDS domain even more important to

have a finely constructed mesh. This is done through mesh sizing in the level of both surface area and volume. Other higher priority regions such as inlet and outlet (s) of the artery, aneurysm and FDS wall. All six patients have elements in the vicinity of 25M with again ICA patients having a greater number of elements than MCA patients due to the greater size of their arteries and the aneurysms. Mesh elements for each patient with all cases are shown on Table 2.3.

Table 2.3. Number of elements for each patient geometry

	Number of elements (Million)		
Patient number	Before Surgery	48 Wire	64 Wire
Patient 1	1.23M	21.3M	25.4M
Patient 2	0.91M	24.7M	20.3M
Patient 3	1.19M	19.3M	20.7M
Patient 4	0.97M	20.8M	16.0M
Patient 5	0.94M	23.8M	23.5M
Patient 6	1.39M	19.5M	22.4M

Difference in number of elements directly dependent on the size of the artery and the aneurysm. ICA patients having larger dimensions would lead them to have higher amount of mesh elements. However, comparing some ICA and MCA patients may prove otherwise. This is due to the existence of ophthalmic artery in MCA geometries in this case and also selection of fluid domain is not critical if important regions are included in it. The same percentage of element size fineness is selected while constructing the mesh. Initially it was expected to have higher number of elements for all 64 wire cases compared to their 48 wire correspondents. However, this was proven wrong with patients 2, 4 and 5. This is due to the fact that removing all the FDS wires except the ones on the neck. Therefore, the number of elements depend on the neck EMSA values for each patient where when EMSA gets lower, the number of elements should get lower as there will be less metal surface coverage existing in the domain. Posing as an example for all patients in Figure 2.2, full geometry and cross section views of patient 2 mesh structures are shown. In the cross-section view from bottom to up the mesh fineness and density differences can be seen for the artery, FDS region and aneurysm.

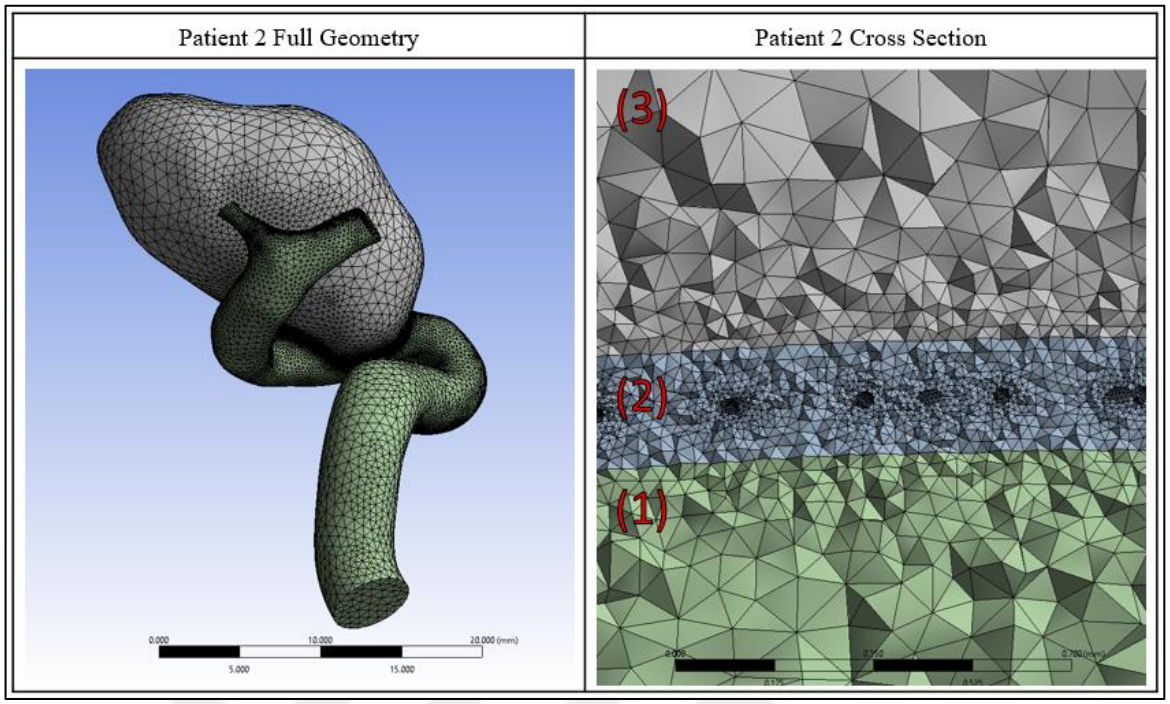

Figure 2.2. Mesh example of patient 2 with 64 wire FDS implanted

2.4. BOUNDARY CONDITIONS

In order to simulate the patient specific model as it is in physical life setting up the boundary conditions are crucial. Each parameter will shape the simulation for the specific case existing within the patients' arteries. The first step in preparing a real-life circumstance to the fluid domain, meshing is done appropriately. Each boundary condition is specific to the patient which makes the simulations as close as possible to the real-life scenario. This section is the explanation of all related numerical relations, equations and physical laws constructing physical model and the patient specific circumstances.

Womersley velocity profile is constructed for all six patients using MATLAB [99–101]. Being time and location dependent, Womersley velocity profile helps in constructing the required blood flow cycle with diastole and systole waveforms existing in it. Constructing the Womersley profile for each patient is done through a series of in-house built code. In order to obtain the profile in the patient specific way as desired, inputs for several parameters need to be plugged in. Those parameters are average inlet velocity that is obtained from VFR, mean artery diameter, pressure gradient, which is measured before surgery, dynamic viscosity of blood, density of blood, heartbeat rate of the patient, time step size value which

is eventually going to be used in the simulation solution and cardiac cycle count that is desired to obtain after the solution of the simulation.

Womersley velocity profile is a derivation from periodic pressure gradient. Being time and location dependent, Womersley velocity profile yields much more sensitive velocity profiles compared to pulsatile flow [102] velocity profile. The availability of constructing patient specific velocity profile by considering age, gender, VFR, HBR, mean artery diameter, density and dynamic viscosity of the blood makes this way of constructing velocity profiles closer to real-life scenario [103].

$$u_z(r,t) = Real\left(\frac{-j\alpha(\omega)}{\omega} e^{i\omega t}\left[1 - \frac{J_0\left(\sqrt{-j}W_0\frac{r}{R}\right)}{J_0\left(\sqrt{-j}W_0\right)}\right]\right) \tag{2.1}$$

Volumetric flow rate is required to calculate an average velocity as the code requires a flow with the unit of m/s. Each patient has different volumetric flow rate depending on their gender, age and the location of the aneurysm [104].

For each patient, volumetric flow rate is taken from the literature and through that average inlet velocity is obtained and calculated, respectively.

$$VFR = Q = \frac{dV}{dt}\left(\frac{m^3}{s}\right) \tag{2.2}$$

VFR is obtained by the fluid flow of certain volume V in the duration of time t. VFR is a parameter that is derived from volume with respect to time.

$$v = \frac{Q}{A}\left(\frac{m}{s}\right) \tag{2.3}$$

$$V = \frac{Q}{A}\frac{\left(\frac{ml}{min}\right)}{(m^2)} \rightarrow \frac{Q}{A}\frac{\frac{10^{-3}}{60}\left(\frac{l}{s}\right)}{(m^2)} \rightarrow \frac{Q}{A}\frac{\frac{10^{-3}}{60}\left(\frac{dm^3}{s}\right)}{(m^2)} \rightarrow \frac{Q}{A}\frac{\frac{10^{-6}}{60}\left(\frac{m^3}{s}\right)}{(m^2)} \tag{2.4}$$

VFR value taken from the literature has the units of ml/min. MATLAB code for Womersley requires inlet velocity value in the units of m/s. Therefore, the conversion from ml/min to m^3/s is done and shown at (2.4).

Table 2.4. Parameters used to obtain average velocity values for each patient

Patient #	VFR (ml/min)	Artery Cross Section Area (m^2)	Average velocity (m/s)
Patient 1	244	$21.3x10^{-6}$	0.191
Patient 2	218	$19.2x10^{-6}$	0.184
Patient 3	247	$16.8x10^{-6}$	0.328
Patient 4	110	$8.58x10^{-6}$	0.214
Patient 5	125	$5.73x10^{-6}$	0.319
Patient 6	149	$10.2x10^{-6}$	0.244

Pressure gradient array is taken from literature [105]. Heart rate (HR) is taken as 75 beats per minute, density and molar mass of the blood are taken as 1120 kg/m^3 and 64458 g/mol, respectively on the hemodynamical properties of blood flow in patient specific carotid artery with stenosis [106].

After obtaining each parameter that are required in constructing the velocity profile, they are inserted in the MATLAB code which generates the Womersley velocity profile in CFX expression language. Womersley velocity waveform constructed in the Setup section of the simulation shows the physical behavior of the code. After solving the simulation, the maximum velocity at inlet is plotted for the entirety of the simulation. An example maximum inlet velocity for patient 1 is shown with Figure 2.3. With that figure the regions of systole and diastole during three cardiac cycles can be seen. This serves as a check and identification action to investigate the integrity of the implemented code to physical relation and obtaining the peak systole and diastole instances.

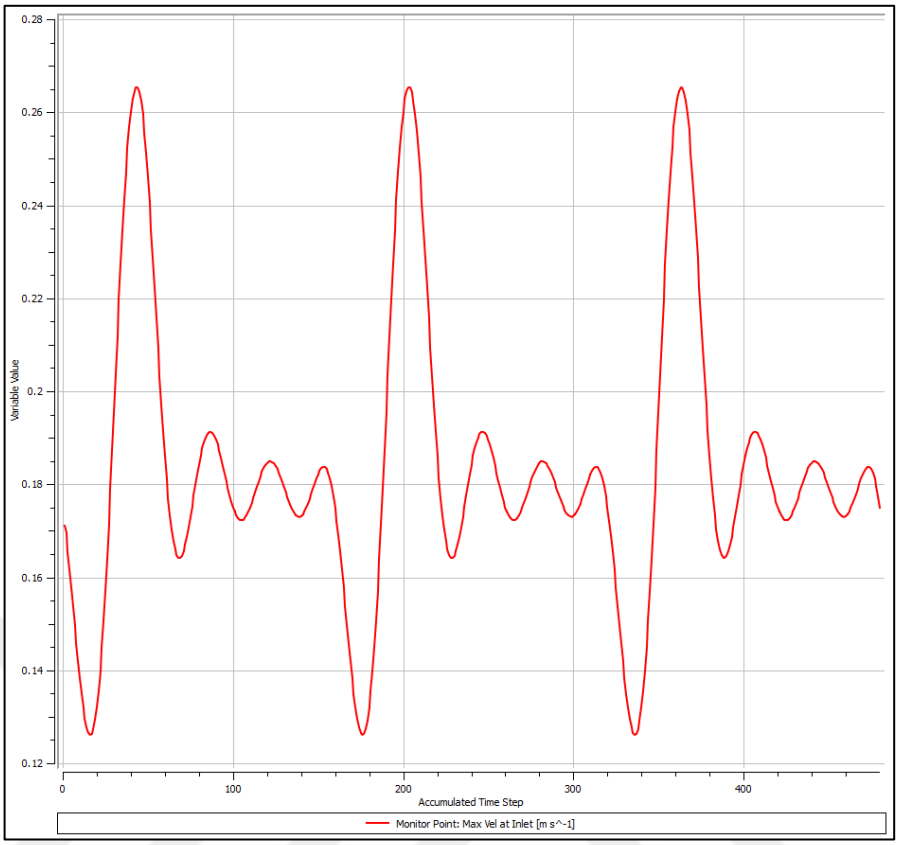

Figure 2.3. Maximum velocity at inlet using Womersley velocity profile of the blood flow for patient 1

Outlet pressure is implemented to each fluid domain as 80 mmHg [107]. The outlet pressure condition is defined as openings for each branch of the artery that are not inlet. The fluid-solid interaction is taken as rigid due to computational limitations. Flow regime is selected as subsonic where flow direction is appointed as normal to the boundary condition.

One of the most crucial boundary conditions to define in order to get a circumstance that is as close as possible to reality, blood is modeled as a non-Newtonian fluid. Those type of fluids have the shear thinning characteristic and this is made possible to implement to the simulations by using the Bird-Carreau model. The main importance of this blood model is to be able to let the fluid differ between 0.00345 Pa.s and 0.056 Pa.s [108].

$$\mu = \mu_{\infty} + (\mu_0 - \mu_{\infty})[1 + (\lambda\dot{\gamma})^2]^{(n-1)/2} \tag{2.5}$$

Shear rate $\dot{\gamma}$ which is varying with the velocity is implemented in (2.5) to employ dynamic viscosity of the blood μ. There, the maximum viscosity μ_0 and minimum viscosity μ_∞ are taken as 0.056 Pa.s and 0.00345 Pa.s, respectively. Time constant λ and the power law constant n are taken as 3.313 seconds and 0.3568.

Each patient simulations are solved for three cardiac cycles. The main reason in doing three cycles is to get rid of the initiation errors from the first cycle and have two relatively similar cycles in order to observe the functions. One cardiac cycle is set last as 0.8s with a time-step size of 0.005s. This sums up to a total of 480 time steps for one simulation. Constructing the solver for each simulation is done by defining several solving schemes. As advection scheme high resolution is selected. Second order backward Euler transient scheme is chosen as the solver with the residual target of 1E-4 defined. Transient fluid flow simulations are conducted within each time-step and at every mesh element where continuity (2.6) and momentum equations in cylindrical coordinates (2.7), (2.8) and (2.9) are governed. For the cylindrical coordinates the flow of the blood is accepted to be through the artery which is the z momentum. Assumption of fully developed flow makes it independent of time component and having laminar flow means no vortices caused by turbulence which means that there is no flow on theta (θ) axis. As the flow accepted to be fully developed and existing on z component, towards the artery walls which is the r momentum yields to be zero. Having these incorporated into the following equations yield the initial given Womersley equation (2.1) that is dependent on time and artery diameter and therefore the velocity profile on z axis.

$$\frac{\partial \rho}{\partial t} + \frac{1}{r}\frac{\partial}{\partial r}(\rho r u_r) + \frac{1}{r}\frac{\partial}{\partial \theta}(\rho u_\theta) + \frac{\partial}{\partial z}(\rho u_z) = 0 \tag{2.6}$$

$$\rho\left(\frac{\partial u_r}{\partial t} + u_r\frac{\partial u_r}{\partial r} + \frac{u_\theta}{r}\frac{\partial u_r}{\partial \theta} + u_z\frac{\partial u_r}{\partial z} - \frac{{u_\theta}^2}{r}\right) = -\frac{\partial P}{\partial r} - \left[\frac{1}{r}\frac{\partial (r\tau_r)}{\partial r} + \frac{1}{r}\frac{\partial (\tau_{\theta r})}{\partial \theta} + \frac{\partial (\tau_{zr})}{\partial z} - \frac{\tau_\theta}{r}\right] + \rho g_r \tag{2.7}$$

$$\rho\left(\frac{\partial u_\theta}{\partial t} + u_r\frac{\partial u_\theta}{\partial r} + \frac{u_\theta}{r}\frac{\partial u_\theta}{\partial \theta} + u_z\frac{\partial u_\theta}{\partial z} - \frac{u_r u_\theta}{r}\right) = -\frac{\partial P}{\partial \theta} - \left[\frac{1}{r}\frac{\partial (r^2\tau_{r\theta})}{\partial r} + \frac{1}{r}\frac{\partial (\tau_\theta)}{\partial \theta} + \frac{\partial (\tau_z)}{\partial z} - \frac{\tau_{\theta r} - \tau_{r\theta}}{r}\right] + \rho g_\theta \tag{2.8}$$

$$\rho\left(\frac{\partial u_z}{\partial t}+u_r\frac{\partial u_z}{\partial r}+\frac{u_\theta}{r}\frac{\partial u_z}{\partial \theta}+u_z\frac{\partial u_z}{\partial z}\right) = -\frac{\partial P}{\partial \theta}-\left[\frac{1}{r}\frac{\partial(r\tau_{rz})}{\partial r}+\frac{1}{r}\frac{\partial(\tau_{\theta z})}{\partial \theta}+\frac{\partial(\tau_z)}{\partial z}\right]+\rho g_z \quad (2.9)$$

2.5. MESH AND TIME STEP SIZE INDEPENDENCY

In order to construct series of simulations independent from the number of elements during mesh and time step, mesh convergence and time step size analyses were run. For a randomly selected geometry the mesh elements are constructed for 20M, 25M, and 30M elements. The time step size values of 0.001s, 0.005s and 0.01s are defined to identify the time independent step size value. The setup of these simulations is constructed with the boundary conditions that are going to be used for the actual simulations as well.

After solving those three simulations, dynamic viscosity values for each time step during the last cardiac cycle is listed down in an Excel (Microsoft Office 365) sheet. In order to find the mesh and time independent domain, relative dynamic viscosity values are compared with each other. Comparing all dynamic viscosity differences for each simulation showed that all simulations have less than five percent difference which shows that the number of elements and time step size values are all in the mesh independent region. To have the most optimal computational time during the solution of the simulations the proximity of 20M elements and the exact time step size of 0.005s are chosen to be defined for each patient with FDS.

2.6. INVESTIGATED PARAMETERS WITH THE SIMULATIONS

Various parameters are investigated in this thesis in order to have the most complete understanding about supraphysiologic forces occurring in blood flow which lead to vWD. Each parameter was investigated thoroughly from contours generated on curved planes to vertical contours perpendicular to neck region of the aneurysm. For some parameters their values were calculated for each time step in the third cardiac cycle. Investigation of different parameters required different approaches to calculate, observe and present. As an example,

investigating shear stress and shear strain rate values requires a sensitive investigating approach due to the possible exceeding of threshold values in these parameters would lead to vWF activation. Therefore, for these types of instance-important parameters, at each time step calculation is done to form a graph to understand the behavior of the flow.

Shear stress and shear strain rate values are obtained at curved planes to construct visual contours and for each time step to form graphs. These curved planes formed in such a way for each patient that they are passing from the center of every FDS wire existing in the neck region. The behavior of those two parameters is constructed on graphs by calculating each value at each time step of the third cardiac cycle. Different from the shear stress parameter, not only on a curved plane but also on a vertical contour, shear strain rate is calculated. The vertical contour is perpendicular to the FDS which is generated to observe the blood flow being affected by the implantation of FDS.

The effect of supraphysiological forces on blood are investigated through a special method. With the help of shear stress and shear strain rate contours it can already be inspected whether there are supraphysiological forces in act. However, the intensity of these forces, in other words the true impact, cannot be known by only inspecting those shear contours. Blood flow which gets aggravated by the FDS, has a proportion of volume which has supraphysiological forces. The investigation is done by calculating the amount of blood volume which has 10 Pa or more shear stresses and obtaining the percentage of that supraphysiological part of the blood volume to the total blood flow's volume. This is calculated for each time step by obtaining the blood volume with supraphysiological forces and the total blood volume for the whole third cardiac cycle. Through this, it can be known that whether high shear stress and shear strain rate levels do actually affect a meaningful proportion of the blood flow. The results are gathered numerically for each time step and plotted on a graph. The aggravated blood volumes are plotted on the fluid domain as well for visual inspection to understand in- and outflow regions.

Besides shear stress and shear strain rate parameters, time-averaged wall shear stress (TAWSS) and oscillatory shear index (OSI) are calculated for each model. TAWSS and OSI parameters are implemented as transient statistic parameters to the setup of the fluid domain as additional variables. Similar to other variables that are in the simulations, the TAWSS and OSI are calculated for each time step for three cardiac cycles. However, different than the rest of the variables they are plotted only for the last time step sizes of each simulation.

The understanding behind this is to show the values obtained and averaged for the whole of the results obtained throughout all three cardiac cycles. These results are plotted on the walls of the whole fluid domain. This way the high shear induced and therefore weaker and rupture prone regions can be identified on the artery and aneurysm.

$$TAWSS = \frac{1}{T}\left(\int_0^T |WSS(s,t)|\, dt\right) \tag{2.10}$$

As it can be seen from (2.10), TAWSS is calculated within the integral of 0 to T which is the period of the cardiac cycle (0.8s). From the initiation of the blood flow until the cardiac cycle is completed the TAWSS value can be calculated through this method. This integral gives the time averaged value of each WSS values existing at every time step of the cardiac cycle at the "s" location on the artery wall. This parameter is added to the simulation's transient statistics section as an additional variable using the CFX language. Higher values of TAWSS starting from 25 Pa may lead to endothelial damage for the patient [109].

$$OSI = 0.5\left(1 - \frac{\left|\int_0^T WSS(s,t)\, dt\right|}{\int_0^T |WSS(s,t)|\, dt}\right) \tag{2.11}$$

OSI given in equation (4.11) represents the deviation in the pre-existing axial direction of the WSS in a cardiac cycle. Lower OSI values are associated with less disturbance in the flow. High OSI values, where 0.5 can be the highest, lead to higher disturbance that is leading to deviations in the direction of WSS vector which is causing a disturbed alignment of endothelial cells [32,76].

Maximum WSS values on artery walls of each model are calculated for each time step. The results are plotted on a WSS versus time-step graph in order to understand the behavior of WSS pre- and post-FDS implantations. With each model, the aneurysm and FDS domains are subtracted from the domain, as in Figure 2.4, while calculating the resulting WSS values per each time-step in the third cardiac cycle. This way, the maximum WSS values are calculated only on the artery walls for every model.

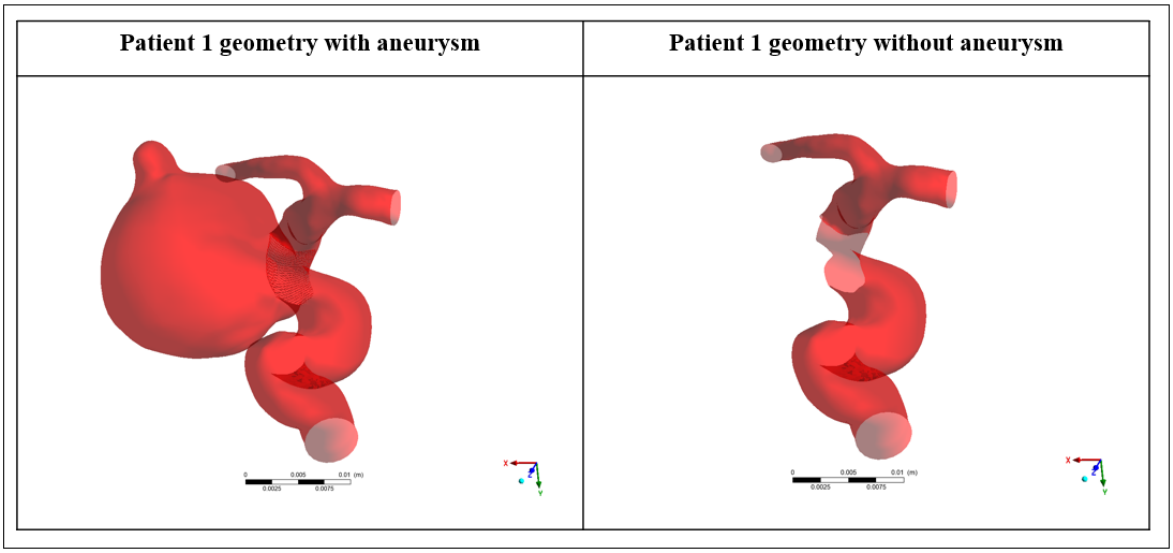

Figure 2.4. Domains with and without aneurysm for patient 1

As introduced in the introduction section, it may be important to inspect the strut differences on 48 and 64 wire FDS geometries for the same patient. The strut opening area and the angle difference of the junction point where two wires coincide are calculated for each FDS for each patient.

Table 2.5. Opening area values and FDS strut wire junction angles for each patient with 48 and 64 wire FDS

Patient #	48 Wire Strut Opening Area (mm^2)	64 Wire Strut Opening Area (mm^2)	48 Wire Junction point angle (degrees)	64 Wire Junction point angle (degrees)
Patient 1	0.296	0.231	31.92	54.73
Patient 2	0.078	0.065	36.97	63.37
Patient 3	0.092	0.103	46.70	89.24
Patient 4	0.315	0.311	52.29	97.45
Patient 5	0.059	0.053	62.42	87.10
Patient 6	0.130	0.061	61.45	100.67

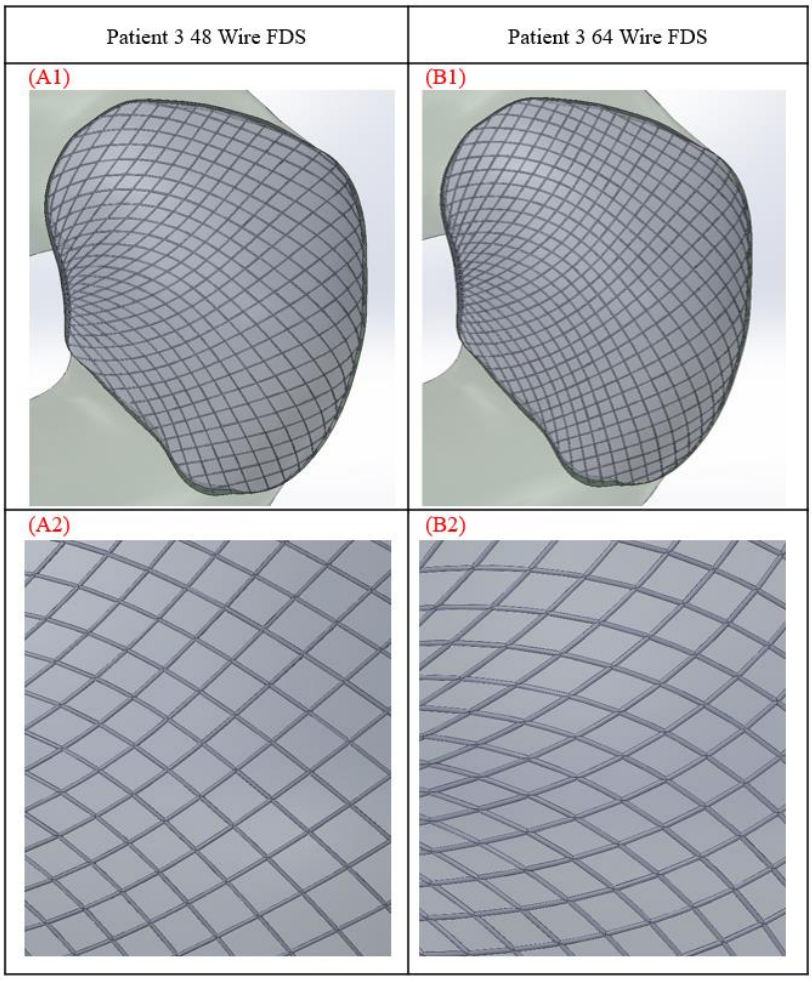

Figure 2.5. Patient 3 after virtual stent implantation model where 48 and 64 wire FDS's are shown on the neck (A1), (B1) and up-close (A2), (B2) for strut shapes, respectively.

It can be seen from Table 2.5 that for every patient except patient 3, the strut opening areas are larger with 48 wire FDS type compared to 64 wire. This alone is not enough to come up with conclusion after obtaining the simulation results. However, looking at angles at the wire junction for 48 and 64 wire FDS implantation, there is a clear distinction between the two FDS types. For every patient FDS with 48 wires has considerably smaller degrees of angles compared to the 64 wire FDS. The value of the difference between junction point angle between two wires for two different FDS could have an influence on the shear stress and shear strain rate differences for 48 and 64 wire FDS as well.

Dynamic viscosity is calculated for each time step and plotted during systole and diastole instances for each patient. The most effective way to visually present these results are found to be by plotting the dynamic viscosity on a vertical plane along the height of the aneurysm sac. This way it is aimed to observe the dynamic viscosity change before and after FDS implantation. Decrease in dynamic viscosity and therefore tendency to have stagnation is the desired situation in the aneurysm sac following FDS treatment. In this research it is used as a supplementary parameter where mesh independence is done and compared with each other using dynamic viscosity as aforementioned in this chapter. Also, to observe different effects of same 48 and 64 wire FDS's on different patients.

3. RESULTS

The investigation of blood flow characteristics is done in three ICA sidewall and three MCA bifurcation aneurysms. Patients 1, 2, and 3 having ICA aneurysms are at the ages of 56, 64, and 39, respectively. Patients 4, 5, and 6 having MCA aneurysms are at the ages of 60, 54, and 29, respectively. For each patient, three simulations were constructed in case of no stent implantation (NSI), 48-wire FDS, and 64-wire FDS implantation. Implanted FDSs have the same EMSA values at the non-implanted position with identical wire thicknesses.

Simulations with no stent implantation are done to investigate the blood flow through the model and obtain the values of the parameters which show if the blood flow is pathological. By using those data, it can be comparable to the FDS implanted models whether the FDS implantation increases the shear levels in the blood flow. Similarly, simulations with 48 and 64-wire FDS implantations are done to compare the effects of different wire numbers for an FDS on the blood flow and if one of them is more preferable with respect to the created shear levels.

Detailed data is shared further in this section in order to have more in-depth knowledge about what is happening in a cycle with increments of 0.01 seconds where one cardiac cycle takes 0.8 seconds [110–112]. The maximum shear stress values for each time step through the third heartbeat cycle, the percentage of blood volume exposed to supraphysiological forces compared to the total blood flow, rupture-prone areas on the artery and differences between 48 and 64-wire FDS implantation in blood flow are the issues that are discussed in this part of this thesis.

The DSA images of three ICA and three MCA patients are used in the study. The results gathered from all the simulations are taken in the same position and alignment with the DSA images for convenience and validation purposes. Dynamic viscosity, OSI, and TAWSS contours are taken precisely as the angiography images, whereas shear stress and shear strain rate contours are taken with a slight rotation to get a top view of the neck area with FDS. The chosen blood flow directions in each model are taken so that all of them are in the same axes.

3.1. PARAMETERS AFFECTING VON WILLEBRAND FACTOR

Activation of the von Willebrand factor occurs due to the supraphysiological level of shear stress and shear strain rate in the blood flow. Every FDS modeled and implanted at each patient's neck region of the aneurysms. The implantation of the FDS dramatically increases shear stress and shear strain rate values for every patient, as expected. This activation of vWF increases the possibility of a cerebral hemorrhage, since FDS implantation causes acquired type 2a von Willebrand disease [47].

3.1.1. Shear Stress

Shear stress is one of the main parameters that need to be inspected in the blood flow affected by the FDS implantation. The results' legends range from 0 to 10 Pa due to the shear stress threshold being 10 Pa. From Figure 3.1 to Figure 3.3, the results are obtained for shear stress from the simulations with no stent implantation, 48 Wire, and 64 Wire FDS implantations. At each figure, the contours are taken from diastole and peak systole instances at the third cardiac cycle.

In Figure 3.1, it can be seen that the shear stress values for the no stent simulations have values that are not supraphysiological levels. Both patients have sidewall ICA aneurysms with relatively large aneurysms with relatively large artery diameter, and neck area compared to MCA patients. After FDS implantation, even during diastole the shear stress is way above the 10 Pa limit for Patient 1. During peak systole, both patients have quite a larger region of inflow with supraphysiological shear stress values. At first glance, the shear stress values for both patients are higher with 48-wire FDS implantation. The increase in shear stress values is highly significant for both patients.

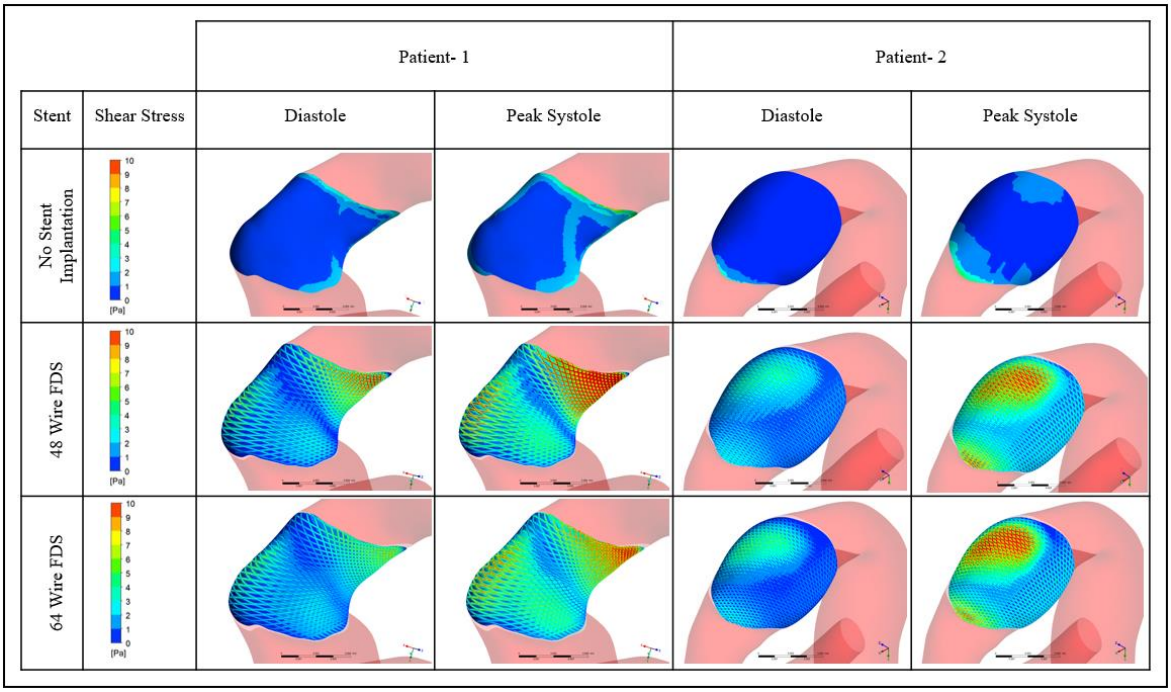

Figure 3.1. Shear stress contours for patients 1 and 2

The simulation results for patient 3, in Figure 3.2, show a high increase in shear stress towards the outer part of the neck region. Compared to the other ICA aneurysms, the supraphysiological shear stress area is widest for the patient 3 Regardless the FDS wire number, the shear stress levels are higher than 10 Pa even during diastole.

The contours representing the shear stress data for patient 4 reveal that supraphysiological levels are not reached before the stent implantation. With the implantation of both FDS, the critical threshold is surpassed at the peak systole instance. Even though the shear stress values are below 10 Pa during diastole, the activation of vWF happens during each peak systole.

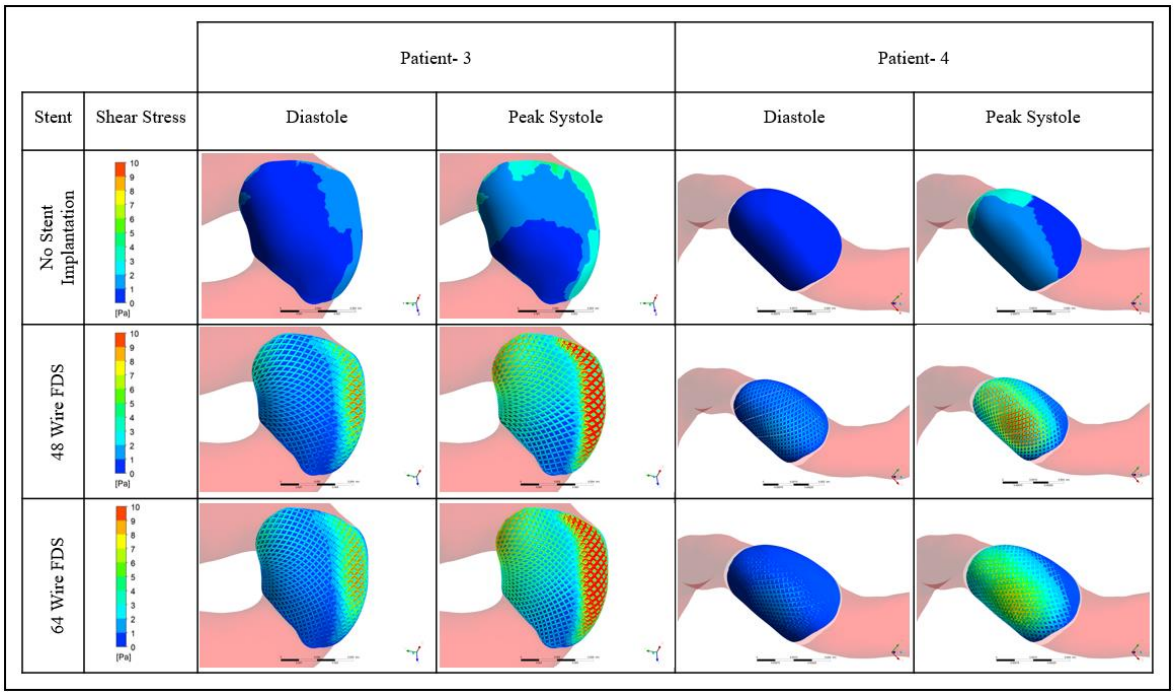

Figure 3.2. Shear stress contours for patients 3 and 4

Shear stress contours of patient 5 shows one of the widest supraphysiological region out of all the results. This is due to the small artery diameter and the higher EMSA value compared to the other two MCA patients. The wider inflow area of this patient also means that the blood flow passing through the neck region increased to supraphysiological levels at a higher volume. This will be investigated further in the following section with a detailed insight into the situation. Despite the fact that shear stress values seem lower than other patients, there is still pathological flow after FDS implantations for patient 6.

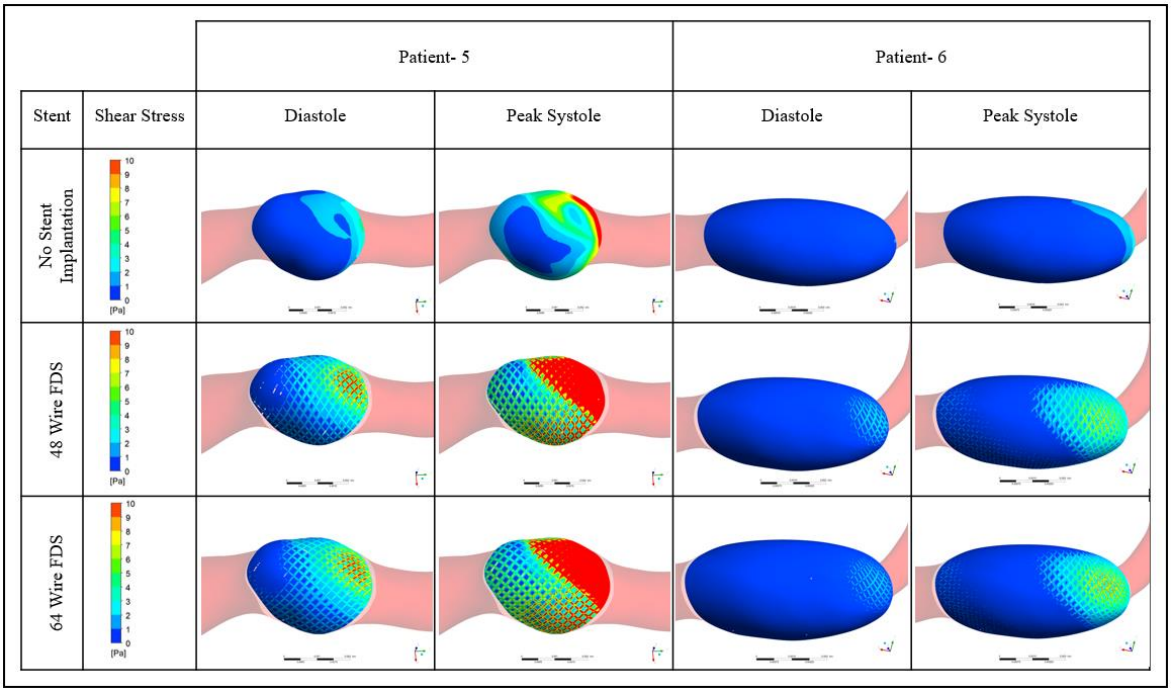

Figure 3.3. Shear stress contours for patients 5 and 6

3.1.2. Shear strain rate

Shear strain rate is the other main parameter to investigate in vWF activation. In the blood flow, shear strain rate values that are greater than 5000 s^{-1} are the signs of a pathological flow [75]. The increase in shear strain rate values is dramatic with the implantation of both FDS types.

Shear strain rate values for each simulation result are inspected in this part of the study. Strain rate values in the blood results in the elongation of the vWF multimers inside the blood. This is crucial for blood flow and vWF multimer activation. Within a pathological flow, the vWF multimers start to elongate, get activated and then get cleaved by ADAMTS-13 enzyme. This long-standing activation leads to von Willebrand disease. Therefore, it is desired not to reach supraphysiological levels in the blood flow. Unfortunately, as shear stress contours showed and shear strain rate contours to be discussed, implantation of an external tool to the human body dramatically alters the hemodynamics, and as in this study it is mentioned, causes the vWD for aneurysms that are considered to be large [47].

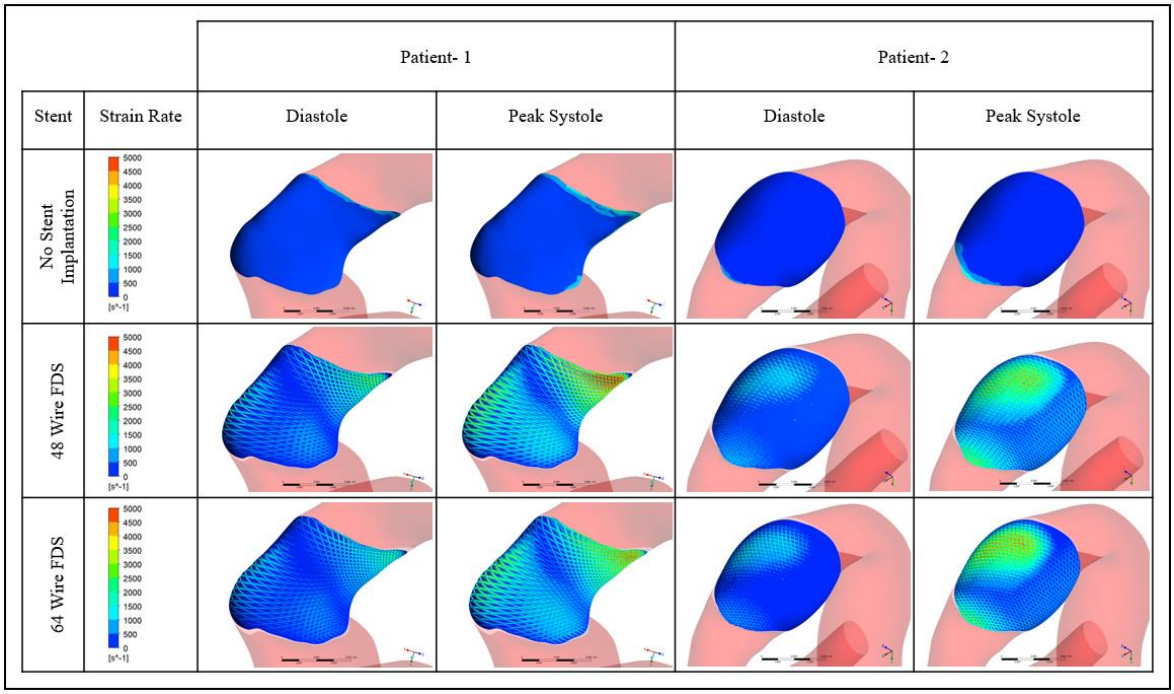

Figure 3.4. Shear strain rate contours for patients 1 and 2

Similar to shear stress contours, the legend for shear strain rate is limited to the supraphysiological level of 5000 s^{-1}. Each location with a higher strain rate value is depicted with the color red. Shear strain rate values for patients 1 and 2 are shown in Figure 3.4. Both patients before the treatments are not showing pathological flow. Indeed, if the aneurysm is left untreated, it will eventually enlarge up to a size that would result in rupture. Therefore, treatment for each patient with an aneurysm is necessary. As mentioned earlier, FDS is one of the most effective and desirable methods to treat aneurysms, making this study even more important to point out why cerebral hemorrhages still occur after successful treatments. Following the FDS implantation, for both patients each FDS affects the blood flow to increase the shear strain levels to a supraphysiological level.

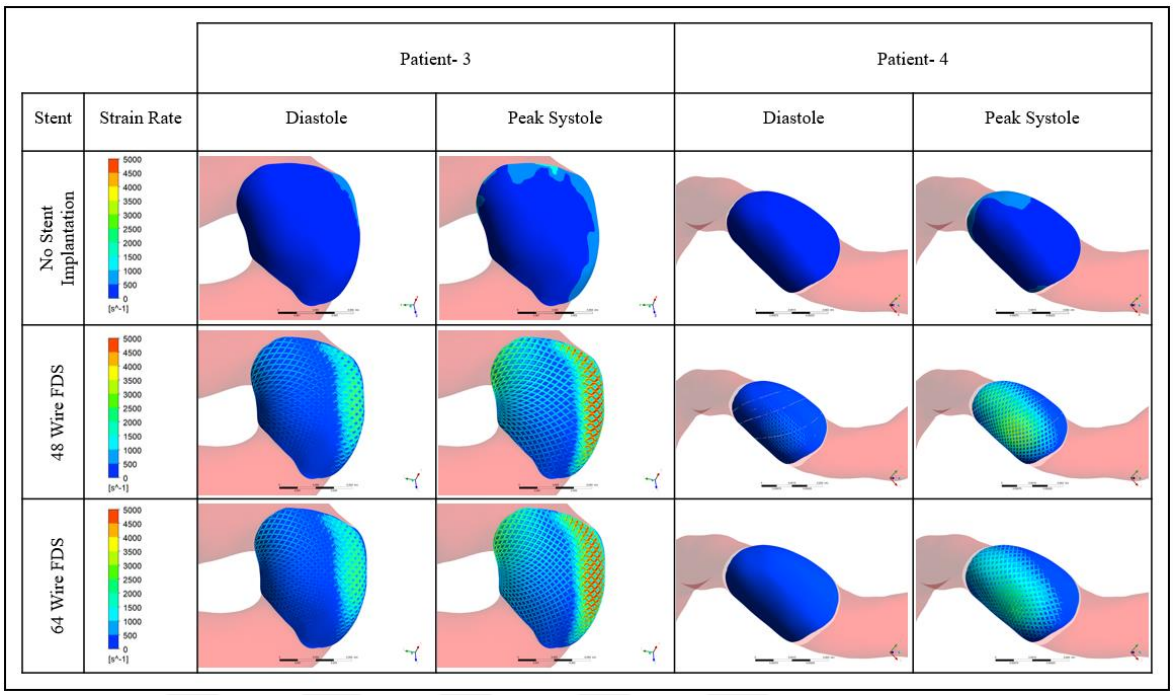

Figure 3.5. Shear strain rate contours for patients 3 and 4

Patient 3 has a non-pathological flow before an FDS implantation. Due to the morphology of the artery having an aneurysm, shear strain rate values are getting higher around the neck of the aneurysm. Nevertheless, these increased regions are well below the threshold value of 5000 s^{-1}, even during peak systole. After the implantations of 48 and 64 wire FDS's, the threshold value is exceeded for both cases, making both flows pathological. Patient 3 has the highest shear strain rate compared to the other two ICA patients. An important factor for this situation is the smaller artery diameter of patient 3. The inflow region during peak systole is quite significant which is occurring due to the aneurysm being located precisely on the bend of the artery.

Patient 4 also has safe shear strain rate values without stent implantation. The implantation of FDS however yield pathological flow. Despite the shear strain rate values being lower than the threshold value during diastole, threshold exceeding values exist for peak systole instances. This means that at every heartbeat cycle activation of vWF may occur.

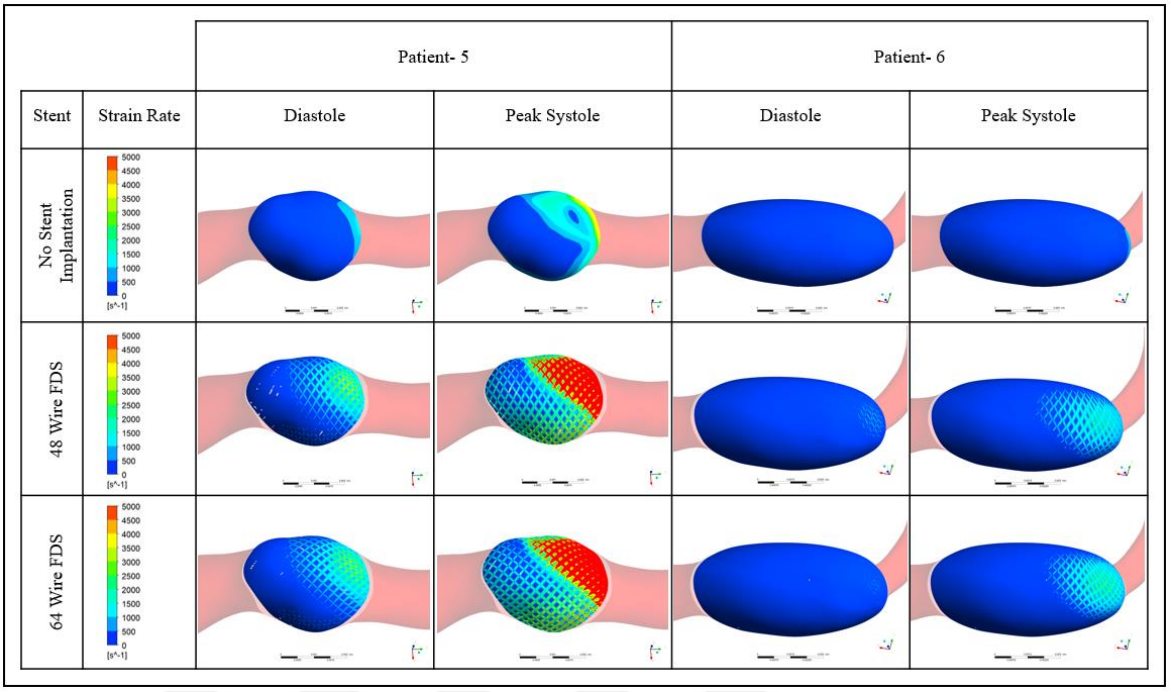

Figure 3.6. Shear strain rate contours for patients 5 and 6

The remaining two MCA patient results are shown in Figure 3.6. Patient 5 already has shear strain rate values above the threshold value of 5000 s^{-1}. This shows the importance of the influence of artery and aneurysm morphology on blood flow. Having the smallest artery diameter and small neck diameter, the shear strain rates for patient 5 are much greater than the activation value for both diastole and peak systole instances with the implantations of both FDS types. The inflow region through the FDS is prominent for this patient.

Patient 6 has the least problematic flow compared to the other patients. The simulation results obtained from the no-stent model shows that even at peak systole shear strain rate values are almost in normal limit. Nonetheless, pathological flow occurs after the FDS implantations. Compared to the rest of the patients, this patient has a lot smaller total area affected by high shear strain rates, but still, the threshold rate is reached in a time range of before and after the instance of peak systole.

3.1.3. Shear strain rate contours vertical to the FDS

Investigating shear strain rate at a vertical plane which is perpendicular to the FDS is constructed to observe the blood flow before and after FDS. For each patient, the peak systole instance is taken. With this investigation, the activation of vWF depending on shear strain rate can be inspected. The difference of this approach is to understand and show that indeed only near the FDS domain the vWF is getting activated by having supraphysiological shear strain rate values.

ICA patients' shear strain rate contours are shown in Figure 3.7, which contains the contours from NSI, 48, and 64 wire FDS models. Before this approach, it was already proven under the Shear strain rate section, and now it is clear that the shear strain rate is above 5000 s^{-1} near FDS wires. Seeing the artery and aneurysm domains blue in these contours state that even during peak systole, the only supraphysiologic (vWF activating) region is near FDS wires.

MCA patients have a significant increase in shear strain rate in the vicinity of the FDS wires, just like the ICA patients. Interestingly, among all six patients, patient 5 has the highest shear strain rate values already existing in the neck region of the aneurysm before any FDS treatment is applied. Therefore, as expected it has the most striking shear strain rates existing in the artery near FDS wires.

The thickness of the increased shear strain rate region is understood to be related to the high shear values such as in the cases of patients 3 and 5 whose shear stress and shear strain rate values are two of the highest in this study. This also can lead to more blood volume exposing supraphysiologic forces and thus more vWF multimer activation. It is important to not mix this approach's intention by investigating vertical contours with diminishing the striking reality of supraphysiological shear levels occurring. The main goal of this section is to show the direct effect of FDS wires' existence in the artery leading to supraphysiological forces being exerted on blood flow and presenting another perspective on vWF activation.

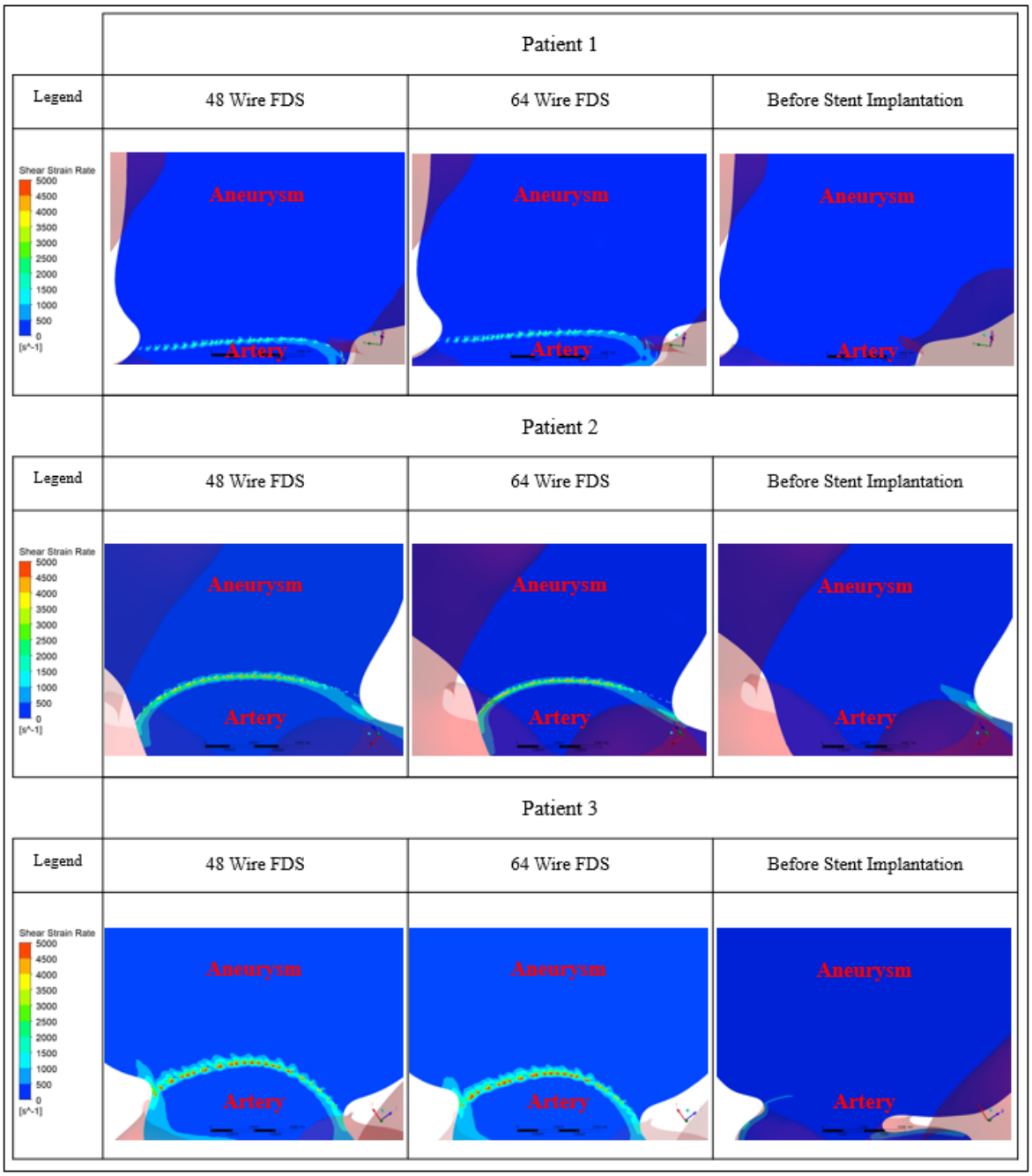

Figure 3.7. Shear strain rate for ICA patients plotted on vertical contours perpendicular to the artery

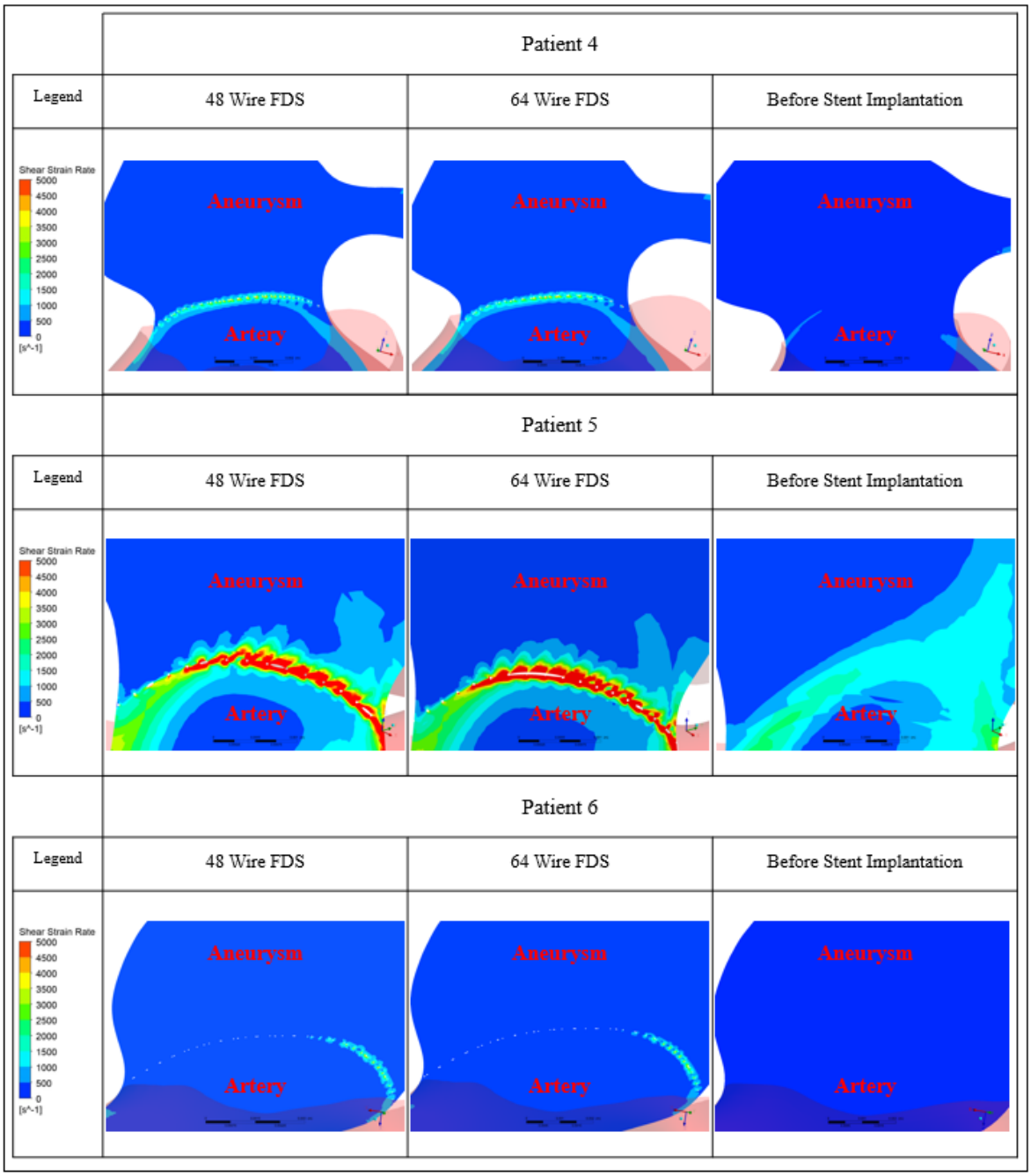

Figure 3.8. Shear strain rate for MCA patients plotted on vertical contours perpendicular to the artery

3.1.4. Maximum values affecting the blood flow

Shear stress and shear strain rate values vary highly for each patient. These differences can occur due to several factors, such as artery and aneurysm morphologies, patient age, and the features of the implanted FDS. Therefore, investigating the maximum values for each patient in each circumstance gives a thorough insight compared to the contour figures.

Table 3.1. Maximum shear stress values for each patient

Patient #	48 Wire FDS (Pa)	64 Wire FDS (Pa)	No Stent Implantation (Pa)	48 vs. NSI (%)	64 vs. NSI (%)
Patient 1	88.62	87.92	21.67	309.0%	305.8%
Patient 2	52.66	30.35	11.93	341.3%	154.3%
Patient 3	143.7	124.9	19.90	622.1%	528.1%
Patient 4	36.86	32.57	6.532	464.3%	398.6%
Patient 5	349.7	340.7	39.27	790.5%	767.6%
Patient 6	39.18	35.68	2.673	1366%	1235%

Maximum shear stress values are listed for each model with and without FDS implantation in Table 3.1. The patients with 48-wire FDS implanted models have higher shear stress values compared to 64-wire FDS implanted models. The impact of FDS implantation on the patient is indisputable. The values show all results of the eighteen simulations, which are for three per patient. Shear stress values are compared between NSI model and FDS implanted models. That comparison clearly points out the immense increase in exerted shear to the blood and therefore causes vWF activation. It is important to observe that the supraphysiological forces are reached for blood flow with each FDS implanted model.

Table 3.2. Maximum shear strain rate values for each patient

Patient #	48 Wire FDS (s^{-1})	64 Wire FDS (s^{-1})	No Stent Implantation (s^{-1})	48 vs. NSI (%)	64 vs. NSI (%)
Patient 1	15359	14359	2673.7	474.5%	437.1%
Patient 2	9197.9	8616.9	3147.2	192.3%	173.8%
Patient 3	21516	19716.7	2403.9	795.0%	720.2%
Patient 4	5925.8	5441.6	1583.7	274.2%	243.6%
Patient 5	57259	51335	5437.3	953.1%	844.1%
Patient 6	11197	9797.9	283.75	3847%	3353%

Similarly, to the maximum shear stress table, maximum shear strain rate values are shown in Table 3.2 for FDS implanted models and no stent models for each patient. The impact of FDS implantation is also critical in shear strain rate values. This is clearly shown with the comparison columns showing the percent increases for each patient with each wired FDS model. The values obtained from 48-wire FDS models for each patient are higher than those from 64-wire FDS models. This result shows that shear stress and shear strain rate values are higher for each patient with 48-wire FDS implanted models. This can be due to the resulting effective metal surface area (EMSA) values of the implanted stents.

Observing similarity in supraphysiological values for both shear stress and shear strain rate can be seen as an expected result. However, shear stress and shear strain rate parameters are proportional to each other for Newtonian fluids in laminar flow. For the case of non-Newtonian fluids, which is the defined fluid for all the fluids in this study, the viscosity is being altered in time leads to a change in velocity and therefore resulting in a change in shear stress [113,114]. Therefore, it is crucial to investigate both shear stress and shear strain rate values for each patient with every simulation model.

3.1.5. Average values affecting the blood flow in a cycle

In this section, the averages of the maximum values for the whole cardiac cycle and the comparisons between FDSs and before FDS treatment models are shown. Averaged value calculations contain all 80-time steps (i.e., total simulation time of 2.4 seconds divided by

the time step size of 0.005 s gives 480-time steps. Half of these time steps are saved, therefore 80 time steps are available for each cardiac cycle) for all eighteen simulations.

Table 3.3. Average shear stress values

Patient #	48 Wire FDS (Pa)	64 Wire FDS (Pa)	No Stent Implantation (Pa)	48 vs. NSI (%)	64 vs. NSI (%)
Patient 1	48.21	47.67	13.19	261.4%	265.5%
Patient 2	22.71	12.06	7.253	213.1%	66.3%
Patient 3	70.79	65.46	8.026	715.6%	782.0%
Patient 4	11.22	9.638	2.253	327.8%	398.2%
Patient 5	108.9	102.8	24.18	325.3%	350.4%
Patient 6	10.96	7.457	1.268	488.3%	764.4%

Similar to the maximum value tables' structures, the average of maximum shear stress and average of maximum shear strain rates are calculated and presented in Table 3.3, and Table 3.4, respectively. Patients 4 and 6 with 64-wire FDS treatment have average values lower than 10 Pa.

Table 3.4. Average shear strain rate values

Patient #	48 Wire FDS (s^{-1})	64 Wire FDS (s^{-1})	No Stent Implantation (s^{-1})	48 vs. NSI (%)	64 vs. NSI (%)
Patient 1	8694.05	7611.20	1673.95	419.4%	354.7%
Patient 2	3641.70	3361.50	1916.80	89.99%	75.37%
Patient 3	10699.9	10330.4	1148.00	832.0%	799.9%
Patient 4	1753.88	1413.41	543.008	223.0%	160.3%
Patient 5	18388.6	16747.6	2514.22	631.4%	566.1%
Patient 6	5641.70	4241.70	140.160	3925%	2926%

3.2. INVESTIGATION OF SUPRAPHYSIOLOGICAL FORCES IN A CYCLE

The importance of investigating the flow in one full cycle is paramount to grasp the insight of incidents occurring for the blood flow. The behaviors of shear stress and shear strain rate are inspected in this section for each patient with each fluid flow model. Investigating whether the shear values increase and decrease linearly is important for obtaining maximum shear values. The main reason to investigate this is for understanding if the shear stress and shear strain rate values are exceeding the threshold only in the small vicinity of the peak systole instance or to find out that the threshold is being exceeded for more instances. More time spent under pathological flow may increase the activation of more vWF multimers, which may lead to a worse condition eventually [115–117].

All data retrieved through the simulations are taken from the third cardiac cycle, which lasts from 1.6 seconds to 2.4 seconds. The graphs are constructed in a way to be self-explanatory in comparing the results from 48-wire FDS, 64-wire FDS, and no stent implanted models with a straight line indicating the shear stress and shear strain rate thresholds in their respective graphs. All values were obtained at the aneurysm neck region through the volume domain of the stent part in the whole model. Therefore, the maximum value taken for each time step is the highest value in the three-dimensional domain. Investigating values for each time step is a more in-depth approach considering average values being not viable enough to help one to grasp the idea that the blood flow is being exerted to continuous supraphysiological shear stresses and shear strains.

3.2.1. Shear stress values

Investigating maximum shear stress values through a full cardiac cycle shows the exact behavior of fluctuating shear stresses. It is crucial to obtain supraphysiological shear stress values which are above 10 Pa. Next to that it should be taken into consideration the high and low shear stress levels alternating from physiological to supraphysiological.

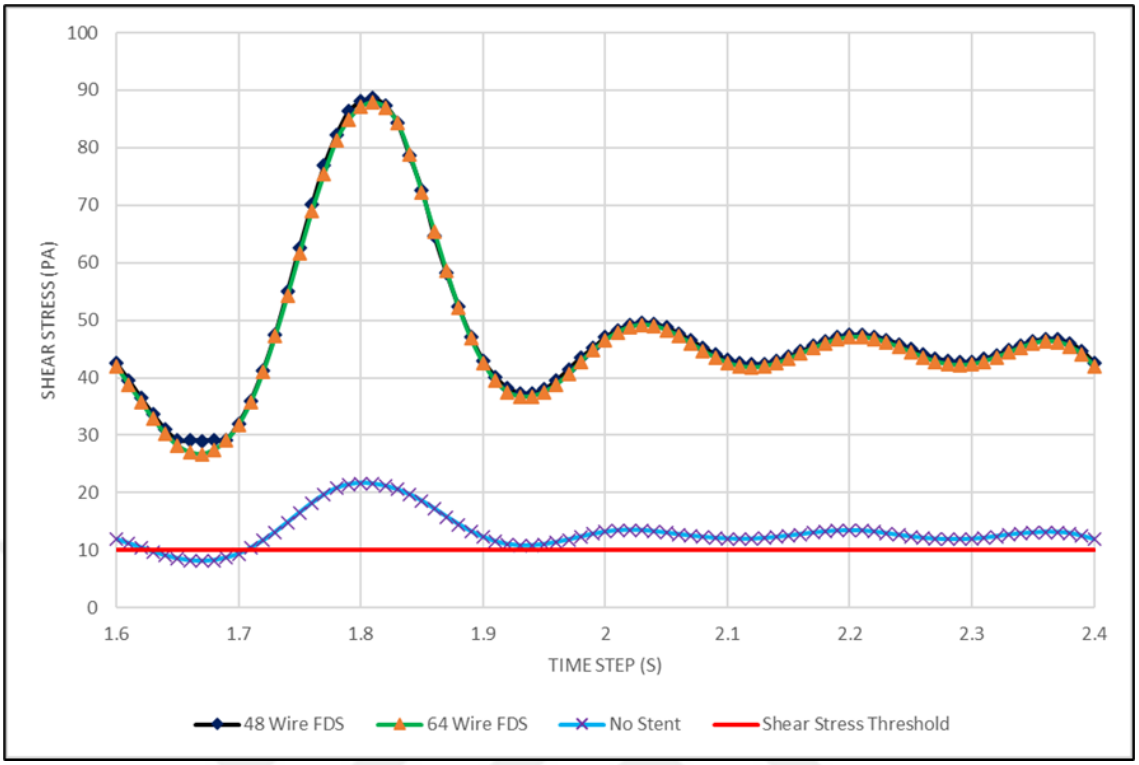

Figure 3.9. Shear stress values for patient 1 during the third cycle

In Figure 3.9 the graph of shear stress values for patient 1 with each model result is shown. The model without any implanted stent is already exceeding the 10 Pa limit during much of the cycle. The maximum shear stresses being above the threshold value points out the vWF activation without an FDS implantation. These results show the maximum shear stresses for each time step which means there are also below threshold value shear stresses available in the domain. This is already available and explained in the contour figures shown earlier. Important aspect at this case is that even though the threshold seems to be exceeded before FDS implantation, with the post FDS surgery shear stress values are increasing in value and the region of supraphysiological forces acting on blood flow is getting enlarged. This causes more multimers to be activated which makes the patient more prone to vWD [118,119].

Results of patient 1 show a dramatic increase with both FDS implantation. The FDS implanted models have pathological flow from the beginning of the cardiac cycle until the end of it. This proves that this patient has a continuous supraphysiological level of shear stress values the whole time.

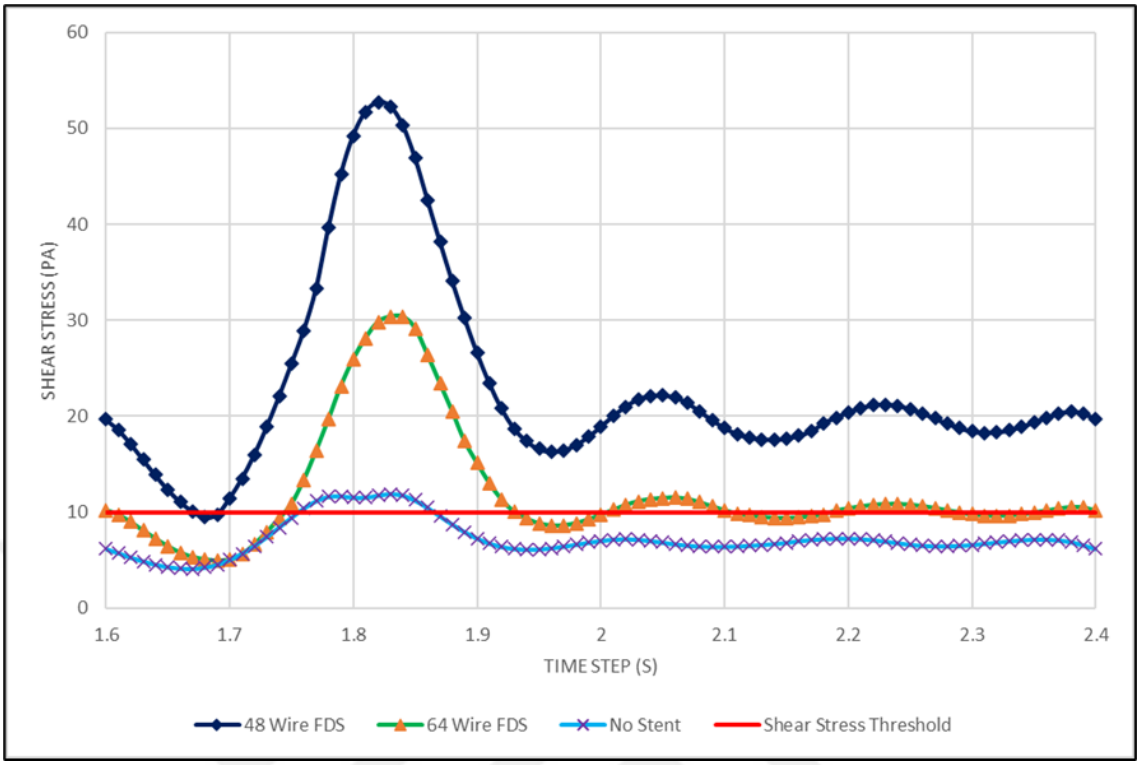

Figure 3.10. Shear stress values for patient 2 during the third cycle

Shear stress values for patient 2 reflect the effect of FDS implantation in turning the blood flow into a pathological one. Throughout the cardiac cycle, shear stress values remained lower than 10 Pa except just before and after peak systole instances. The fluid domain with 48-wire FDS shows five times higher values than the threshold level. This domain also has shear stress values higher than 10 Pa throughout the cycle. The situation is different for 64-wire FDS implanted model, where pathological flow exists for almost 20 percent of the cardiac cycle. This also shows that the wire selection in FDS implanting can have a dramatic role where it can lead to supraphysiological shear stress values.

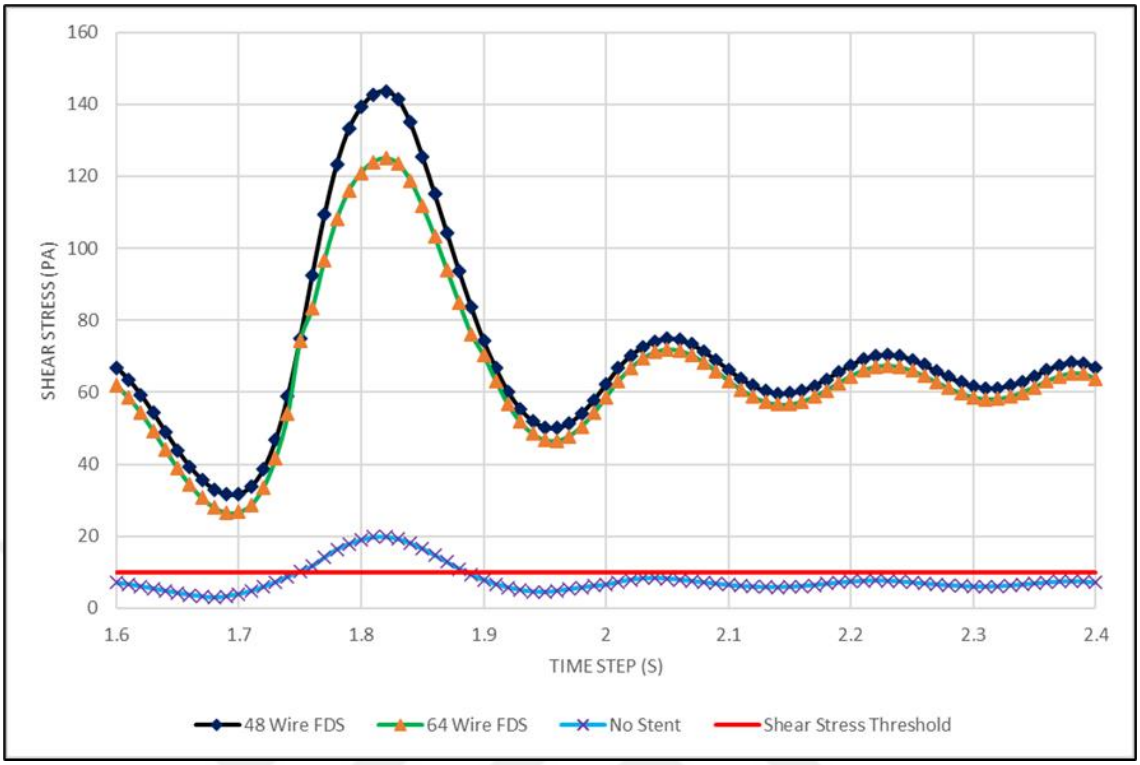

Figure 3.11. Shear stress values for patient 3 during the third cycle

Patient 3 has the highest maximum shear stress values compared to the other two ICA patients throughout the whole cardiac cycle. The artery without an implanted FDS for patient 3 shows a similar behavior as patient 2's model without an implanted FDS. However, unlike patient 2, both 48-wire and 64-wire FDS implanted models have shear stress values that are above 10 Pa limit during the whole cycle. The difference in shear stress values in different FDS models for patient 3 is greater than patient 1 and less than patient 2. The difference is highest during peak systole and least through diastole.

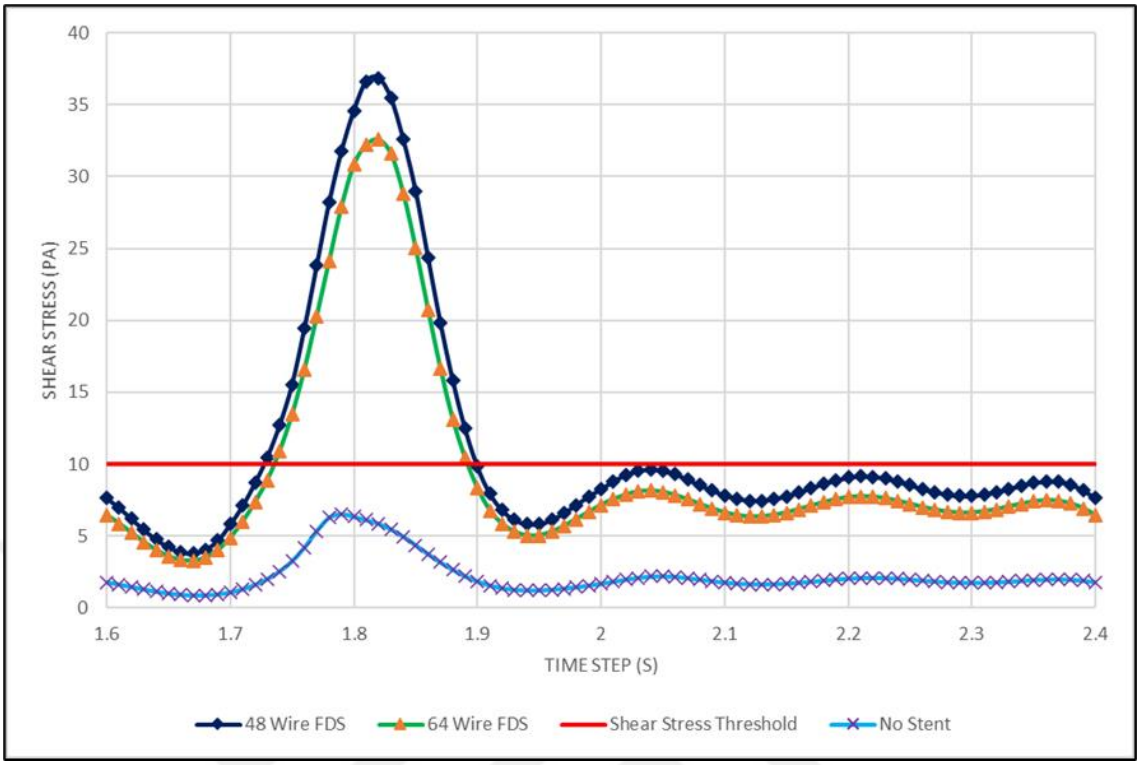

Figure 3.12. Shear stress values for patient 4 during the third cycle

The blood flow for patient 4 is not pathological before an FDS implantation. The maximum shear stress values are almost half the threshold value of 10 Pa. Therefore, this proves that vWF activation in the blood did not exist before FDS implantation. Post FDS implantation results for both 48 and 64 wire stents prove the increase in shear stress values to a point where the threshold value is exceeded and conclusively, vWF multimers getting activated. Even though patient 4 has the lowest maximum shear stress values after FDS implantations, the level of increase and resulting shear stresses are well-above 10 Pa for a long duration before and after peak systole.

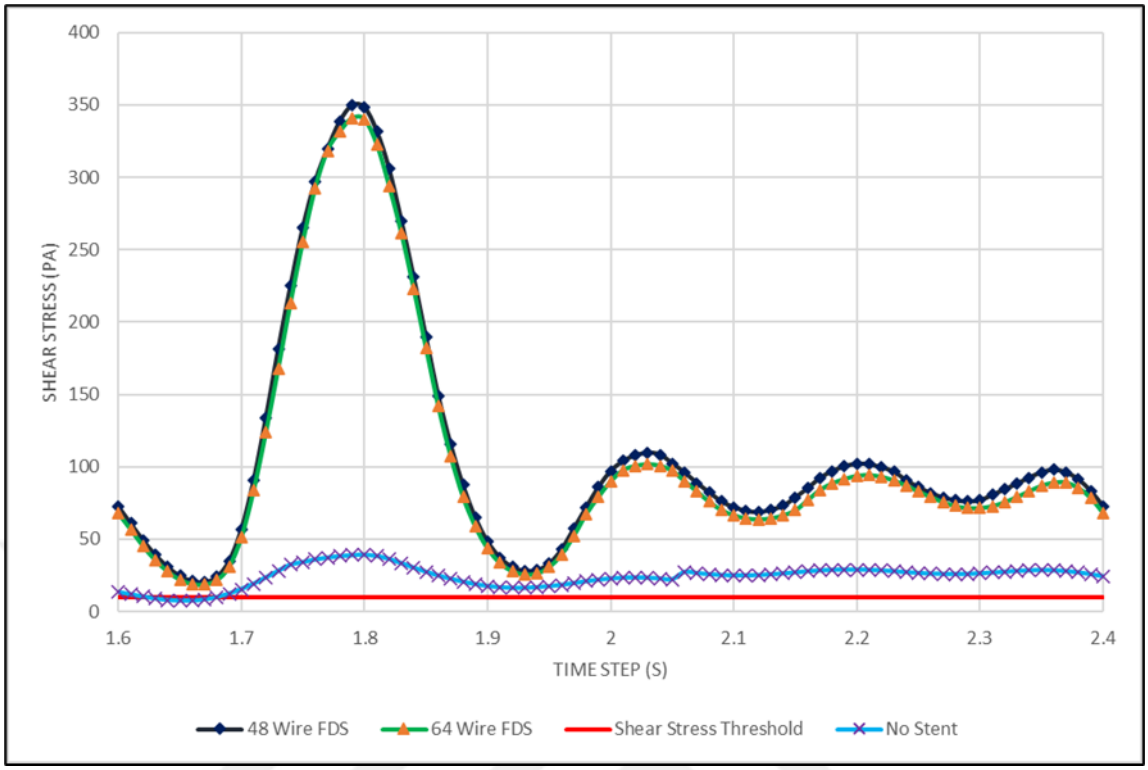

Figure 3.13. Shear stress values for patient 5 during the third cycle

The results of patient 5 presented in Figure 3.13, show increase in shear stresses strikingly. Having above threshold shear stress values before treatment, patient 5 gets exposed to a great amount of shear stress values post-FDS treatment with both 48 and 64 wired ones. The margins of systolic maximum shear stresses between FDS and after FDS implantation are the biggest compared to every other patient result in this study. It is important to point out the fact that the activation of vWF multimers starts at 10 Pa, and for that very multimer because the activation has already begun, it does not make a huge difference to have such a value of around 350 Pa. On the other hand, having such high shear stress existing on a large amount of region as seen on Figure 3.3 causes a larger amount of vWF activation.

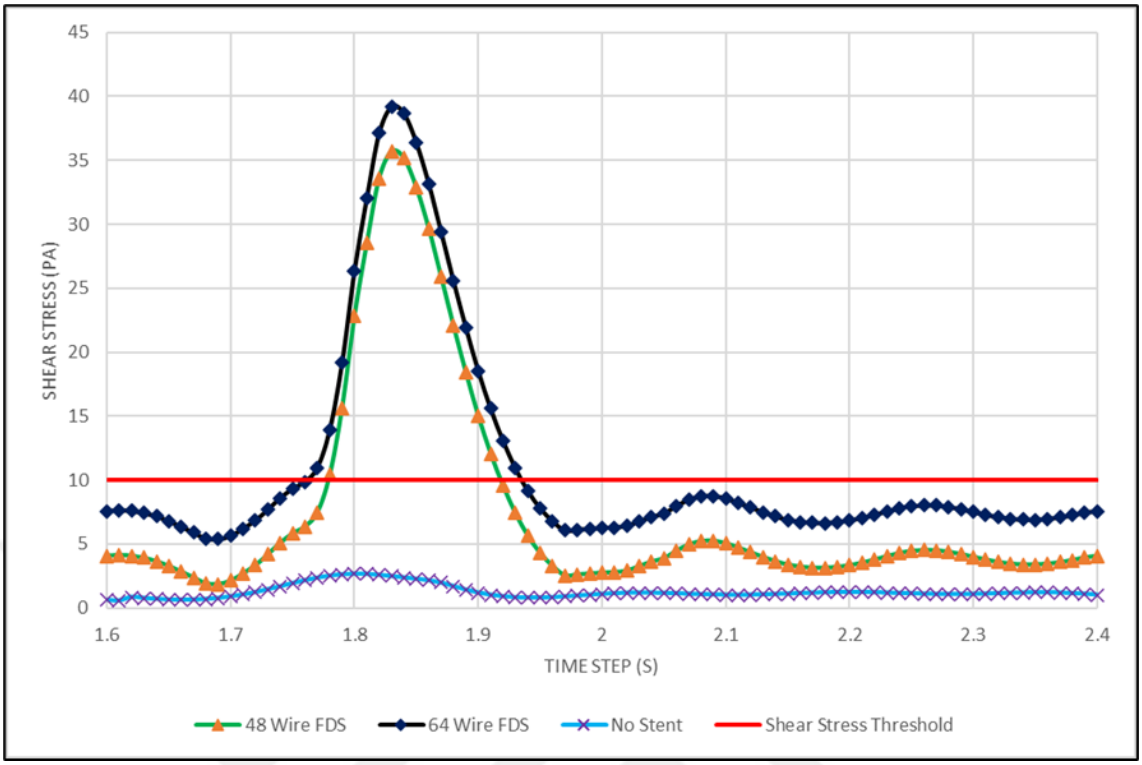

Figure 3.14. Shear stress values for patient 6 during the third cycle

Patient 6 has healthy blood flow before FDS implantation. During peak systole, the maximum shear stress value reaches 2.67 Pa, which is much less than the threshold value and as seen in Figure 3.14, during the full cycle, shear stress values show a stable behavior. Implantations of both FDSs change the healthy blood flow into a pathological one. Supraphysiological shear stresses are confirmed for 20 percent of the cardiac cycle. Activation of vWF multimers is evident.

3.2.2. Shear strain rate values

Shear strain values throughout the third cardiac cycle for all six patients and eighteen simulation models are represented in this section. Shear strain rate is the other parameter with shear stress where both can indicate the activation of vWF multimers and therefore leading to vWD. By investigating shear strain rate values, it can be understood better that shear stress and shear strain rate values are not behaving related with each other, and one patient can have supraphysiological shear stress value at a time step and at the very time step have a healthy shear strain rate value.

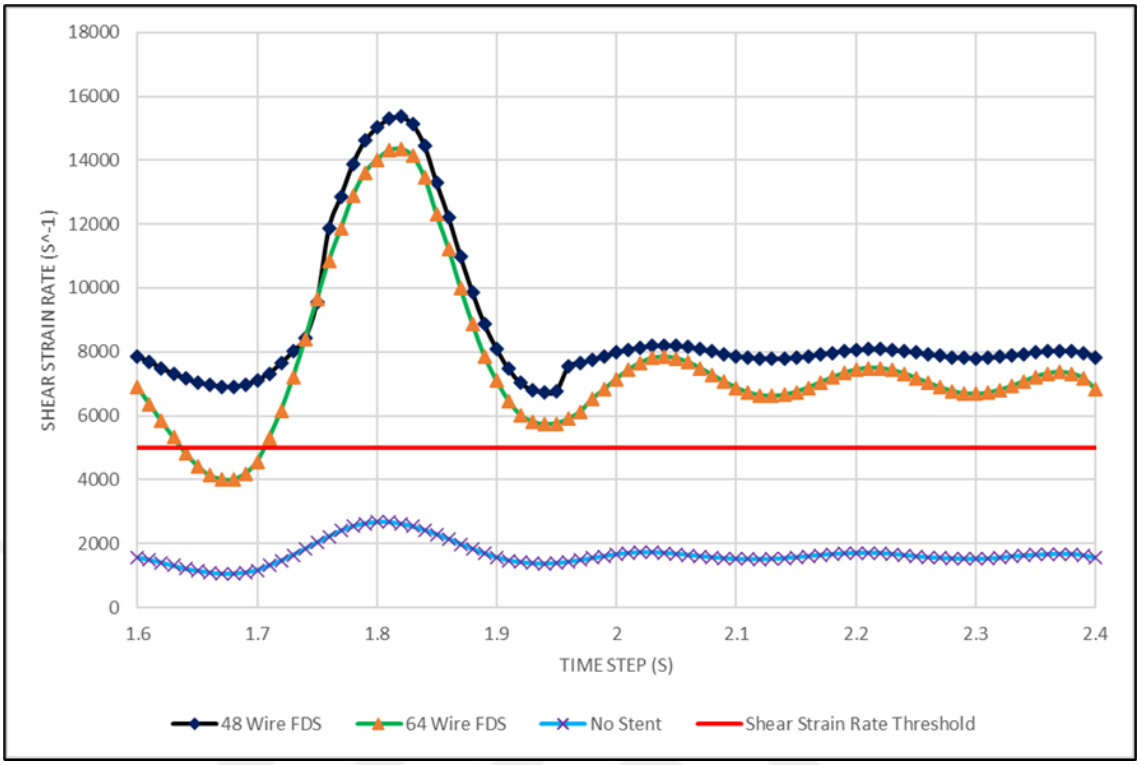

Figure 3.15. Shear strain rate values for patient 1 during the third cycle

Before FDS treatment, patient 1 had no vWF activation due to shear strain rate. For each time step within the cardiac cycle, shear strain rate values are well below the threshold value of 5000 s^{-1} as presented in Figure 3.15. Treatment done with 48-wire FDS yields supraphysiological shear strain rate values during the cardiac cycle. Activation of vWF is positive with this FDS. Post 64-wire FDS treatment, shear strain rate values are lower compared to 48-wire FDS but higher than the 5000 s^{-1} limit. Converting the non-supraphysiological shear strain rate values to shear strain rate values, both FDS implantations cause a pathological blood flow for the patient.

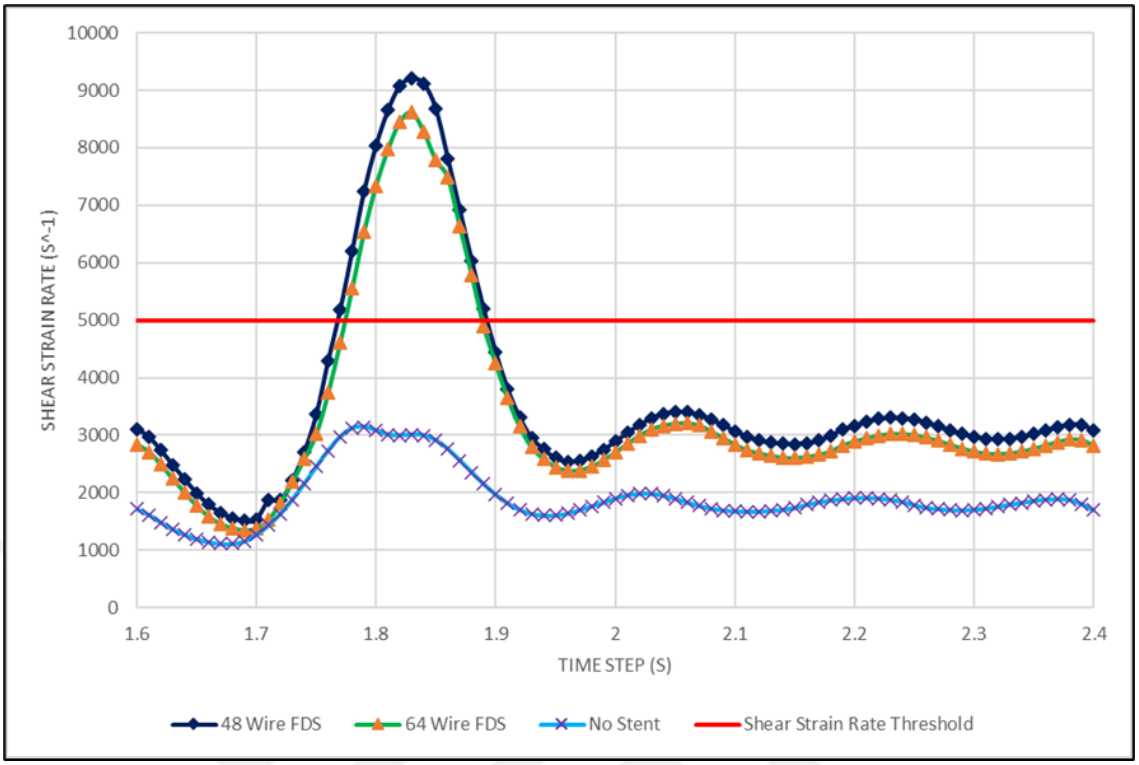

Figure 3.16. Shear strain rate values for patient 2 during the third cycle

Healthy blood flow exists throughout the cardiac cycle for patient 2 before FDS implantation. Post FDS treatment multiplies the shear strain rate values during systole by more than three times. A striking difference between shear strain rate and shear stress values post 48 wire FDS implantation exists. As presented in Figure 3.10, shear stress values are above the critical value of 10 Pa for every time step in the cycle where shear strain rate values exceed the critical value of 5000 s^{-1} only during systole instances, as shown in Figure 3.16. This shows two parameters being unrelated with each other when it comes to reaching supraphysiological levels and conclusively activating vWF. For this patient, vWF activation occurs also due to shear strain rate during systole. However, shear strain rate values go below threshold value during diastole, unlike shear stress values.

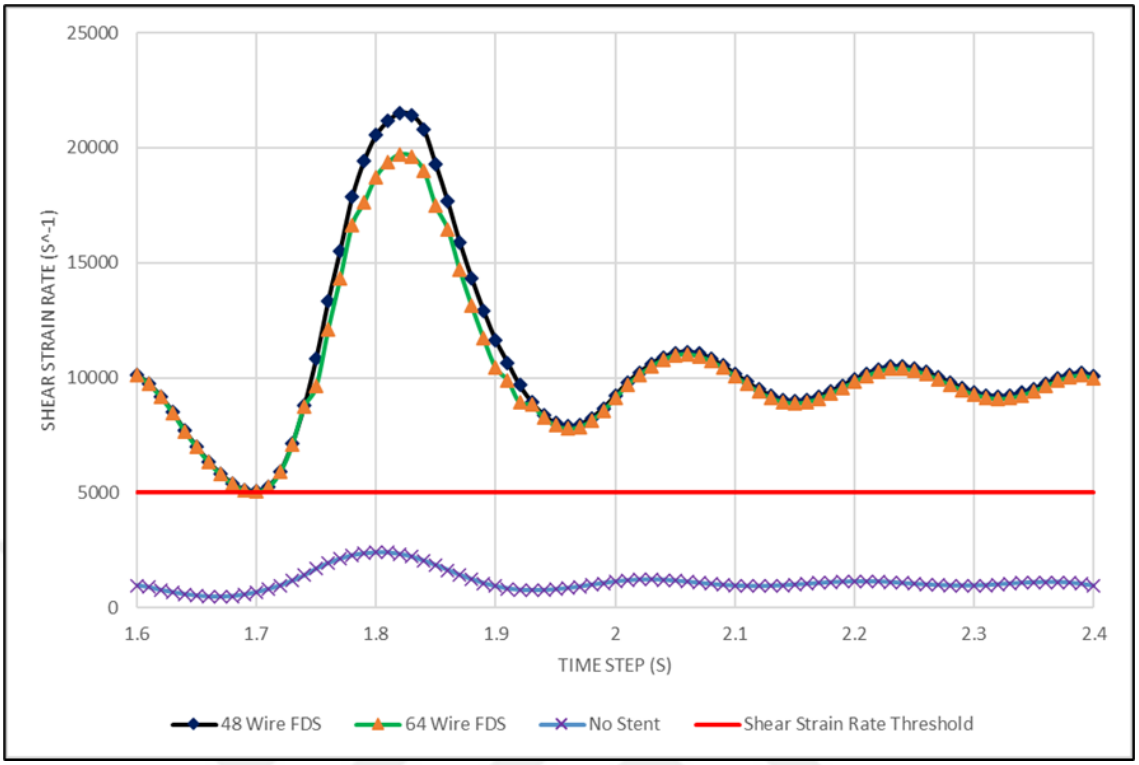

Figure 3.17. Shear strain rate values for patient 3 during the third cycle

The values shown in Figure 3.17 are not exceeding the threshold for the model of no stent. Blood flow before FDS treatment is not pathological based solely on shear strain rate. However, activation of vWF is done by shear stress values during systole, shown in Figure 3.11. Post-FDS treatments with both FDS, blood flow becomes pathological with supraphysiological values existing along the cardiac cycle.

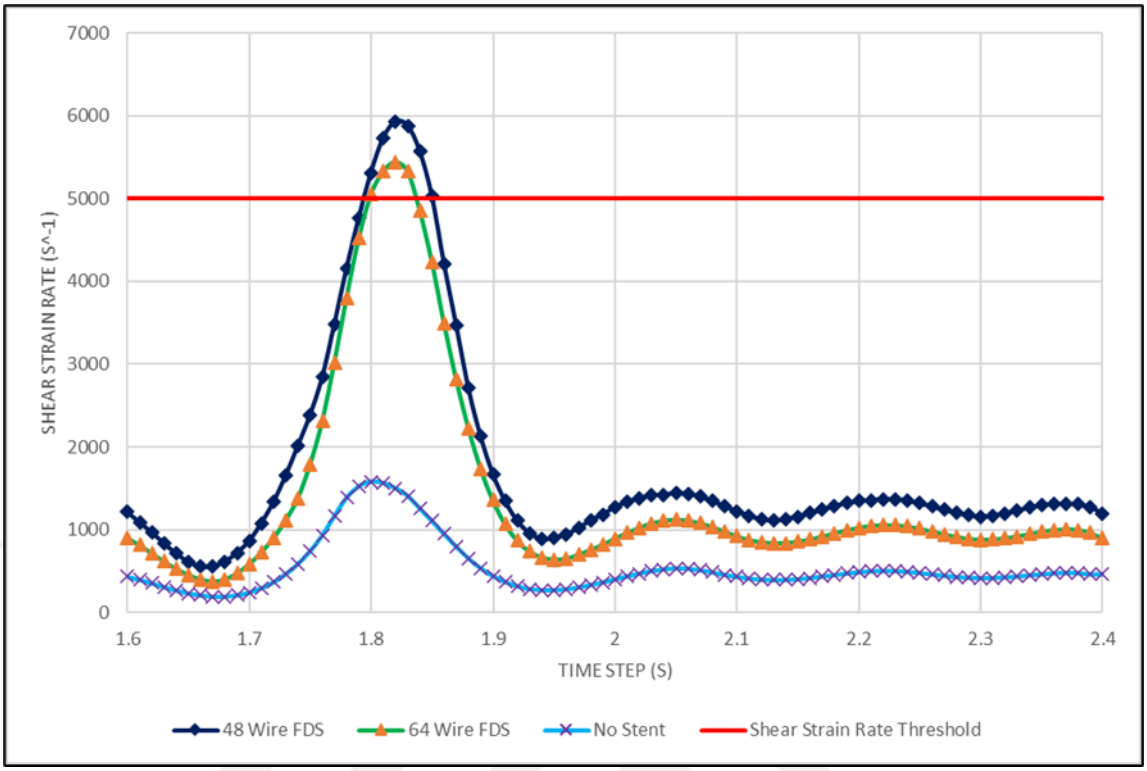

Figure 3.18. Shear strain rate values for patient 4 during the third cycle

Before FDS treatment, patient 4 has shear strain rate values varying from 5 to 15 percent of the threshold value, according to shear strain rate and shear stress, which are presented with Figure 3.18 and Figure 3.12 respectively. There is no activation of vWF with the no stent implanted model for patient 4. Post FDS treatment, for both FDS types, shear strain rate values are exceeding 5000 s^{-1}. This happens only in the time frame of just before and after peak systole. Implantation of 48-wire FDS yields higher values of shear strain rate compared to the 64-wire FDS. The supraphysiological shear strain rate values prove the activation of vWF multimers. This patient is also the first patient to have both shear stress and shear strain rate values lower than threshold values of 10 Pa and 5000 s^{-1} for the model before the implantation of any FDS.

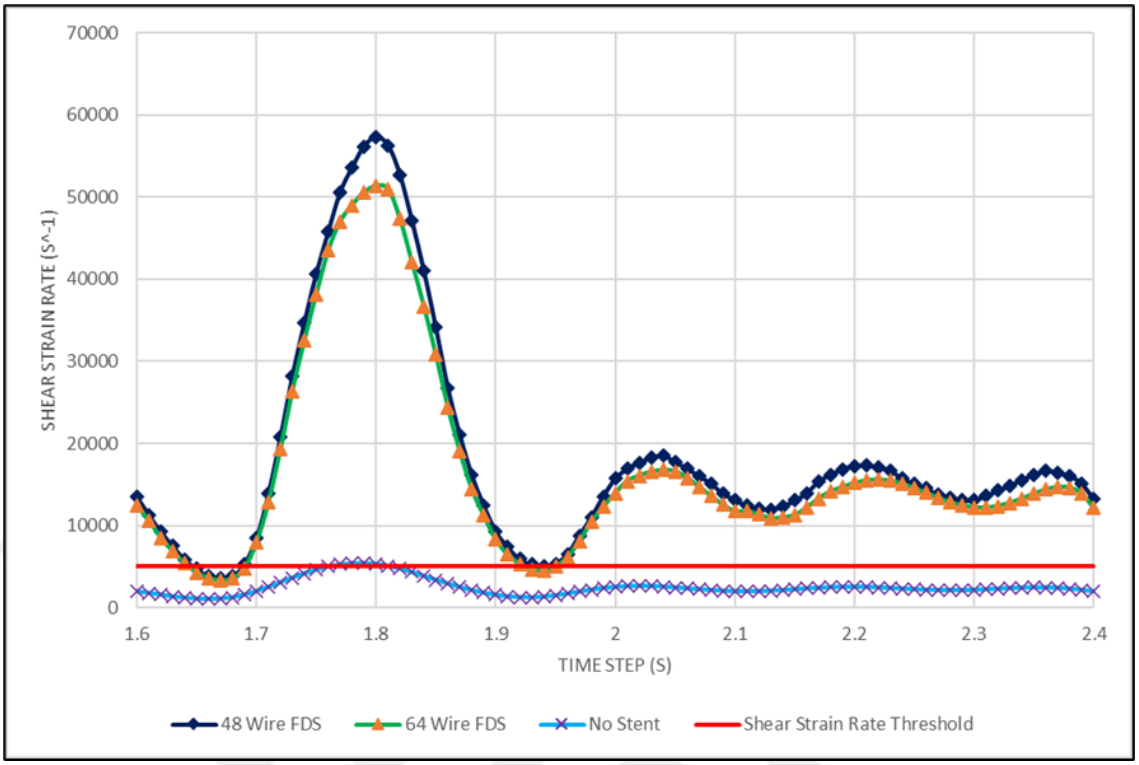

Figure 3.19. Shear strain rate values for patient 5 during the third cycle

Patient 5 has the highest maximum shear strain rate values compared to all the other patients. Activation of vWF multimers may be possible during peak systole instance for the before treatment model. However, there is no doubt left with the implantations of both FDS models. Similar to the rest of the patients, higher maximum shear strain rate values are reached with the addition of 48 wire FDS to the artery. After both FDS treatments, almost whole the cardiac cycle, the shear strain rate values are supraphysiological and pathological flow is existent, activating the vWF multimers. The dramatic increase in both shear stress and shear strain rate with the treatments done by both FDS models for patient 5 can be related to the lower artery diameter compared to all other patients.

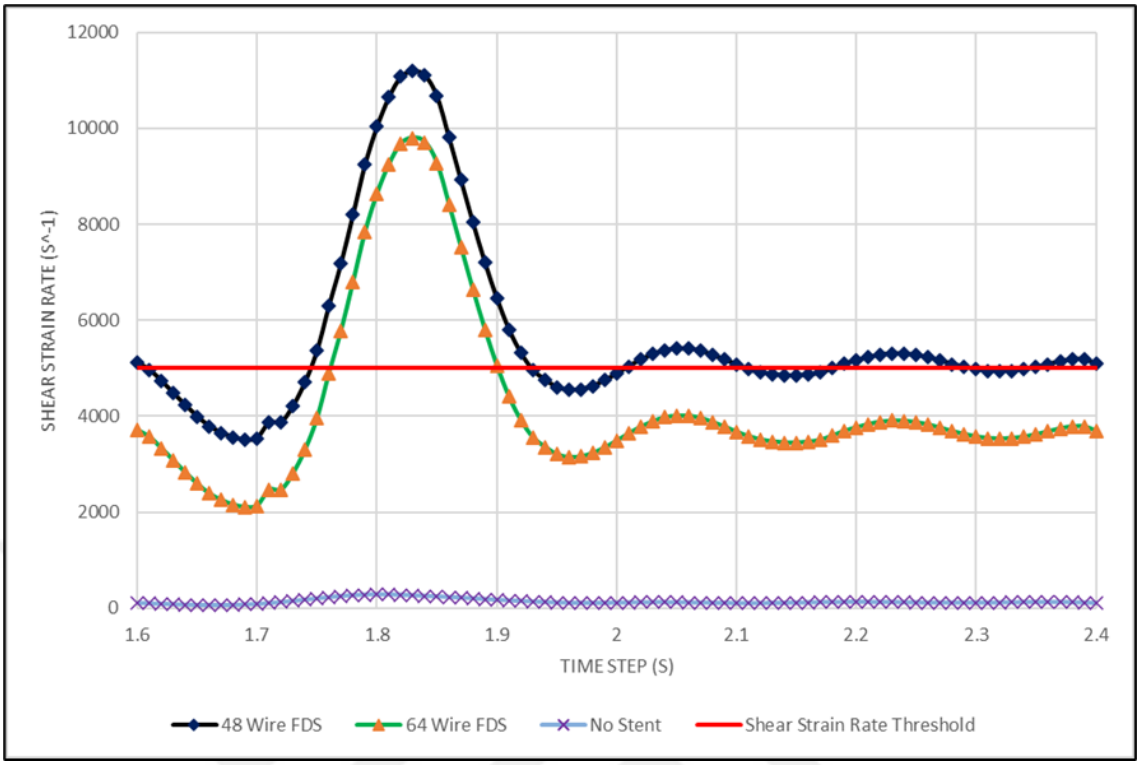

Figure 3.20. Shear strain rate values for patient 6 during the third cycle

Patient 6 has the least fluctuating shear strain rate in comparison with all the other patients before treatment status. Even though an almost healthy flow exists for this patient, shear stress is well-under threshold like shear strain rate; with implantations of 48 and 64 wire FDSs pathological flow starts to exist. Supraphysiological levels of shear strain rate are reached for most of the cardiac cycle, where 48-wire FDS has greater maximum values than 64-wire FDS. From an almost non-responsive shear strain rate value along the cardiac cycle to a well above threshold value proves the activation of vWF multimers for this patient.

3.3. VOLUME PROPORTION OF SUPRAPHYSIOLOGIC FORCES IN FDS

Investigating shear stress values and shear strain rates proved the activation of vWF for every patient after having an FDS implantation. All these cases, even the ones where pathological flow is not reached during peak systole instance, have transformed to possess pathological flow with FDS treatment. A highly important investigation is carried out in this section that focuses on the volume of the blood which has supraphysiological forces to lead to above threshold shear stress and shear strain rate values.

In previous sections, it was proven that the above threshold shear values are reached with FDS implantations. In this section, the scope is about how big of an impact FDS implantation has on blood flow. This impact is investigated by calculating the amount of blood volume with 10 Pa or higher shear stress values in the aneurysm neck region where the FDS domain exists. The calculations are done for the three-dimensional body of FDS, and conclusively a ratio of aggravated blood volume to the total volume available in the neck region is obtained for every model in this study at each time step for the whole range of the cardiac cycle. The volume of each implanted FDS in the neck region is calculated separately for every patient and every model to obtain the aforementioned comparison in percentage. These results point out how much of the blood volume entering through and leaving from FDSs has shear stress values which lead to a pathological flow.

The importance of calculating the percentage is to have a dimensionless value. Not only the neck region FDS volumes are different for each model, but also ICA and MCA have anatomically large size differences. Therefore, calculations are made for each time step, the blood volume which got induced by supraphysiological forces are obtained, and the percentage of those volumes to total blood volumes are found. Having zero percentage shows that there is no amount of supraphysiological forces existing within blood for that instance in the cardiac cycle.

Calculating the blood volume which has supraphysiological shear forces being exerted provides another aspect of understanding the importance of the activated amount of vWF multimers. It is logical to expect a patient to have high blood volume with supraphysiological forces existing if the shear stress values are also accordingly high. To have a slight truth, this comment is not entirely correct. This is proved in this section where results point to the different tendency of aggravated blood volume percentages, compared to higher shear stress values existing in 48-wire FDS treated models.

A comparison between 48 and 64-wire FDS models is available for each patient, bringing a new discussion. So far, investigating maximum shear stress and shear strain rate values yielded the result that 48-wire FDS models have higher values for both parameters than the 64-wire FDS models. Therefore, it is essential to observe the results to see whether the higher shear stress values and shear strain rate values existing in 48-wire FDS models also exert supraphysiological values to larger volumes.

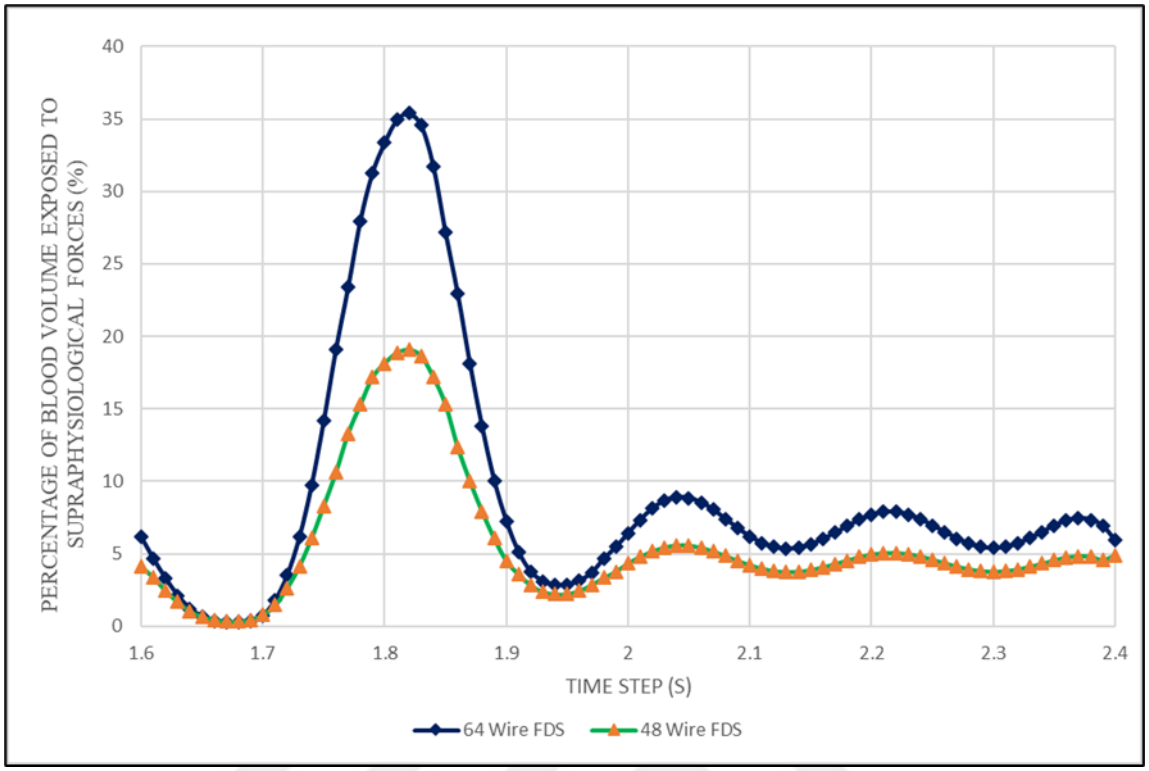

Figure 3.21. Percentage of blood volume exposed to supraphysiological forces to total blood volume at neck region for patient 1 after 48 and 64 wire FDS implantations

The amount of blood volume for each time step that are exposed to 10 Pa above shear stress when the blood passes through stent struts at the neck region is calculated. Then percentages of blood volumes exposed to supraphysiological forces to total blood volumes are calculated. Plotting the results for patient 1, Figure 3.21 is obtained which shows almost 20 percent and over 35 percent of blood volume which are exposed to supraphysiological forces are existent for 48-wire and 64-wire FDS models, respectively. For both models reaching their peak at peak systole instance, the 64-wire FDS implanted model yielded more than 15 percent higher supraphysiologic force-induced volume than the 48-wire FDS model. Having the main differences during systole moments, 64 wire FDS model has equal or higher aggravated blood volume throughout the cycle. This shows that more blood volume exposed to supraphysiological forces exists at 64 wire FDS model, and therefore more vWF multimers are being activated for the same model.

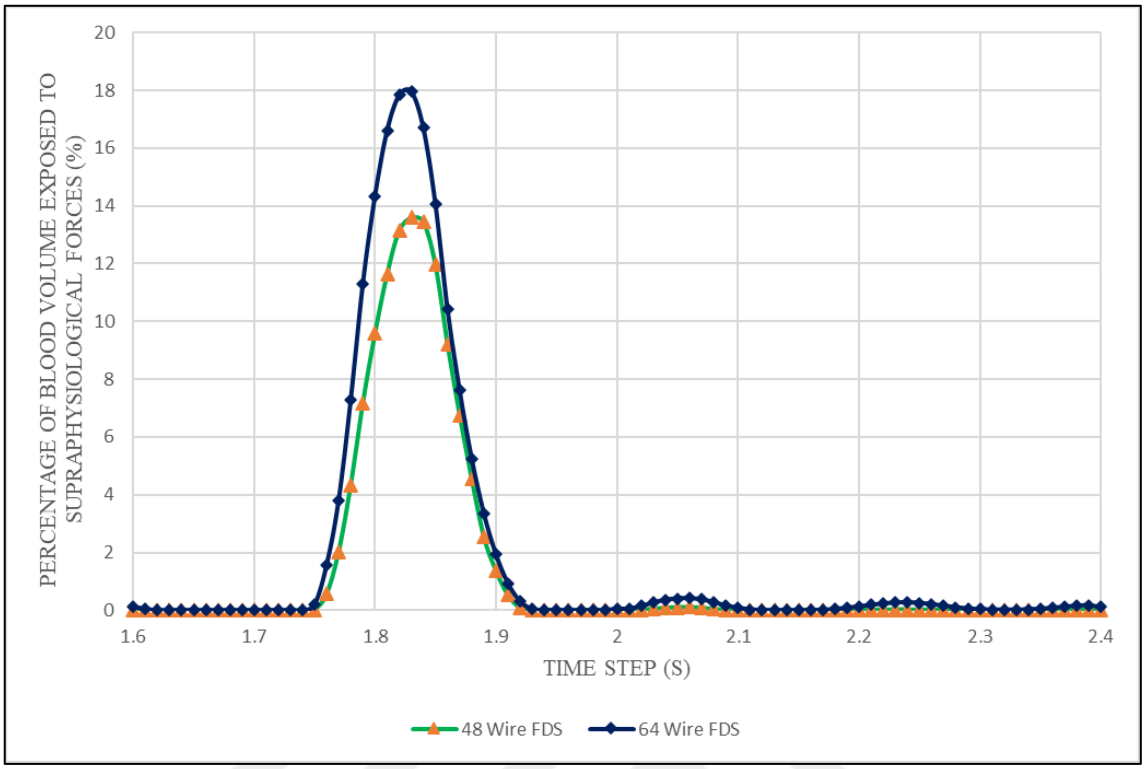

Figure 3.22. Percentage of blood volume exposed to supraphysiological forces to total blood volume at neck region for patient 2 after 48 and 64 wire FDS implantations

Patient 2 has a higher aggravated blood volume percentage with 64-wire FDS treated model compared to the 48-wire FDS. The difference between the two models is observed at around 4 percent, which makes 48-wire FDS almost 25 percent less than the 64-wire FDS model. Even though the shear stress and shear strain rate values are much higher with 48-wire FDS implantation, the blood volume exposed to supraphysiological forces is higher for 64-wire FDS. Having almost one-fifth of the total volume of blood being aggravated due to supraphysiological forces at peak systole instance shows the above threshold values presented in earlier sections are not merely existent in an infinitesimal region.

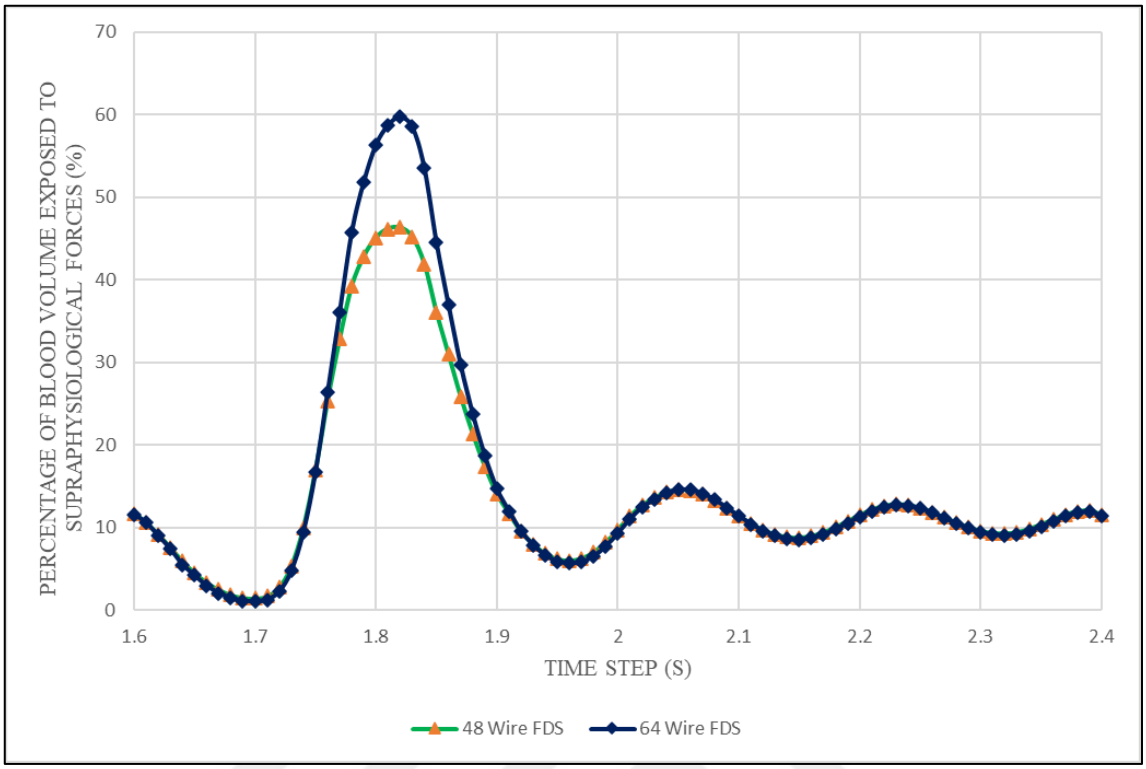

Figure 3.23. Percentage of blood volume exposed to supraphysiological forces to total blood volume at neck region for patient 3 after 48 and 64 wire FDS implantations

Patient 3 yielded the highest percentages among the other two ICA patients. Similar to the other two patients, 64 wire FDS model has more blood volume being exposed to supraphysiological forces. Reaching a 60 percent aggravation rate, patient 3 has more blood volume with activated vWF than inactive ones for systole instances. Implantation of 48-wire FDS indeed returns lower aggravated blood volume, but almost 50 percent of blood volume exposed to supraphysiological forces exists during peak systole. This patient also has more vWF-activated blood volume after the implantation of 64-wire FDS.

After inspecting the percentages obtained for patient 3, it is clear that there tends to be a higher supraphysiologic shear force induced amount of volume for higher maximum shear stress values for ICA patients.

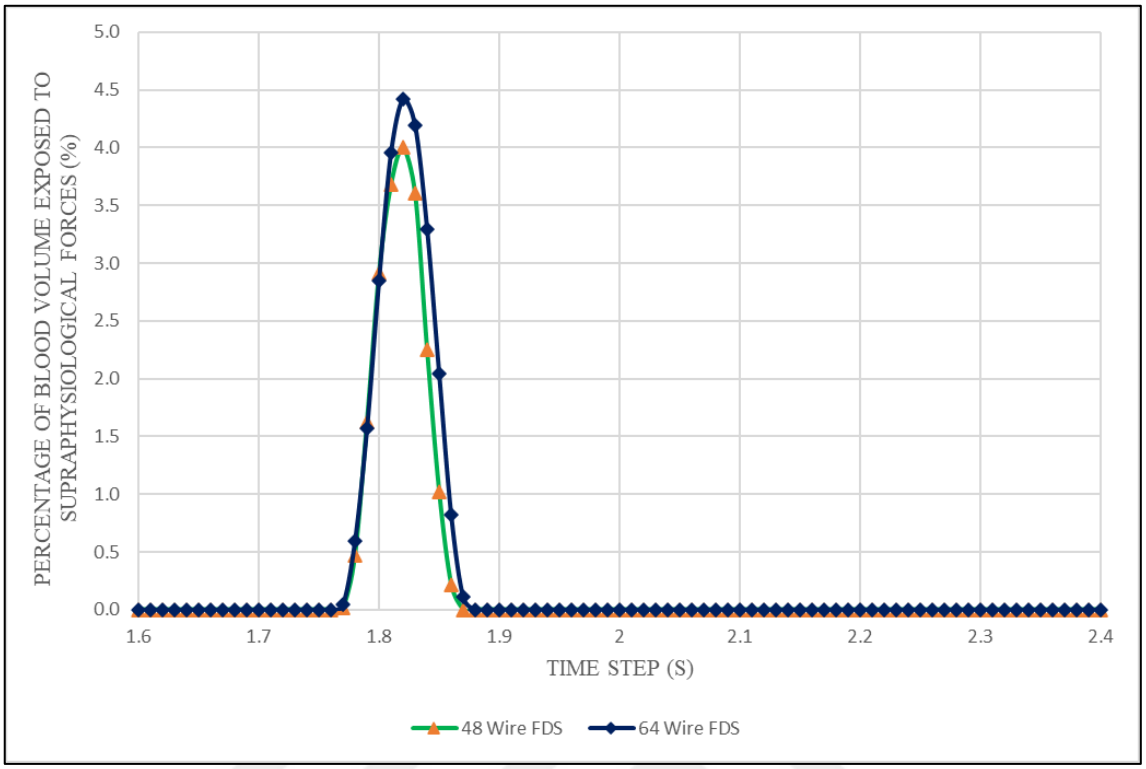

Figure 3.24. Percentage of blood volume exposed to supraphysiological forces to total blood volume at neck region for patient 4 after 48 and 64 wire FDS implantations

Patient 4 has a much lower percentage of blood volume exposed to supraphysiological forces than ICA patients. This is due to having much smaller neck areas for MCA patients. Compared to ICA, less blood with high shear stress is passing through for MCA patients, but also this leads to having smaller inflow regions. Therefore, percentages are dropping as well for MCA patients. Treatment done with 64-wire FDS causes higher blood volume which is being exposed to supraphysiological forces than the results of 48-wire FDS. This difference is largest during peak systole, as expected. Therefore with Figure 3.24, it can be seen that the implantation of 64-wire FDS results in more activated vWF multimers.

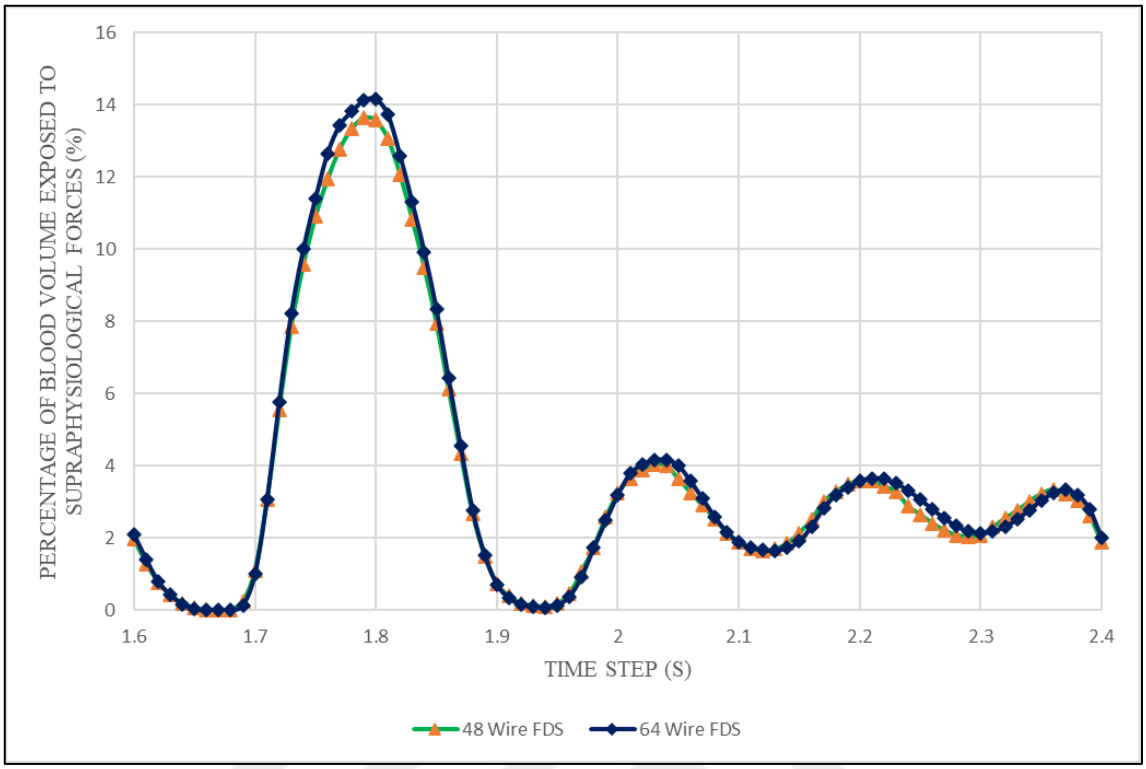

Figure 3.25. Percentage of blood volume exposed to supraphysiological forces to total blood volume at neck region for patient 5 after 48 and 64 wire FDS implantations

Having the highest shear stress and shear strain rate values in this study, patient 5 has a lower percentage of blood volume that is exposed to supraphysiological forces to total blood volume when compared with all ICA patients. This shows the importance of inspecting the blood volume above threshold shear stress values. By doing that, it can be understood that more vWF multimers are being activated for ICA patients due to a greater amount of blood volume above 10 Pa shear stress values. Simulation results with 64 wire FDS model show that more blood volume have aggravated values than 48-wire FDS treatment.

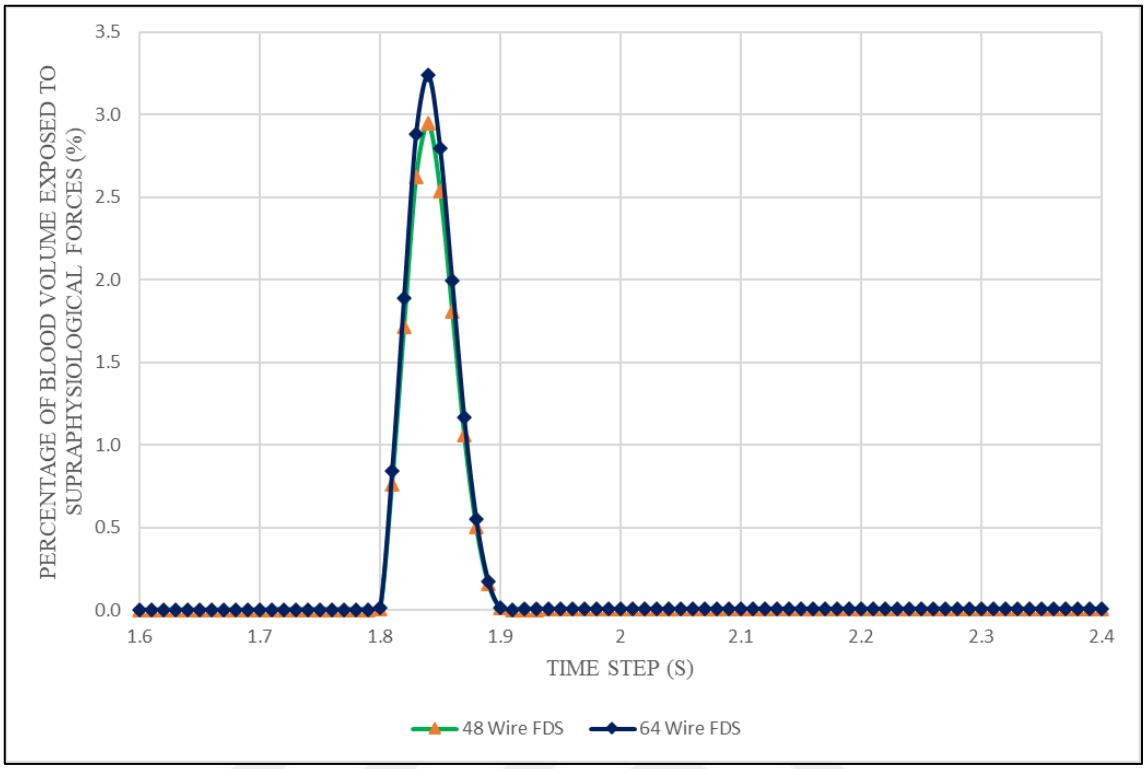

Figure 3.26. Percentage of blood volume exposed to supraphysiological forces to total blood volume at neck region for patient 6 after 48 and 64 wire FDS implantations

Patient 6 has second to lowest shear stress values, as shown earlier. Plotting Figure 3.26 reveals the case where patient 4 has slightly higher blood volume which is exposed to supraphysiological forces, meaning more vWF is being activated compared to their domain volumes. This proves the importance of inspecting the aggravated blood volume percentage and not settling to calculating the shear values solely. Because ICA patients' higher shear stress values align with having a higher percentage of blood volume that is exposed to supraphysiological forces to the total blood volume for each patient's neck region FDS volume.

Overall, it can be seen that ICA aneurysm models have larger percentages of blood exposed to supraphysiologic forces than MCA patient models. This is caused by the larger aneurysm diameter, which has a wider neck for ICA patients. When a wide neck diameter exists, the blood volume that is exposed to supraphysiological forces is calculated to be larger in amount, but also the region it occupies overall in the neck domain is getting larger. Similarly, MCA models having smaller neck diameters yield a lower percentage of exposed blood volume to total blood volume. Patient 5 has the highest maximum shear stress and shear

strain rate values in this study; but nevertheless, it has lower percentage value compared to patient 2, which has the lowest shear values within ICA patients. As shown earlier, patient 4 had the least shear stress and shear strain rate values compared to the two MCA patients. Nonetheless, FDS implantation for patient 4 causes a higher percentage of blood volume to have supraphysiologic shear values compared to patient 6.

For all the patient models where 64-wire FDS is implanted, the percentage of blood volume exposed to supraphysiologic forces to total blood volume is greater than 48 wire FDS models. Earlier it was found that shear values are greater for the 48 wire FDS model. However, having more wires affects the dimensions of the region where blood can be exposed to supraphysiologic forces, thus increasing the percentage of blood volume exposed to those forces. This can be due to the EMSA values being different between 48 and 64-wire FDSs. With this investigation, another aspect of vWF activation is pointed out. Even though this margin is not huge for MCA patients, for ICA patients with larger neck diameters, the difference can go more than 15 percent between the two FDSs for the same patient. This shows the importance of wire numbers in FDS types.

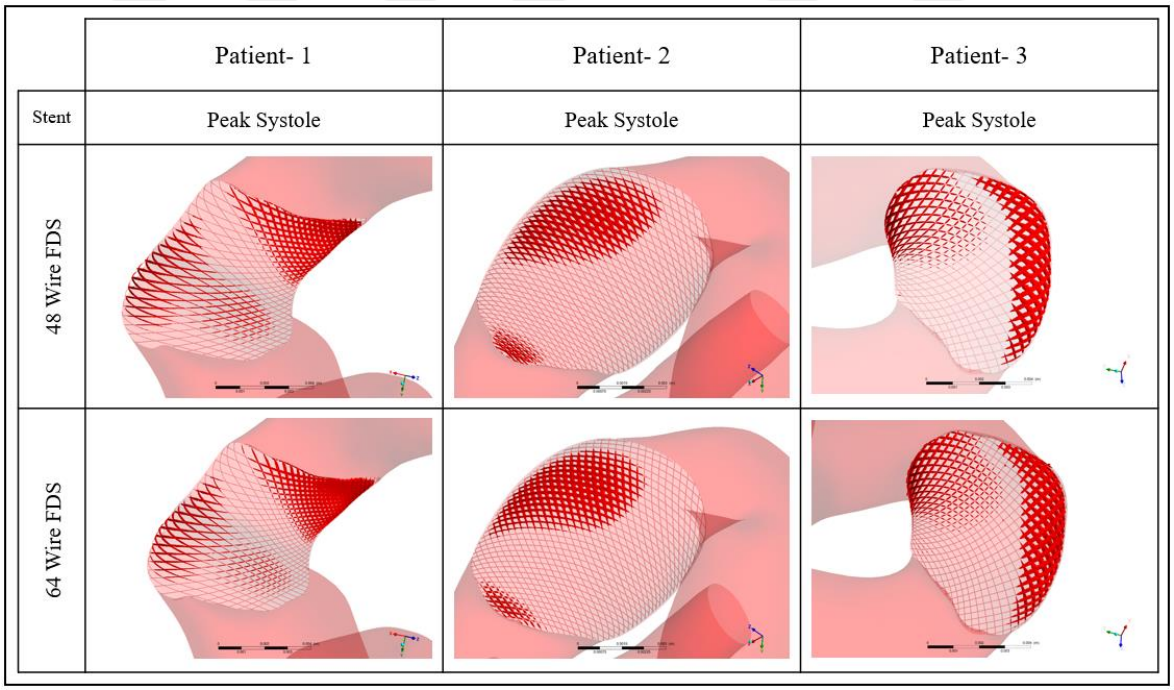

Figure 3.27. Blood particles exposed to supraphysiological forces for ICA patients with the same alignment as DSA images

High shear-induced regions on the stent domain are constructed and shown in Figure 3.27 and Figure 3.28. Dark red colored volumes represent blood particles that have 10 Pa and higher shear stress values. These figures are taken in the same format as DSA images that are available in this study. For ICA patients, it can be seen that the blood volumes that are exposed to supraphysiological forces exist with large and distinctive inflow and outflow regions. Due to the greater size in ICA patients, the amount of blood particles under supraphysiological force exertion is higher for ICA patients. Other than having an insight on the inflow and outflow regions, it is important to see how high shear stress existing blood particles aggregate in each other's vicinity.

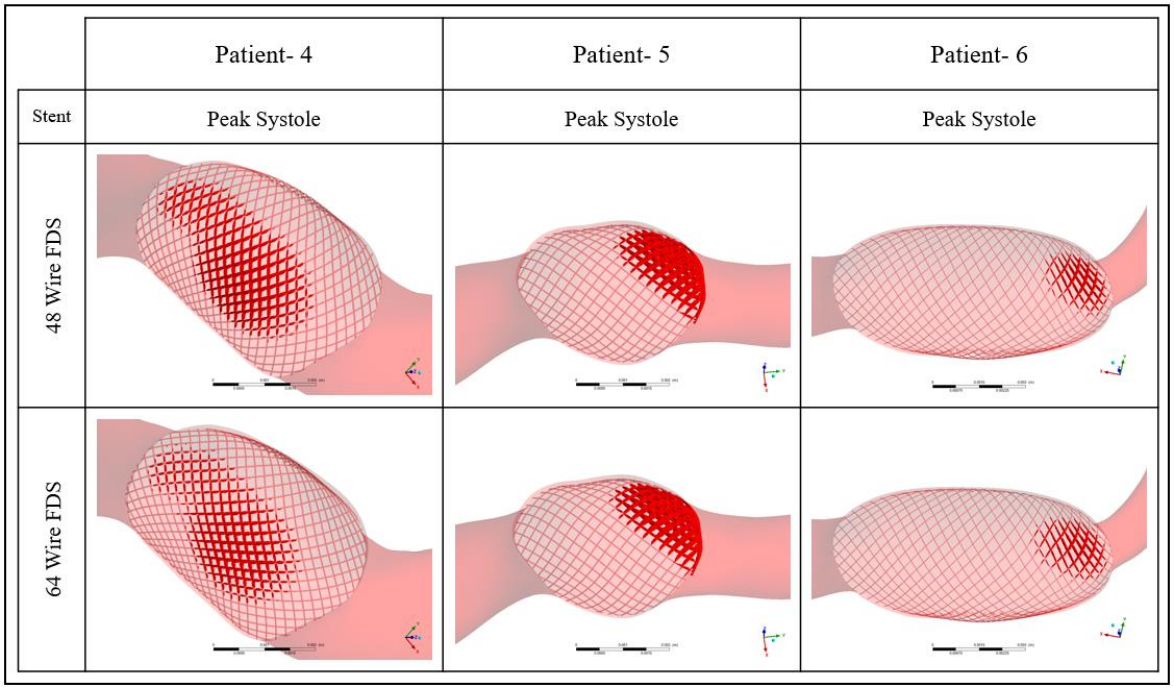

Figure 3.28. Blood particles exposed to supraphysiological forces for MCA patients with the same alignment as DSA images

As shown in the previous section, it is already known that the ratio of the blood volume which is exposed to supraphysiological forces to total blood volume is lower for MCA patients. In Figure 3.28, it can be seen how the blood particles which are being exposed to supraphysiological forces exist during peak systole instances for each patient.

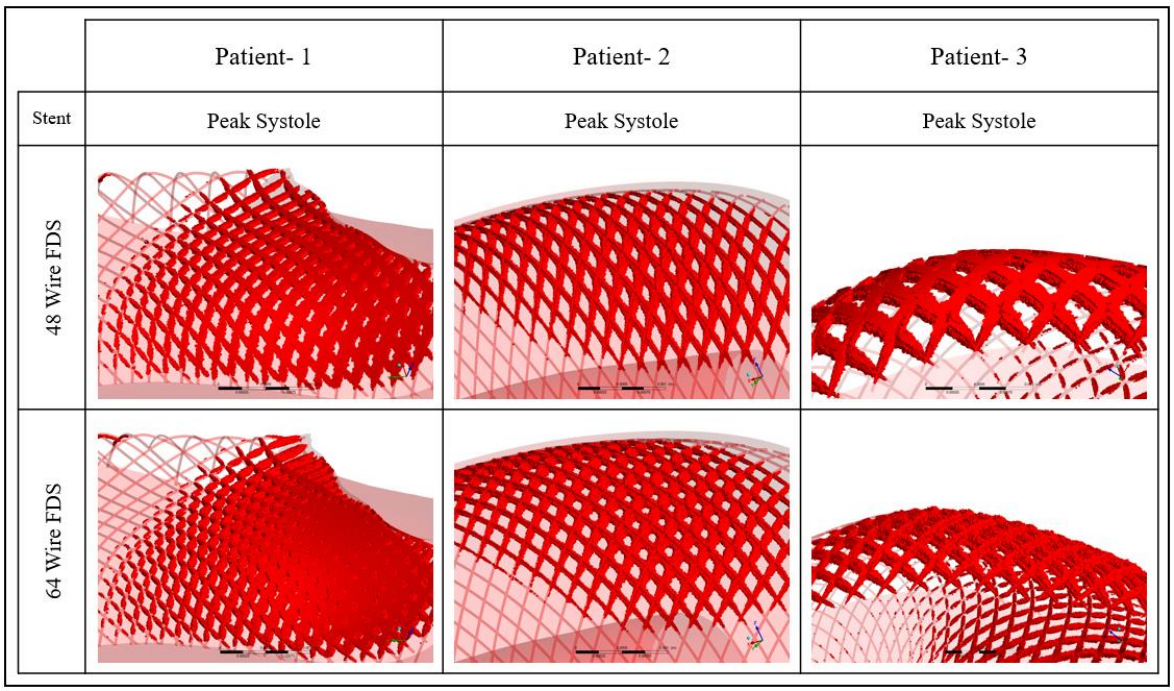

Figure 3.29. Blood particles exposed to supraphysiological forces for ICA patients from a close-up view

Close-up views are constructed to have an even better understanding of how the blood particles entering and leaving the aneurysm through the FDS struts induce high shear stresses in the inflow and outflow regions. For supraphysiological particles, where they are aggregated at some locations, struts are almost fully colored dark red. That shows that even away from the walls of the FDS, the shear stress values are above 10 Pa.

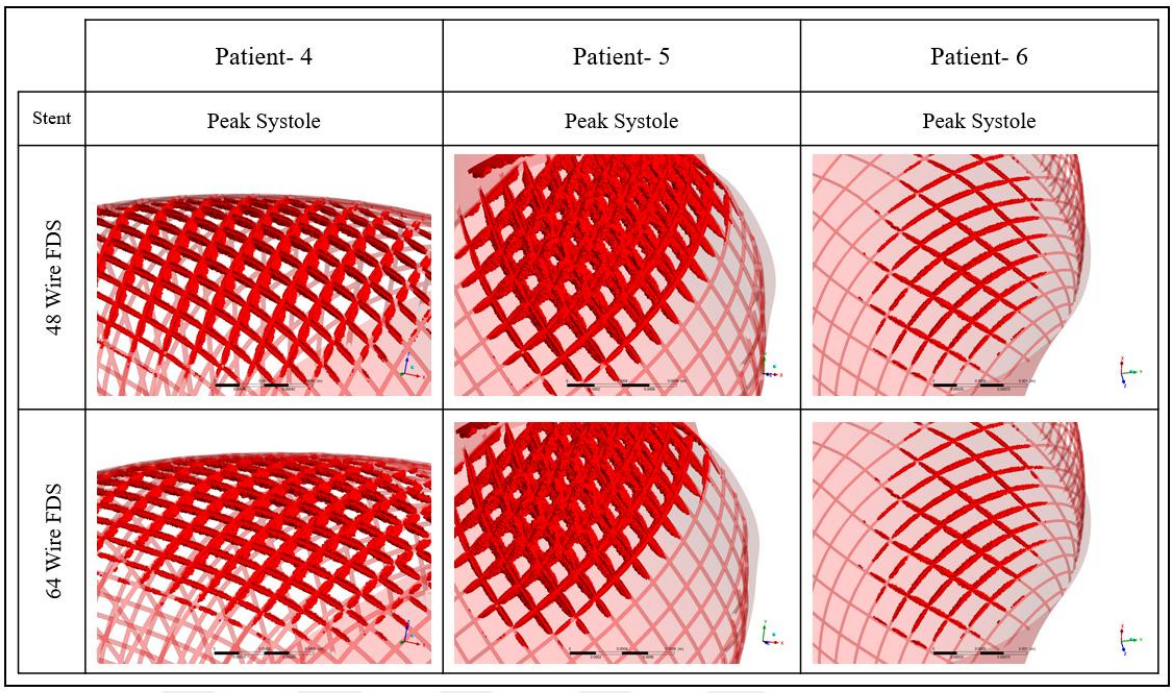

Figure 3.30. Blood particles exposed to supraphysiological forces for MCA patients from a close-up view

3.4. PREDICTION OF RUPTURE-PRONE REGIONS

3.4.1. Time-averaged wall shear stress

TAWSS contours are taken to observe the distribution of shear stress on the walls of the whole model. A surface group is constructed to investigate each model's average shear stress globally. TAWSS provides insight into the model, which shows the locations affected by excessive stress levels. In each model, it can be seen that supraphysiological levels of time-averaged shear stresses are obtained. For convenient comparison, each model's minimum and maximum value range is set as 0 and 10 Pa, respectively. Each contour is constructed at the last time step of the third cycle of the heartbeat. This way the effect of the wall shear stress averaged in time is obtained on the walls of the artery and aneurysm for each simulation.

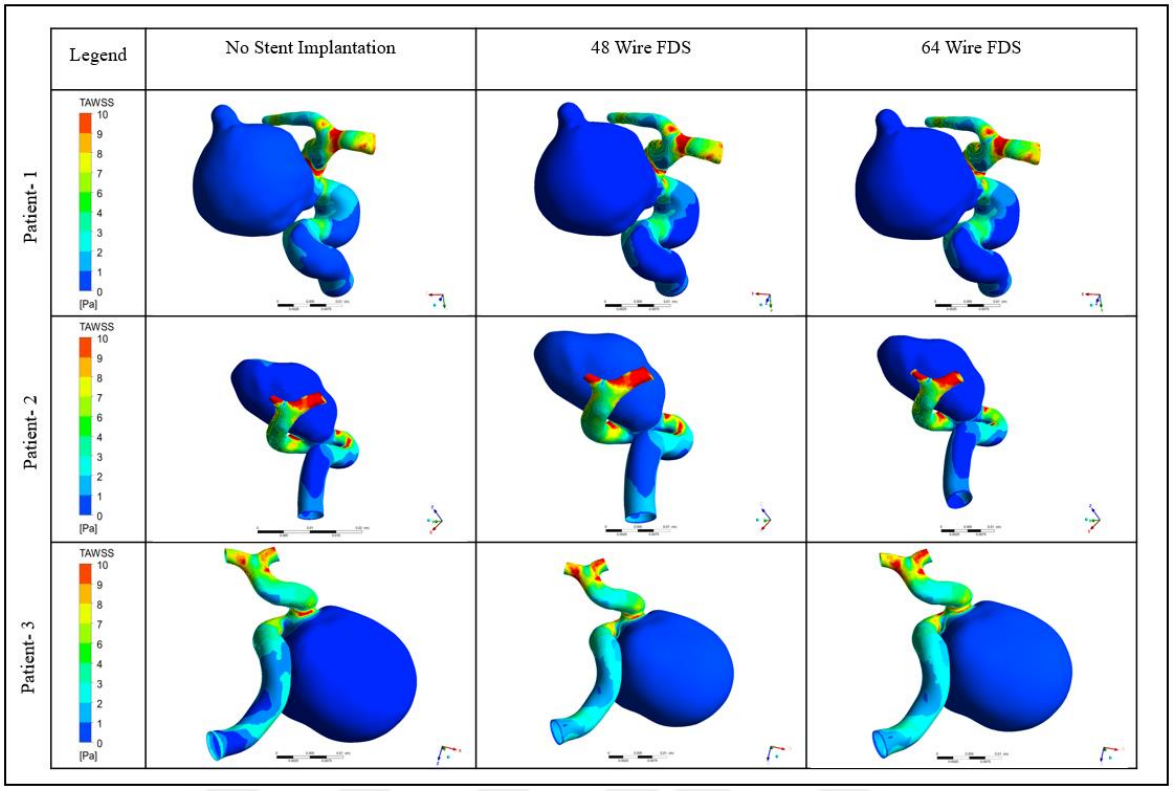

Figure 3.31. TAWSS contours of ICA patients for each model

In the results of patient 1 shown in Figure 3.31, the shear stress values throughout the model without an implanted stent are in the proximity of the supraphysiologic shear stress threshold of 8 to 10 Pa. Those values increase dramatically with the implantation of FDS for both 48-wire and 64-wire FDS. The regions with excessive average shear stress values for the no-stent model get changed slightly after an FDS implantation. High shear stress locations for both 48-wire and 64-wire models are impacting with much higher stress levels compared to the untreated model, but the affected regions seem like as if they are similar. These regions can be called rupture-prone regions as they do not change with the implantations of FDS, but the intensity of shear forces increases to pathological levels.

Similarly, for patients 2 and 3, the distribution of high shear locations is almost the same regardless of FDS implantations. The elevated levels of average shear stress values are obtained after the blood flow encounters with FDS, which is called the distal of the artery. This aggravation in shear stress through distal shows the change in blood flow characteristics due to the existence of an aneurysm. The blood flow that leaves from the aneurysm with and without an FDS is altered to cause higher shear stresses. Indeed, in the FDS implanted

models, the dramatic increase in time-averaged shear stress locations point out the rupture prone zones. Wall shear stress levels on the aneurysm are never reaching supraphysiological shear force levels. This is valid for all ICA models with each stent variation.

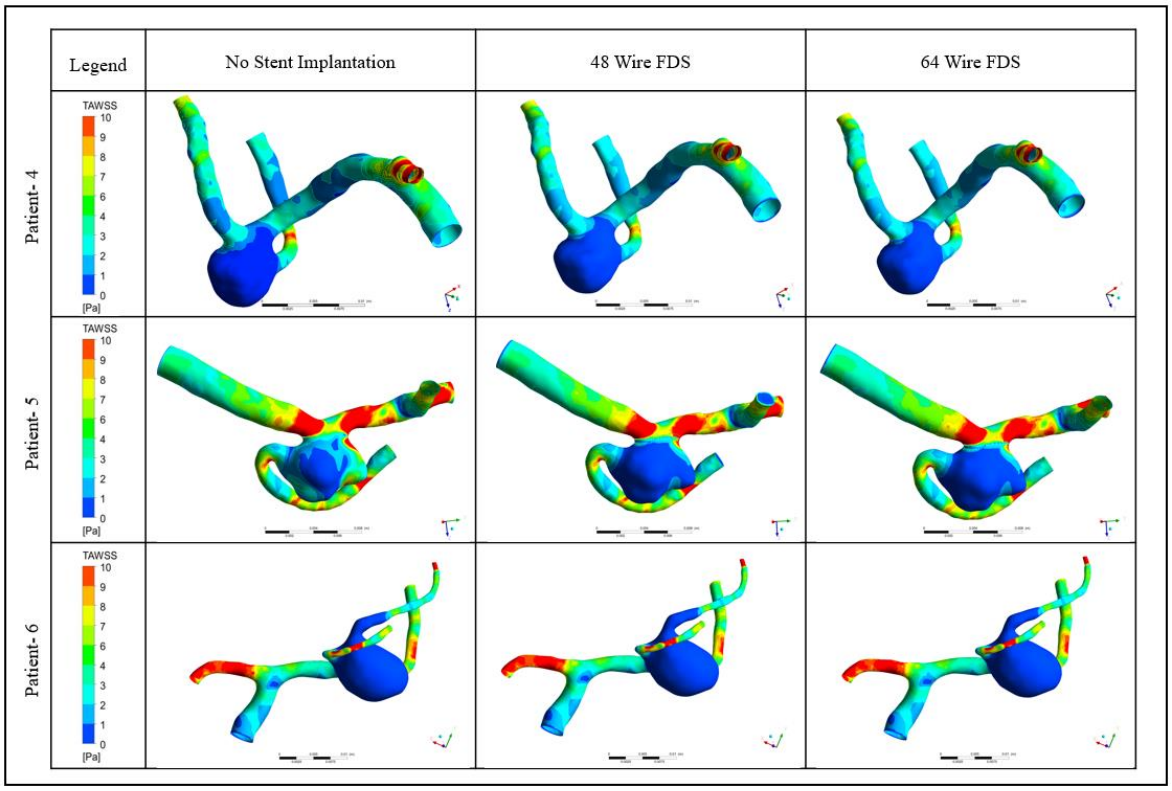

Figure 3.32. TAWSS contours of MCA patients for each model

The simulation results obtained from MCA models show some differences compared to the ICA models (Figure 3.32). One striking difference is that the high shear stress locations are not only through the distal but also existing at the proximal of the artery. An important reason for this is the presence of branching in the middle cerebral artery next to the inlet of the aneurysm. The increased shear stress regions in no stent cases for each patient and the increase in shear stress values of those regions are showing similarity with the ICA models. The rupture-prone zones in MCA models exist in more locations than in the ICA models.

3.4.2. Oscillatory shear index (OSI)

When a disturbance in the flow exists, the OSI parameter is used to describe that disturbance. Ranging from 0 to 0.5, where 0 indicates a low oscillatory flow and 0.5 indicates a high

oscillatory one. High oscillatory flow means that the direction of the WSS vectors are almost 180 degrees changed in direction. Any change occurring in wall shear stress magnitude and direction can be inspected through OSI. This is a valuable information to have, considering if low WSS exists in the same region where OSI is known to be high, this circumstance increases the occurrence of rupture by weakening the artery wall [83]. Results for each patient with no stent implantation, 48 and 64-wire FDS implanted models were compared to investigate the behavior of shear stress and oscillations in it. All calculations are made at the last time step of each simulation to inspect the behavior throughout three cardiac cycles.

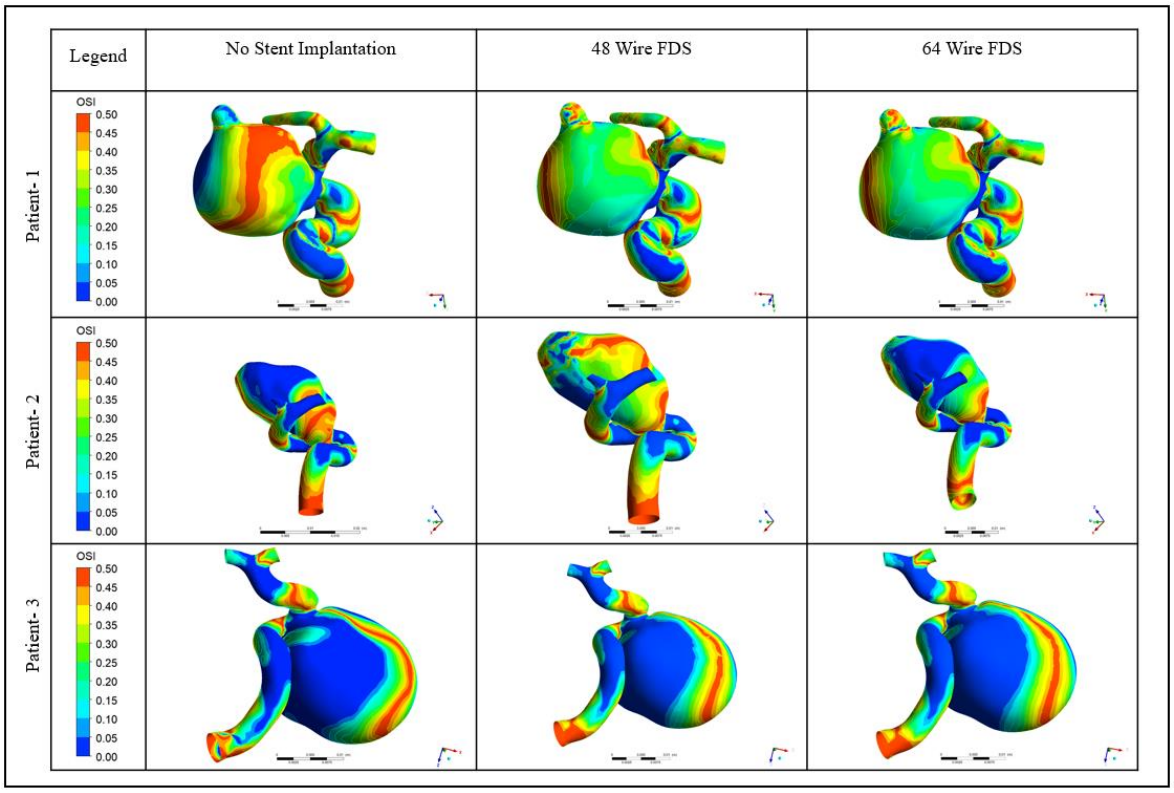

Figure 3.33. Oscillatory shear index contours of patients 1, 2, and 3 without FDS implantation, 48 and 64 wire FDS implantations

The model with no stent implanted for patient 1 shows high oscillatory shear stress behavior on the aneurysm wall and several regions at the proximal and distal. After FDS treatments, high OSI values drop on aneurysm wall significantly, shown in Figure 3.33. At proximal the change in wall shear stress oscillations is minimal. The OSI intensity is increasing at distal after FDS treatments, near already high oscillatory regions before FDS treatment model. Patient 2 has a different case by having an increase in OSI on the aneurysm wall after the

implantation of 48-wire FDS. The oscillatory shear behavior existing on the aneurysm wall for the before treatment case decreased after 48-wire FDS implantation, leading to non-effected areas becoming high OSI regions. 64-wire FDS treatment method lowered the OSI values on the aneurysm wall significantly. There is no significant change in fluctuation for distal with all the models of patient 2.

OSI values on the aneurysm wall are lower following FDS treatments. The dominant area of oscillatory flow existing on the aneurysm wall became smaller post treatments. The significant influence of FDS implantations happens at the distal side of the aneurysm neck. Results obtained from each simulation show that for ICA patients, OSI levels drop on aneurysm wall after FDS treatments for most cases. The tendency of oscillatory shear stresses stayed similar at distal after FDS treatments were done for ICA patients.

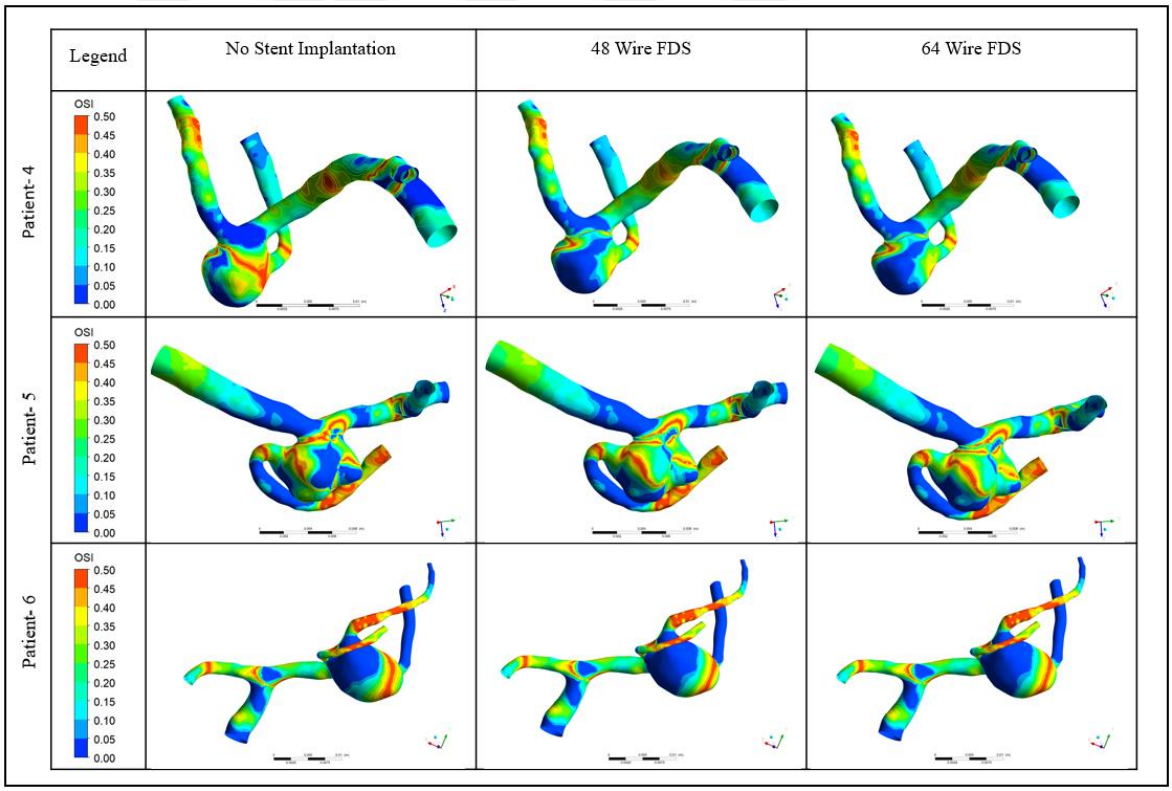

Figure 3.34. Oscillatory shear index contours of patients 4, 5, and 6 without FDS implantation, 48 and 64 wire FDS implantations

Forming OSI contours for patient 4 shows a decrease in fluctuations in shear stresses on the aneurysm wall after FDS treatments. At proximal and distal OSI values stayed quite similar

for before and after treatment models. Patient 5 contours with FDS treatment show a small decrease in OSI on the aneurysm wall for high OSI regions, whereas an increase around the low OSI zones exists. There is almost no difference in oscillatory flow at the distal and proximal. Lastly, for patient 6 each model showed nearly identical results along the domain.

Nevertheless, there is a slight difference in the aneurysm wall where the high OSI region before treatment shrunk minimally with both FDS implantations. Overall oscillatory shear stresses tend to stay similar for MCA patients along the domain with a slight improvement on the aneurysm wall, and no significant increase at distal is obtained. It is expected to have less oscillatory flow occurring for MCA aneurysms which are smaller than ICA aneurysms and tend to rupture at significantly lower rates [120].

3.4.3. Maximum WSS values for the artery in a cycle

Through TAWSS contours, it is explained that high shear stress regions for before FDS implanted models at proximal are increasing their shear stress values while slightly increasing in the area which affects the arterial wall. Maximum wall shear stress values are obtained for each time step for the third cardiac cycle for each model to show this increase after an FDS treatment in this study. The importance of this is to show intensifying shear stresses on the so-called rupture-prone regions with numerical values. In the case of vWF activation, the importance is not dire whether shear stress on the blood has a value slightly above 15 Pa or 50 Pa; for example, the main concern is that the activation occurs after exceeding the threshold value of 10 Pa. On the contrary, in the case of wall shear stress at the artery wall, higher the shear stress, greater the chance of rupture. Therefore, having intensified shear stresses on already high-shear existing regions cause concern with the implantation of FDS.

Obtaining the maximum WSS values at artery walls throughout the third cardiac cycle is done by removing the aneurysm from each patient's geometries. An example of the aneurysm removal for Patient 1 is presented in Figure 3.35. The location of where the aneurysm got removed from the domain is determined according to the FDS location at the neck region. This gives a clear indication in determining where aneurysm region starts to erupt from the artery. Remaining domain consists of only the artery which is necessary to obtain the maximum WSS values at artery walls of each patient.

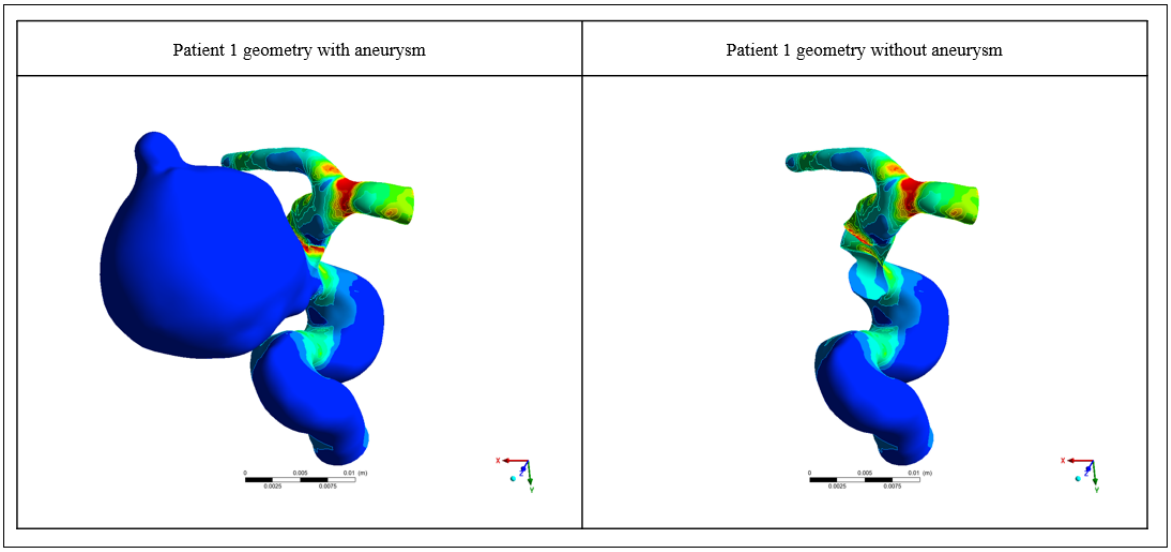

Figure 3.35. Patient 1 geometry with and without aneurysm

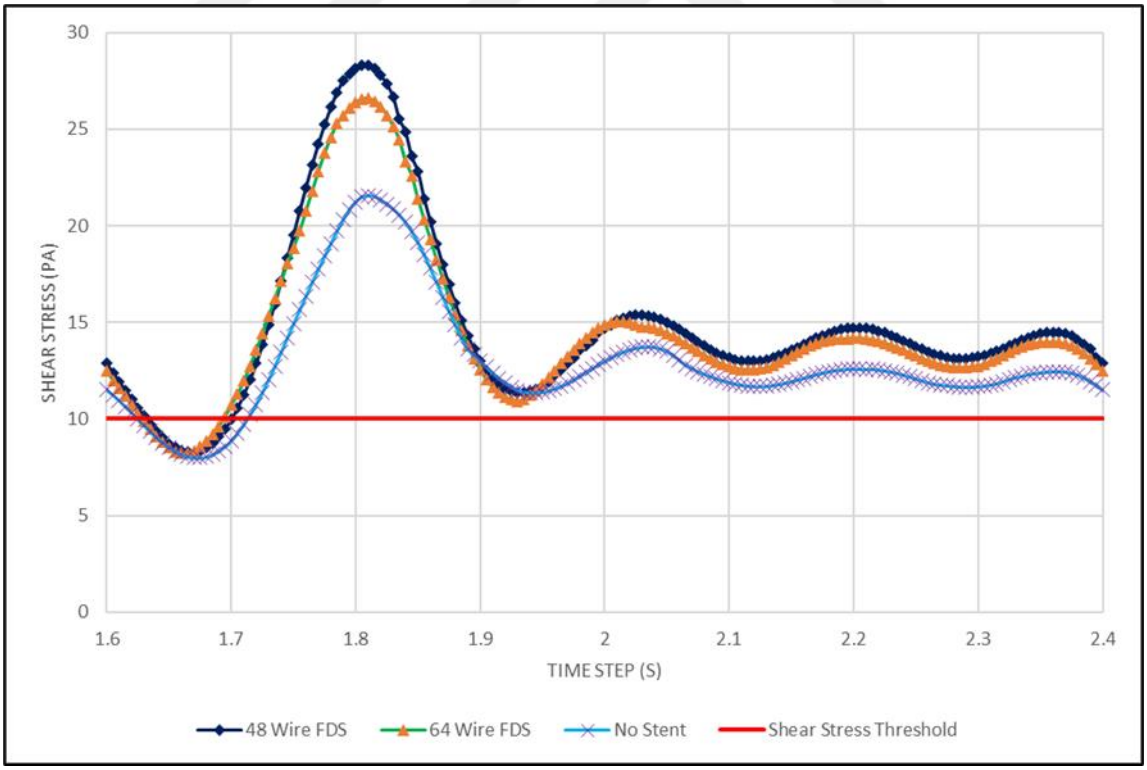

Figure 3.36. Shear stress values at the artery wall for patient 1

Results presented in Figure 3.36 indicate the increase in maximum shear stress values on ICA for patient 1 following the FDS implantations. Higher shear stress values at the

aneurysm neck region after 48-wire FDS treatment compared to 64-wire FDS seems to be transmitted to the wall shear stress values at the artery wall. Implantations of both FDSs lead to a more than 25 percent increase in shear stress during peak systole instances.

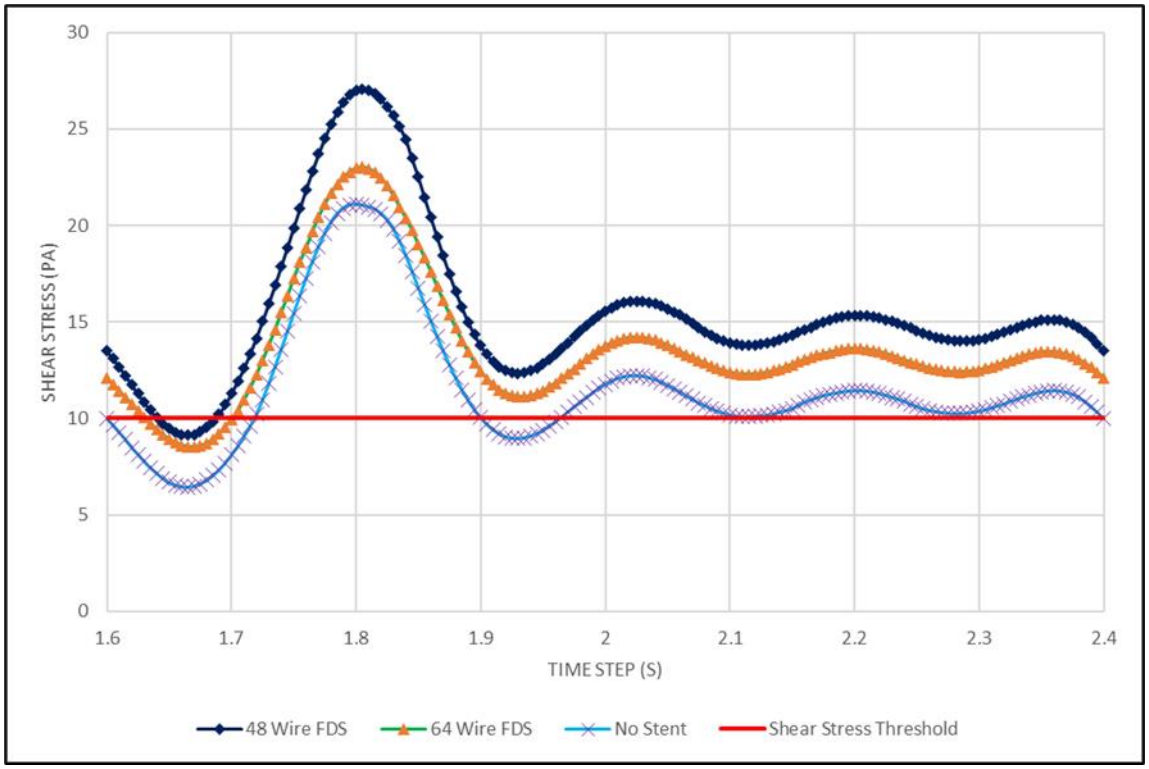

Figure 3.37. Shear stress values at the artery wall for patient 2

Similar to patient 1, an increase in wall shear stress at the artery wall for patient 2 is evident after receiving FDS treatment. It is particularly important to observe the rise for patient 2 following FDS treatments, where contours showed almost identical high TAWSS regions. This proves an increase in shear stress values after treatment for the same rupture-prone regions that existed before treatment. Another important argument can be made about whether the shear stress values occurring at the aneurysm neck are somehow related to the shear stresses at artery walls. Shear stress values obtained for the neck regions for patients 1 and 2 are quite different, where patient 1 has over 30 Pa more shear stresses available at systole. However, comparing their wall shear stress values at their artery wall does not indicate such difference, which can be seen by looking at both Figure 3.36 and Figure 3.37.

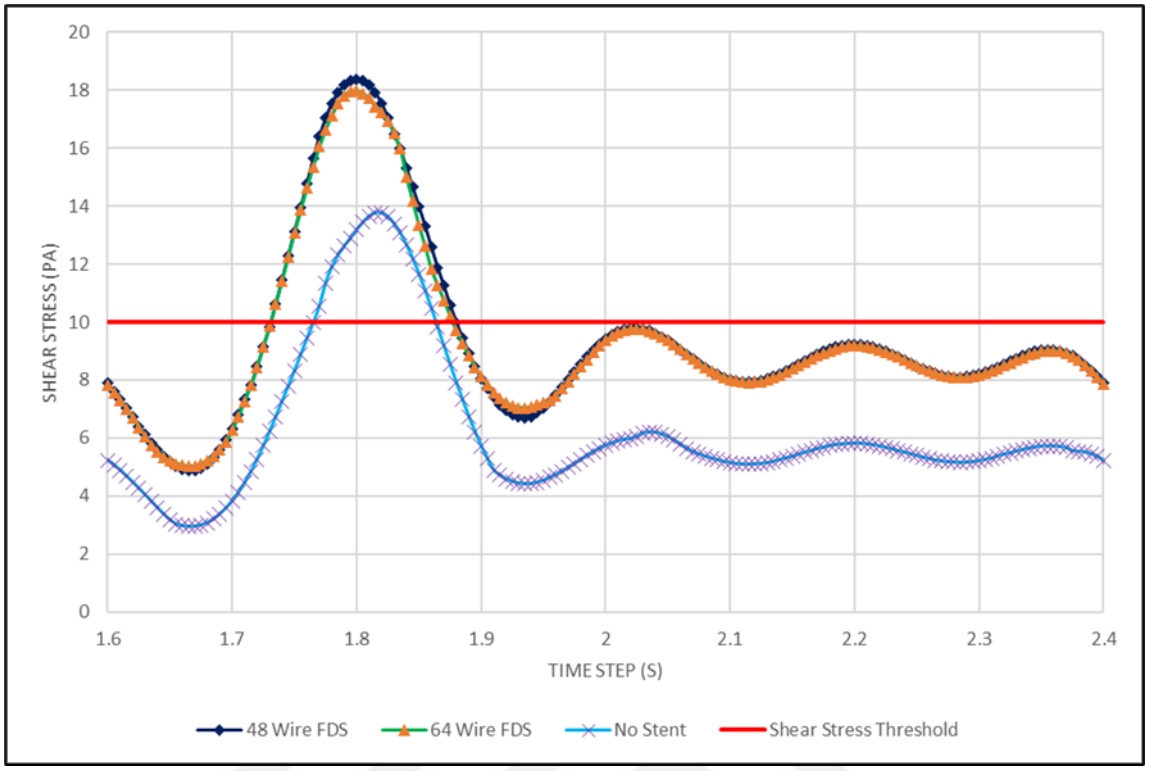

Figure 3.38. Shear stress values at the artery wall for patient 3

Wall shear stress values in Figure 3.38 show the increase with FDS implantations like the other ICA patients. The difference between 48 and 64-wire FDS implanted models is quite small compared to patients 1 and 2's cases. The maximum wall shear stress values for patient 3 are lower for each time step in the cycle compared to patient 1 and 2. Conclusively, implanting FDS increases maximum wall shear stress values at artery walls for every ICA patient and the level of shear stresses available at aneurysm neck does not determine the level of wall shear stresses at artery wall.

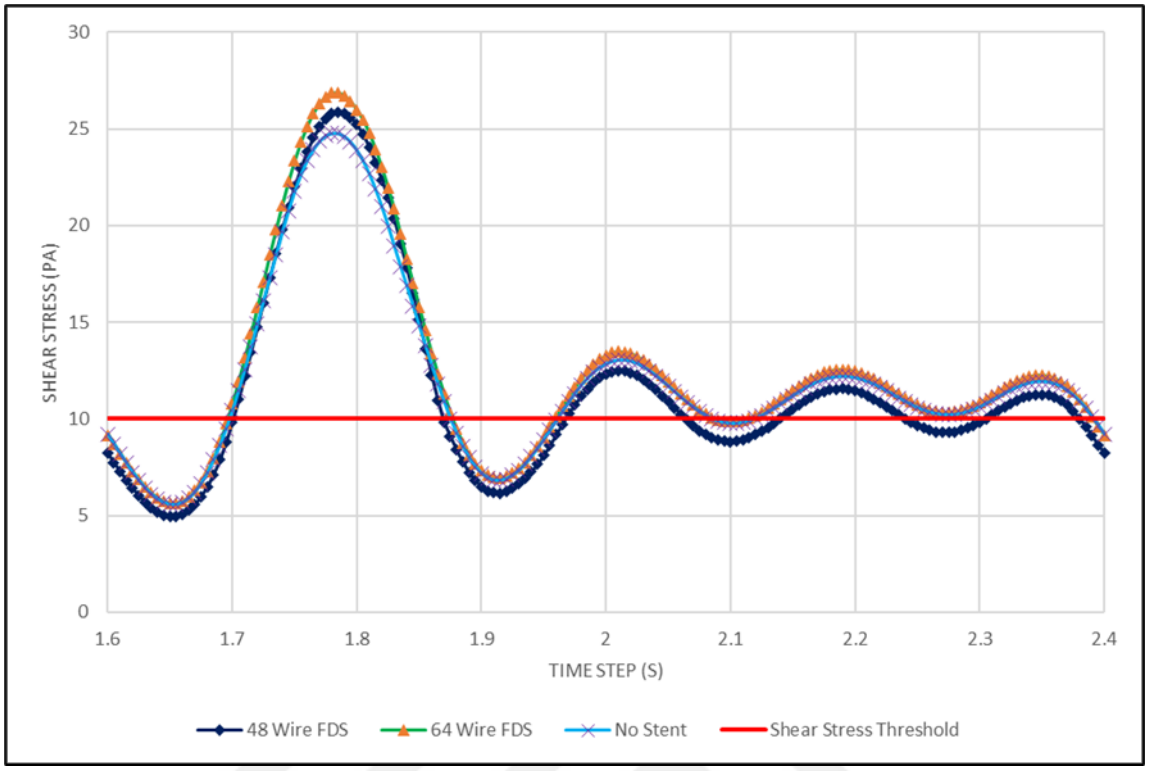

Figure 3.39. Shear stress values at the artery wall for patient 4

There is no significant increase in maximum wall shear stresses after the implantation of both FDSs. An increase exists, highest during peak systole; however, it is not as high as for ICA patients. Interestingly as plotted in Figure 3.39, the higher maximum wall shear stresses are available after 64-wire FDS implantation.

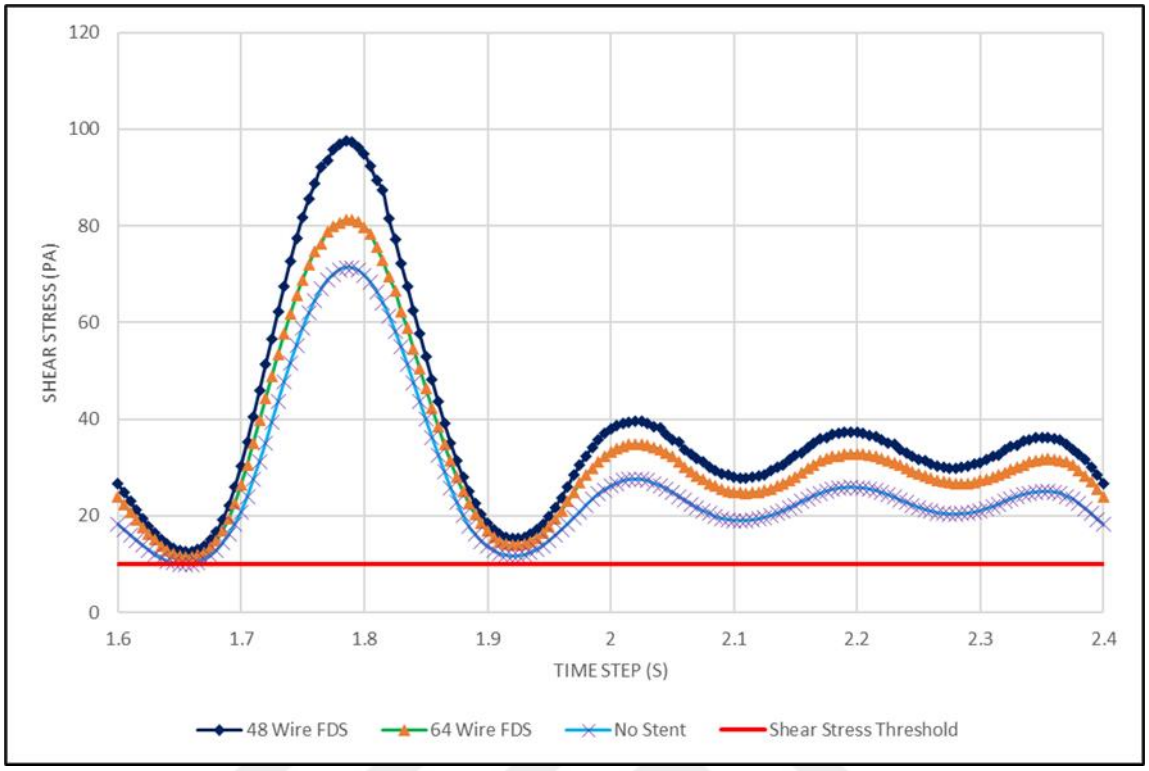

Figure 3.40. Shear stress values at the artery wall for patient 5

Patient 5 has the highest maximum wall shear stress values at the artery wall, like for shear stress values at the neck of the aneurysm. Following the treatment with 48-wire FDS, maximum wall shear stress values are higher than the 64-wire FDS implanted model. This shows a similar result to the ICA patients, where maximum wall shear stresses increase significantly at the artery wall after FDS implantation.

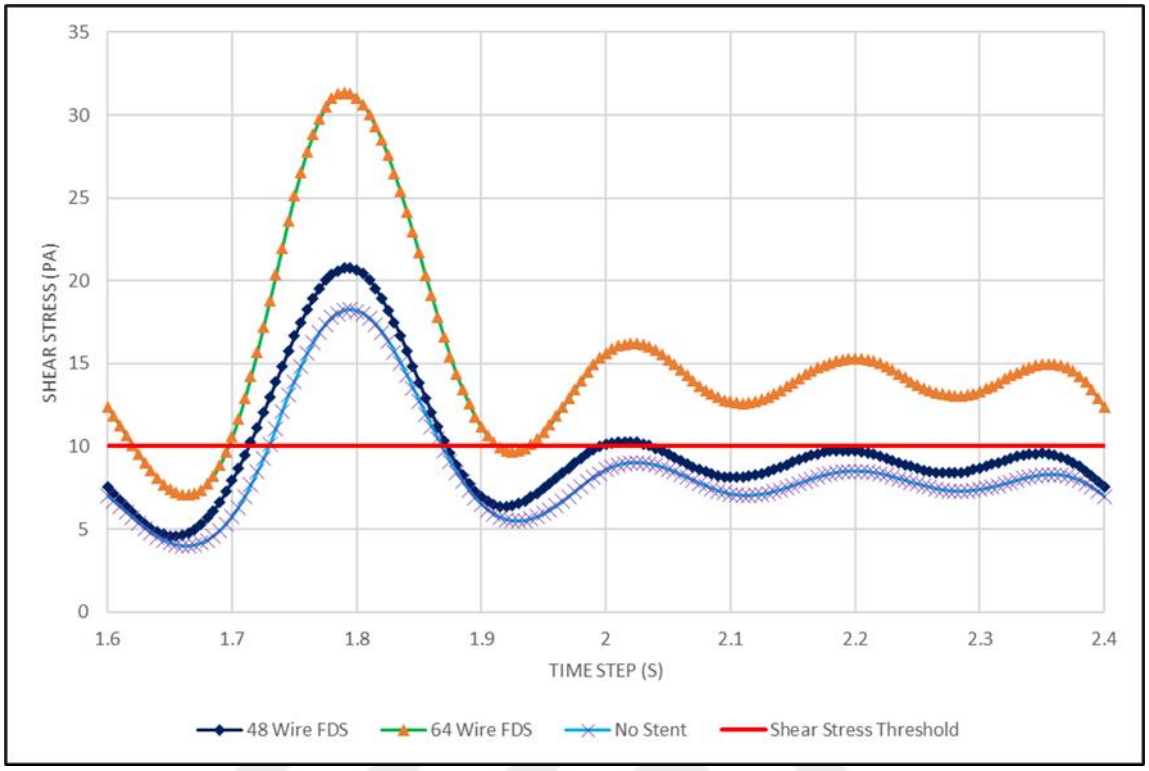

Figure 3.41. Shear stress values at the artery wall for patient 6

Lastly, the data plotted in Figure 3.41 shows an almost 50 percent increase after the treatment of 64-wire FDS when compared to 48-wire. Both FDS implantations increase maximum wall shear stresses at the artery wall. Similar to patient 4 and different than patient 5, higher wall shear stresses are reached with the implantation of 64-wire FDS. In summary, the results obtained for MCA patients show an increase in maximum wall shear stress values after receiving FDS implantations. Unlike ICA patients, the shear stress levels available at the aneurysm neck region may indicate the level of wall shear stress at the artery wall.

3.5. DIFFERENT EFFECTS OF IMPLANTING 48 AND 64-WIRE FDS

Throughout the study main importance has been proving the increase in shear values due to FDS implantations, and a comparison has been provided between 48 and 64 wire FDS models. Initially, all these patients already have pathological flow due to the existence of cerebral aneurysms they have, and they need a treatment where FDS is currently the most prominent endovascular treatment way of cerebral aneurysms (121). Therefore, it is crucial

to select the most effective type of FDS with the least number of complications arising after its implantation, such as vWF activation.

Inspecting the maximum shear stress and shear strain rate values of the FDS with 48 wires resulted in higher values for both ICA and MCA patients. Later, solely focusing on this aspect became not enough as the activation of vWF already takes place by exceeding 10 Pa and 5000 s^{-1} for shear stress and shear strain rate, respectively, further increase after the threshold values does not change the situation for the very activated vWF multimers. However, the amount of blood volume with supraphysiological shear values is critical for the patient. Analyzing the percentage of blood volume that is exposed to supraphysiological forces to total blood volume showed that the 64-wire FDS implanted models had a higher volume of blood which had supraphysiological forces being exerted on in percentage compared to the models where 48-wire FDS implantations took place. Even though the EMSA values are kept at 65 percent for each model, having more wires at the neck region of the aneurysm resulted in more blood particles being exposed to supraphysiological forces compared to each patient's own total available blood volume.

Table 3.5. Maximum shear stress values and the difference between different FDS implantations for each patient

Patient #	48 Wire FDS (Pa)	64 Wire FDS (Pa)	48 vs. 64 (%)
Patient 1	88.62	87.92	0.79%
Patient 2	52.66	30.35	42.4%
Patient 3	143.7	124.9	14.9%
Patient 4	36.86	32.57	13.2%
Patient 5	349.7	340.7	2.64%
Patient 6	39.18	35.68	9.81%

A comparison between 48 and 64-wire FDS implantations on shear stress is made in Table 3.5. The percentage differences in maximum shear stress values with different FDS implantations are shown in that table. The main reason for not having a pattern to the percent differences between the three ICA patients and the three MCA patients is the morphology

difference for each patient. The angle of the artery where the aneurysm was formed plays a crucial role in changing the catalog porosity of the FDS.

Table 3.6. Maximum shear strain rate values and the difference between different FDS implantations for each patient

Patient #	48 Wire FDS (s^{-1})	64 Wire FDS (s^{-1})	48 vs. 64 (%)
Patient 1	15359.40	14359.40	6.96%
Patient 2	9197.94	8616.86	6.74%
Patient 3	21516.70	19716.70	9.13%
Patient 4	5925.84	5441.60	8.90%
Patient 5	57259.40	51335.40	11.54%
Patient 6	11197.94	9797.94	14.29%

Maximum shear strain rate values are higher with the 48-wire FDS treatment method. The difference between the same MCA patients with different FDS models is slightly higher than those of ICA patients.

3.6. FLUID FLOW CHARACTERISTICS IN THE ANEURYSM SAC

Dynamic viscosity (μ) is an important parameter to investigate in order to observe the stagnant regions inside the aneurysm [38]. Stagnation occurrence in the aneurysm sac is a desired result following FDS implantation. Through this parameter, mesh independency is done in this thesis work, and the behavior of the blood flow can be inspected before and after the implantations of FDSs. It is expected to have low dynamic viscosity in the aneurysm due to the high amount of fluid flow entering and leaving the aneurysm with high velocities before the treatment. After the implantation of an FDS, it is desired to have higher dynamic viscosity inside the aneurysm sac due to the majority of the flow being diverted to the artery. Therefore, this parameter is used as one of the several ways to determine the effect of the blood flow occurring in the aneurysm sac. The reason to have these contours in this study is to inspect the correctness of the constructed fluid domains because even though an FDS does

not work efficiently enough to help cure the aneurysm, there will surely be a difference in the blood flow.

Implanting different FDSs can lead to significant differences in dynamic viscosity in the aneurysm sac. However, in this study's case, less than a 5 percent difference is available for every patient between 48 and 64 wire FDS treatments. This is due to the fact that keeping the porosity values at 65 percent for both FDS models. Another benefit of not looking merely into the blood flow characteristics but inspecting what happens to blood particles themselves can be seen in this situation.

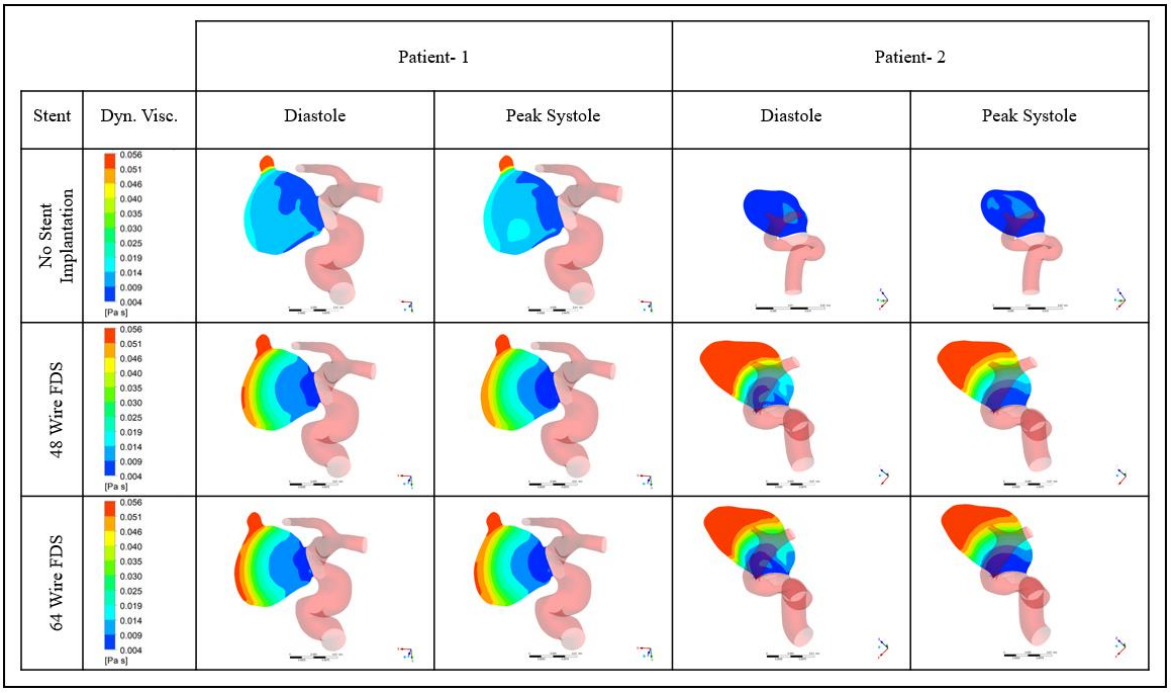

Figure 3.42. Dynamic viscosity contours of patients 1 and 2 without FDS treatment and 48 and 64-wire FDS implantation

Dynamic viscosity contours of patients 1 and 2 are presented in Figure 3.42. The immediate effect of both FDS implantations on blood flow is prominent. The increase in dynamic viscosity shows the effectiveness of the implanted FDSs for both patients. The stagnations occurring for each model with both patients are different due to the efficiency of the same FDS models on different patients. This is due to the changes in EMSA values caused by different artery morphologies.

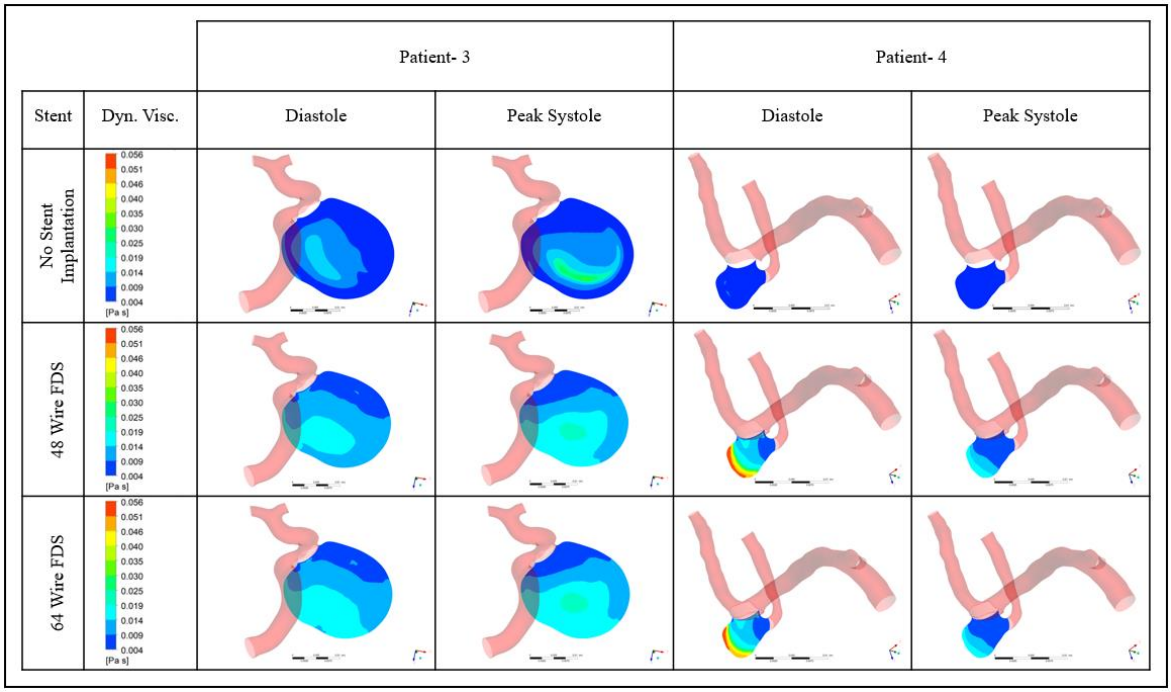

Figure 3.43. Dynamic viscosity contours of patients 3 and 4 without FDS treatment and 48 and 64-wire FDS implantation

A slight increase in dynamic viscosity occurs for patient 3 after FDS treatments. The level of improvement is less compared to the first two patients. Patient 4 has dynamic viscosity change after receiving treatment as well. The stagnant region starts to exist with diastole, but after a new cycle begins, it vanishes with systole.

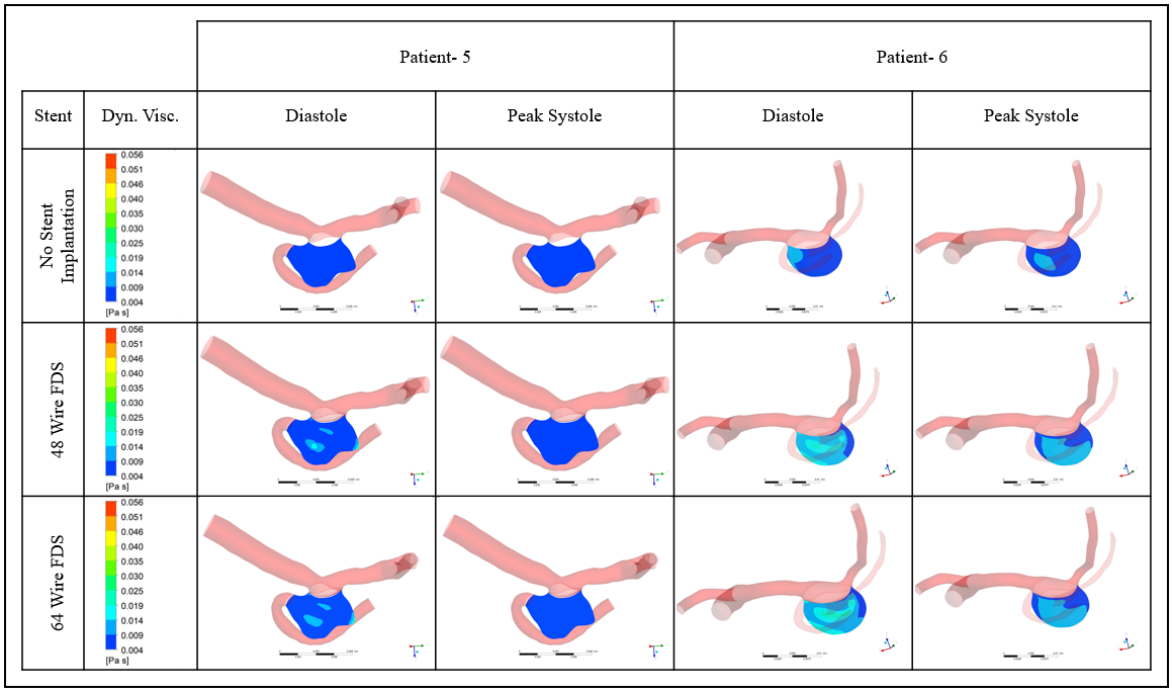

Figure 3.44. Dynamic viscosity contours of patients 5 and 6 without FDS treatment and 48 and 64 wire FDS implantation

Patient 5 has the least change in dynamic viscosity after getting FDS implantations. This should be expected, considering this patient's excessive maximum shear stress and shear strain rate values. This also shows that the higher flow of the fluid in velocity is related to dynamic viscosity, which yields higher shear values, which are also dependent on the age of the patient and artery diameter.

4. CONCLUSION

The influence of FDS implantation on blood passing through stent struts into the aneurysm after FDS implantation was investigated in ways never done before. Six patients with ICA and MCA aneurysms, three each, were investigated with and without FDS treatment. The goal was to observe a greatly impacted blood flow where dramatic increase in shear stress and strain rate values would exist which is known to be causing AvWD through reducing vWF activity. The results obtained from patient specific fluid flow domains prove the increase in shear stress and shear strain rate following FDS treatment for all ICA and MCA patients in this study. DSA images retrieved from the hospital enabled the construction of those patient specific geometries where highly sensitive artery diameter, aneurysm height and aneurysm neck diameter values are calculated. After generating the patient specific CAD models, virtual stent implantation of the FDS implantation made it possible to physically place the FDS models to each patient. With that, varying patient morphologies and their various geometrical effects on FDS struts and neck region porosity were observed. Building the fluid domain with patient specific Womersley velocity profiles, defining blood as a non-Newtonian fluid and constructing the remaining boundary conditions realistically makes it possible to investigate FDS implantation with different FDS models to different artery and aneurysm morphologies. The power of CFD comes in comparing different treatment type reactions on the same patient where in reality one patient can only get once, an unchangeable FDS treatment with a life-lasting duration.

Simulation results have been obtained for all three ICA and three MCA patients and processed. For every patient in the vicinity of the peak systole, shear stress and shear strain rate values exceeded their threshold values of 10 Pa and 5000 s^{-1}, respectively. This leads to the conclusion that FDS implantation was directly related to supraphysiological shear force occurrences being exerted on blood vessels. The vWF multimer activation was proved numerically which causes delayed intracranial aneurysmal or parenchymal hemorrhages due to cleaved vWF proteins that lead to AvWD. These results are crucial for surgeons and radiologists to relate the FDS implantation and two complications of delayed aneurysmal or parenchymal hemorrhages within thirty days even for patients which had successful treatments initially. The results presented in several different ways for both shear stress and shear strain rate values. Curved planes on the FDS neck region showed inflow and outflow

regions clearly where shear forces became the highest. Vertical planes perpendicular to the aneurysm proved the effect of FDS on shear strain rate and the increasing behavior of shear strain rate when the fluid comes closer and merely passes through the FDS struts. Surfaces were generated on the fluid domain walls to investigate the WSS on artery wall, OSI and TAWSS on whole fluid domain walls. WSS values calculated on artery wall to inspect any shear stress and strain rate increase on the distal of ICA or MCA artery to comment on the relation of this with the parenchymal microhemorrhages. OSI and TAWSS values are calculated for the whole cycle on the domain walls. The existence of low WSS values and high OSI values in the same region are observed for every patient. This situation increases the likelihood of rupture.

The percentage of blood particles exposed to supraphysiological forces for ICA and MCA patients compared to the total flowing blood was calculated. The importance of this investigation was calculating how much of the blood in the flow increased its shear stress and shear strain rate values to pathological levels after interacting with FDS wires. This proves the shear stresses and strain rates are exceeding for a large amount of blood flow and not barely exceeding over threshold values in only peak systole instances. This was a crucial result, as not only do higher shear forces affect blood vessel but also higher shear forces affect more blood vessels. This eventually leads to more vWF multimers getting elongated, cleaved and evidently getting reduced in their activity to not be able to act as the clotting agent for aggregated thrombi. As a future work, calculating the blood volume which was induced by supraphysiologic forces may lead to obtain how many vWF multimers get activated in a cardiac cycle. With that there can be a calculation to define a numerical threshold of activated vWF multimers. This can be a category in preliminary tests for patients before FDS treatment to reduce complications.

Investigation of TAWSS and OSI values show the striking effect after FDS treatment where the walls of the whole fluid domain having high shear stresses and shear strain rates before treatment have much higher shear values on the same regions for each patient. These regions are named as rupture prone regions in this study and classify highly sensitive regions on the distal of the artery walls where rupture was most likely to occur. Second to the delayed aneurysm hemorrhage complication, delayed parenchymal microhemorrhage complication type following FDS treatment within thirty days may be linked with this characteristic of rupture prone regions on artery walls. However, the models available in this study cannot

specifically prove the relation between this complication type with the obtained rupture prone regions available on the artery distal. As another future work, the distal side of ICA or MCA geometries can be included in the fluid flow domain with longer branches of the artery system. Because this possible relation was not known before this study, the distal side of the artery was taken from the DSA data in a way to reduce the number of mesh elements for the domain and to prevent excessive computational times of the simulations. Inspecting OSI and TAWSS regions on the patient specific domains present an important finding where low shear stresses and high OSI values existing on the same places of the domain walls create a circumstance where rupture risk is greatly increased. This is a widely known and accepted case which can most likely also be a supplementary finding for delayed hemorrhages following FDS treatment.

Results for giant ICA aneurysms align with the hypothesis of exceeding threshold values for shear stresses and shear strain rates activating vWF multimers. Significantly smaller MCA aneurysms with more than half the height and neck diameter of ICA aneurysms, show the similar behavior of having increased shear forces following FDS treatment. This was a highly important result testifying the supraphysiological forces being reached for MCA aneurysms as well at similar risk levels after FDS implantation on the contrary where it was thought that aneurysm neck diameters larger than 8 mm would lead to delayed bleeding due to vWD following FDS treatment.

Hypothesis of having FDS treatment with different wire numbers leading to significantly varying effects on hemodynamics was investigated in this thesis as well. Comparisons between both 48 and 64 wire FDS treatments for the same patient show that there are indeed significant differences in hemodynamics. These differences are consequent between every ICA and MCA patient overall, though the 48 wire FDS model causes higher shear stresses and shear strain rates. Even though the porosity values are the same for both 48 and 64 wire FDS implanted in the same patient, different shapes of struts are formed by each patient morphology. The angle difference between wires with unlike strut shapes leads to a distinct opening area values. The value of the difference between junction angle between two wires for two different FDS convincingly have an influence on the shear stress and shear strain rate differences for 48 and 64 wire FDS as well. Smaller angles at the wire junctions most likely lead to higher shear stresses and strain rates due to the smaller areas existing with smaller angles at the wire junctions. However, comparing the percentage of blood volumes

which are exposed to over the threshold shear stresses and strain rates show the higher volume of vWF activation with 64 wire FDS for the same patient. Having higher shear stress and strain rate values may be less significant compared to having more blood vessels affected from the exceeding of the shear threshold levels. The main reason behind this was due to having too high of a shear stresses or shear strain rates may not have more severe effects compared to a lower shear stress or strain rate value, considering both values being over the threshold values. However, having excessive shear forces for bigger blood volume could mean more blood vessel undergoing supraphysiological shear forces and therefore more vWF multimers getting activated and cleaved, impacting the clotting effectiveness and capability within the blood flow. Conclusively, the 48 wire FDS choice was more beneficial than 64 wire FDS. Maximum shear stress rates are indeed higher at 48 wire models, but each patient had a larger blood volume that was exposed to supraphysiological forces with 64 wire FDS treatments. Also, the difference in maximum shear stress and shear strain rates is less important than more blood volume having activated vWF multimers. Having a hemodynamically worse case by stents with higher wire numbers, multiple stent implementation may increase the shear stress and strain values even higher and may aggravate a greater volume of blood. Therefore, affecting less amount of blood by 48 wire FDS implantation, it was more beneficial to consider and choose FDS models with less wire numbers considering the desired porosity levels being reached.

Conclusively, this research points out the FDS treatment's direct effect on reducing vWF activity by increasing the shear stresses and shear strain rates greatly above the physiological levels and converting the blood flow into a pathological one leading to type 2A AvWD. Next to the main inspection of vWF activity, supplementary searches conducted in this thesis present two major outcomes. Inspecting the shear stress and strain rate changes during a full cardiac cycle for the total blood volume showed not only an instantaneous activation of vWF but also the volume percentage of how much blood had become aggravated. The other important finding was that shear stresses effect a similar area where in the same region the tendency for the directional changes of the shear stresses for each patient resulted in being called as rupture prone regions on the distal of the artery.

REFERENCES

1. Rinkel GJE, Djibuti M, Algra A, Van Gijn J. Prevalence and risk of rupture of intracranial aneurysms: A systematic review. Stroke. 1998;29(1):251–6.

2. Hop JW, Rinkel GJE, Algra A, Van Gijn J. Case-fatality rates and functional outcome after subarachnoid hemorrhage: A systematic review. Stroke. 1997;28(3):660–4.

3. Cebral JR, Castro MA, Burgess JE, Pergolizzi RS, Sheridan MJ, Putman CM. Characterization of cerebral aneurysms for assessing risk of rupture by using patient-specific computational hemodynamics models. Am J Neuroradiol. 2005;26(10):2550–9.

4. Ajiboye N, Chalouhi N, Starke RM, Zanaty M, Bell R. Unruptured Cerebral Aneurysms: Evaluation and Management. Sci World J. 2015;2015.

5. Brinjikji W, Kallmes DF, Cloft HJ, Lanzino G. Age-related outcomes following intracranial aneurysm treatment with the Pipeline Embolization Device: A subgroup analysis of the IntrePED registry. J Neurosurg. 2016;124(6):1726–30.

6. le Roux AA, Wallace MC. Outcome and Cost of Aneurysmal Subarachnoid Hemorrhage. Neurosurg Clin N Am. 2010;21(2):235–46.

7. Kaminogo M, Yonekura M, Shibata S. Incidence and outcome of multiple intracranial aneurysms in a defined population. Stroke. 2003;34(1):16–21.

8. De Rooij NK, Linn FHH, Van Der Plas JA, Algra A, Rinkel GJE. Incidence of subarachnoid haemorrhage: A systematic review with emphasis on region, age, gender and time trends. J Neurol Neurosurg Psychiatry. 2007;78(12):1365–72.

9. Ghods AJ, Lopes D, Chen M. Gender differences in cerebral aneurysm location. Front Neurol. 2012;MAY(May):1–6.

10. Turan N, Heider RAJ, Zaharieva D, Ahmad FU, Barrow DL, Pradilla G. Sex Differences in the Formation of Intracranial Aneurysms and Incidence and Outcome of Subarachnoid Hemorrhage: Review of Experimental and Human Studies. Transl Stroke Res. 2016;7(1):12–9.

11. Nieuwkamp DJ, Setz LE, Algra A, Linn FH, de Rooij NK, Rinkel GJ. Changes in case fatality of aneurysmal subarachnoid haemorrhage over time, according to age, sex, and region: a meta-analysis. Lancet Neurol [Internet]. 2009;8(7):635–42. Available from: http://dx.doi.org/10.1016/S1474-4422(09)70126-7

12. Daniel R, Souza MR De, Pipek LZ, Fagundes CF, Solla DJF, Carlos G, et al. External validation of the Glasgow coma scale-pupils in low- to middle-income country patients with traumatic brain injury: Could " motor score-pupil " have higher prognostic value ? Surg Neurol Int. 2022;13(510):0–4.

13. Fréneau M, Baron-Menguy C, Vion AC, Loirand G. Why Are Women Predisposed to Intracranial Aneurysm? Front Cardiovasc Med. 2022;9(February):1–10.

14. Stirone C, Duckles SP, Krause DN. Multiple forms of estrogen receptor-α in cerebral blood vessels: Regulation by estrogen. Am J Physiol - Endocrinol Metab. 2003;284(1 47-1):184–92.

15. Cebral JR, Mut F, Weir J, Putman CM. Association of Hemodynamic Characteristics and Cerebral Aneurysm Rupture. AJNR Am J Neuroradiol. 2011;32(2):264–70.

16. Friedman JA, Piepgras DG, Pichelmann MA, Hansen KK. Small cerebral aneurysms presenting with symptoms other. Neurology. 2001;57(1):1212–6.

17. Wiebers OD. Unruptured intracranial aneurysms : natural history , clinical outcome , and risks of surgical and endovascular treatment. Lancet. 2003;362(Vol 362):103–10.

18. Keedy A. An overview of intracranial aneurysms. McGill J Med. 2006;9(2):141–6.

19. Kallmes DF, Ding YH, Dai D, Kadirvel R, Lewis DA, Cloft HJ. A New Endoluminal , Flow-Disrupting Device for Treatment of Saccular Aneurysms. Stroke. 2007;38(8):2346–53.

20. D'Urso PI, Lanzino G, Cloft HJ, Kallmes DF. Flow Diversion for Intracranial Aneurysms: A Review. Stroke. 2011;42(8):2363–8.

21. Pistocchi S, Bartolini B, Piotin M. Flow Diverters at and Beyond the Level of the Circle of Willis for the Treatment of Intracranial Aneurysms. Stroke. 2012;43(4):1032–8.

22. Saatci I, Yavuz K, Ozer C, Geyik S, Cekirge HS. Treatment of Intracranial Aneurysms Using the Pipeline Flow-Diverter Embolization Device : A. AJNR Am J Neuroradiol. 2012;33(8):1436–46.

23. Peach T, Spranger K, Ventikos Y. Virtual flow-diverter treatment planning : The effect of device placement on bifurcation aneurysm haemodynamics. J Eng Med. 2017;235(5):432–43.

24. Thai N, Dang V, Minh P, Ngoc N. Heliyon Flow diverter stent for treatment of cerebral aneurysms : A report of 130 patients with 134 aneurysms. Heliyon [Internet]. 2020;6(March 2019):e03356. Available from: https://doi.org/10.1016/j.heliyon.2020.e03356

25. Gonzalez LF, Randazzo C, Dumont AS, Jabbour P. Single Center Experience With Pipeline Stent: Feasibility, Technique, and Complications. Neurosurgery. 2012;71(3):619–91.

26. Fiorella D, Woo HH, Albuquerque FC, Nelson PK. Definitive Reconstruction Of Circumferential, Fusiform Intracranial Aneurysms With The Pipeline Embolization Device. Neurosurgery. 2008;62(5):1115–21.

27. Nelson PK, Lylyk P, Szikora I, Wetzel SG, Wanke I. The Pipeline Embolization Device for the Intracranial Treatment of Aneurysms Trial. AJNR Am J Neuroradiol. 2011;32(1):34–40.

28. Starke M, Dumont MDAS, Liu MDH, Rosenwasser R, Moursi MDS El, Gonzalez MDLF. Treatment of Large and Giant Intracranial Aneurysms: Cost Comparison of Flow Diversion and Traditional Embolization Strategies. World Neurosurg [Internet]. 2013; Available from: http://dx.doi.org/10.1016/j.wneu.2013.02.089

29. van Rooij WJ, Sluzewski M. Endovascular Treatment of Large and Giant Aneurysms SUMMARY: AJNR Am J Neuroradiol. 2009;30:12–8.

30. Gonzalez NR, Duckwiler G, Jahan R, Murayama Y, Vinuela F. CHALLENGES IN THE ENDOVASCULAR TREATMENT OF GIANT INTRACRANIAL ANEURYSMS. Neurosurgery. 2006;59(5):113–24.

31. Kojima M, Irie K, Fukuda T, Hirose Y, Negoro M, Arai F. The study of flow diversion

effects on aneurysm using multiple enterprise stents and two flow diverters. Asian J Neurosurg. 2012;7(4):159.

32. Zhang P, Liu X, Sun A, Fan Y, Deng X. Hemodynamic insight into overlapping bare-metal stents strategy in the treatment of aortic aneurysm. J Biomech [Internet]. 2015;48(10):2041–6. Available from: http://dx.doi.org/10.1016/j.jbiomech.2015.03.028

33. Dholakia R, Sadasivan C, Fiorella DJ, Woo HH, Lieber BB. Hemodynamics of Flow Diverters. J Biomech Eng. 2017;139(2).

34. Peach TW, Ngoepe MN, Spranger K, Zajarias-Fainsod D, Ventikos Y. Personalizing flow-diverter intervention for cerebral aneurysms: from computational hemodynamics to biochemical modeling. Int j numer method biomed eng. 2014;30:1387–407.

35. Ollikainen E, Tulamo R, Kaitainen S, Honkanen P. Macrophage Infiltration in the Saccular Intracranial Aneurysm Wall as a Response to Locally Lysed Erythrocytes That Promote Degeneration. J Neuropathol Exp Neurol. 2018;77(10):890–903.

36. Muhammad S, Chaudhry SR, Dobreva G. Vascular Macrophages as Therapeutic Targets to Treat Intracranial Aneurysms. Front Immunol. 2021;12(March):1–9.

37. Himizu KS, Ushamae MK, Izutani TM, Oki TA. Macrophage-mediated Inflammatory Disease. Neurol Med Chir. 2019;126–32.

38. Mutlu O, Olcay AB, Bilgin C, Hakyemez B. Understanding the effect of effective metal surface area of flow diverter stent's on the patient-specific intracranial aneurysm numerical model using Lagrangian coherent structures. J Clin Neurosci [Internet]. 2020;80:298–309. Available from: https://doi.org/10.1016/j.jocn.2020.04.111

39. Mutlu O, Olcay AB, Bilgin C, Hakyemez B. Evaluating the Effectiveness of 2 Different Flow Diverter Stents Based on the Stagnation Region Formation in an Aneurysm Sac Using Lagrangian Coherent Structure. World Neurosurg [Internet]. 2019;127:e727–37. Available from: https://doi.org/10.1016/j.wneu.2019.03.255

40. Mutlu O, Olcay AB, Bilgin C, Hakyemez B. Evaluating the Effect of the Number of

Wire of Flow Diverter Stents on the Nonstagnated Region Formation in an Aneurysm Sac Using Lagrangian Coherent Structure and Hyperbolic Time Analysis. World Neurosurg [Internet]. 2020;133:e666–82. Available from: https://doi.org/10.1016/j.wneu.2019.09.116

41. Meyers PM, Coon AL, Kan PT, Wakhloo AK, Hanel RA. SCENT Trial. Stroke. 2019;50:1473–9.

42. Li Y, Zhang M, Verrelli DI, Chong W, Ohta M, Qian Y. Numerical simulation of aneurysmal haemodynamics with calibrated porous-medium models of flow-diverting stents. J Biomech [Internet]. 2018;80:88–94. Available from: https://doi.org/10.1016/j.jbiomech.2018.08.026

43. Xiang J, Ma D, Snyder K V., Levy EI, Siddiqui AH, Meng H. Increasing flow diversion for cerebral aneurysm treatment using a single flow diverter. Neurosurgery. 2014;75(3):286–94.

44. Suzuki T, Takao H, Fujimura S, Dahmani C, Ishibashi T, Mamori H, et al. Selection of helical braided flow diverter stents based on hemodynamic performance and mechanical properties. J Neurointerv Surg. 2017;9(10):999–1005.

45. Iosif C, Berg P, Ponsonnard S, Carles P, Saleme S, Ponomarjova S, et al. Role of terminal and anastomotic circulation in the patency of arteries jailed by flow-diverting stents: From hemodynamic changes to ostia surface modifications. J Neurosurg. 2017;126(5):1702–13.

46. Pierot L, Spelle L, Berge J, Januel A, Herbreteau D, Aggour M, et al. SAFE study (Safety and efficacy Analysis of FRED Embolic device in aneurysm treatment): 1-year clinical and anatomical results. J Neurointerv Surg. 2019;11:184–9.

47. Oran I, Cinar C, Bozkaya H, Parildar M, Duman S. Reduced activity of von Willebrand factor after flow-diverting stent implantation for intracranial aneurysms: A link to acquired von Willebrand disease? Am J Neuroradiol. 2020;41(1):140–6.

48. Nichols WL, Hultin MB, James AH, Manco-johnson MJ. von Willebrand disease (VWD): evidence-based diagnosis and management guidelines , the National Heart , Lung , and Blood Institute (NHLBI) Expert Panel report (USA) 1. Haemophilia.

2008;14:171–232.

49. Ruggeri ZM. Multimeric Following Pathophysiology. Blood. 1982;59(6):1272–8.

50. Shetty S, Kasatkar P, Ghosh K. Pathophysiology of acquired von Willebrand disease : a concise review. Eur J Haematol. 2011;87(10):99–106.

51. U.S. Department of Health and Human Services NI of H. Von Willebrand disease. Natl Hear Lung, Blood Inst NHLBI. 2008;

52. Zimmerman TS, Dent JA, Ruggeri ZM, Nannini LH. Subunit composition of plasma von Willebrand factor. Cleavage is present in normal individuals, increased in IIA and IIB von Willebrand disease, but minimal in variants with aberrant structure of individual oligomers (types IIC, IID, and IIE). J Clin Invest. 1986;77(3):947–51.

53. Bharati PK, Prashanth RR. Von Willebrand Disease : An Overview. Indian J Pharm Sci. 2011;73(1):7–16.

54. Sadler JE, Mannucci M, Berntorp E, Bochkov N, Boulyjenkov V, Ginsburg D, et al. Impact , Diagnosis and Treatment of von Willebrand Disease *. J Thromb Haemost. 2000;(13):160–74.

55. Von Willebrand EA. Hereditary pseudo-haemophilia. Haemophilia. 1999;5:223–31.

56. Michiels JJ, Vliet HDM Van. Dominant von Willebrand Disease Type 2A Groups I and II due to Missense Mutations in the A2 Domain of the von Willebrand Factor Gene : Acta Haematol. 2009;121:154–66.

57. Dent JA, Berkowitz SD, Ware J, Kasper CK, Ruggeri ZM. Identification of a cleavage site directing the immunochemical detection of molecular abnormalities in type IIA von Willebrand factor. Proc Natl Acad Sci U S A. 1990;87(16):6306–10.

58. Lyons SE, Bruck ME, Bowie EJW, Ginsburg D. Impaired intracellular transport produced by a subset of type IIA von Willebrand disease mutations. J Biol Chem. 1992;267(7):4424–30.

59. Zhang X, Halvorsen K, Zhang CZ, Wong WP, Springer TA. Mechanoenzymatic cleavage of the ultralarge vascular protein von willebrand factor. Science (80-). 2009;324(5932):1330–4.

60. Wu T, Lin J, Cruz MA, Dong JF, Zhu C. Force-induced cleavage of single VWFA1A2A3 tridomains by ADAMTS-13. Blood. 2010;115(2):370–8.

61. Löf A, Müller JP, Brehm MA. A biophysical view on von Willebrand factor activation. J Cell Physiol. 2018;233(2):799–810.

62. Sing CE, Alexander-Katz A. Giant nonmonotonic stretching response of a self-associating polymer in shear flow. Phys Rev Lett. 2011;107(19):1–5.

63. Ying J, Ling Y, Westfield LA, Sadler JE, Shao JY. Unfolding the a2 domain of von willebrand factor with the optical trap. Biophys J [Internet]. 2010;98(8):1685–93. Available from: http://dx.doi.org/10.1016/j.bpj.2009.12.4324

64. Springer TA. Von Willebrand factor, Jedi knight of the bloodstream. Blood. 2014;124(9):1412–25.

65. Rana A, Westein E, Niego B, Hagemeyer CE. Shear-Dependent Platelet Aggregation: Mechanisms and Therapeutic Opportunities. Front Cardiovasc Med. 2019;6(September):1–21.

66. Nascimbene A, Neelamegham S, Frazier OH, Moake JL, Dong J. Review Article Acquired von Willebrand syndrome associated with left ventricular assist device. Blood. 2016;127(25):3133–41.

67. Horiuchi H, Doman T, Kokame K, Saiki Y, Matsumoto M. Acquired von Willebrand Syndrome Associated with Cardiovascular. J Atheroscler Thromb. 2019;26:303–14.

68. Kumar S, Pruthi RK, Nichols WL. Acquired von Willebrand Disease. Mayo Clin Proc. 2002;77(February):181–7.

69. Kalbhenn J, Schlagenhauf A, Schmutz A, Zieger B. Author ' s Accepted Manuscript. J Hear Lung Transplant [Internet]. 2018; Available from: https://doi.org/10.1016/j.healun.2018.03.013

70. Tiede A. Diagnosis and treatment of acquired von Willebrand syndrome. Thromb Res [Internet]. 2012;130:S2–6. Available from: http://dx.doi.org/10.1016/S0049-3848(13)70003-3

71. Berge J, Tourdias T, Moreau JF, Barreau X, Dousset V. Perianeurysmal brain

inflammation after flow-diversion treatment. Am J Neuroradiol. 2011;32(10):1930–4.

72. Kulcsár Z, Houdart E, Bonafé A, Parker G, Millar J, Goddard AJP, et al. Intra-aneurysmal thrombosis as a possible cause of delayed aneurysm rupture after flow-diversion treatment. Am J Neuroradiol. 2011;32(1):20–5.

73. McGuinness BJ, Memon S, Hope JK. Prospective Study of Early MRI Appearances following Flow-Diverting Stent Placement for Intracranial Aneurysms. Am J Neuroradiol. 2015;36(5):943–8.

74. Oran I. Flow-diverting stent and delayed intracranial bleeding: the case for discussing acquired von Willebrand disease. Platelets. 2021;32(3):432–5.

75. Schneider SW, Nuschele S, Wixforth A, Gorzelanny C, Alexander-Katz A, Netz RR, et al. Shear-induced unfolding triggers adhesion of von Willebrand factor fibers. Proc Natl Acad Sci U S A. 2007;104(19):7899–903.

76. Ku DN, Giddens DP, Zarins CK, Glagov S. Pulsatile Flow and Atherosclerosis in the Human Carotid Bifurcation Positive Correlation between Plaque Location and Low and Oscillating Shear Stress. Arterioscler Thromb Vasc Biol. 1985;5(3):293–302.

77. Meng H, Tutino VM, Xiang J, Siddiqui A. High WSS or Low WSS ? Complex Interactions of Hemodynamics Toward a Unifying Hypothesis. AJNR Am J Neuroradiol. 2014;35(7):1254–62.

78. Shojima M, Oshima M, Takagi K, Torii R, Hayakawa M, Katada K, et al. Magnitude and Role of Wall Shear Stress on Computational Fluid Dynamic Study of 20 Middle Cerebral. Stroke. 2004;35(11).

79. Xiang J, Natarajan SK, Tremmel M, Mocco J, Hopkins LN, Siddiqui AH. Hemodynamic-Morphologic Discriminants for Intracranial Aneurysm Rupture. Stroke. 2012;42(1):144–52.

80. Sforza DM, Putman CM, Cebral JR. Computational fluid dynamics in brain aneurysms. Int j numer method biomed eng. 2012;28(0):801–8.

81. Lu G, Huang L, Zhang XL, Wang SZ, Hong Y, Hu Z, et al. Influence of

Hemodynamic Factors on Rupture of Intracranial Aneurysms: Patient-Specific 3D Mirror Aneurysms Model Computational Fluid Dynamics Simulation. AJNR Am J Neuroradiol. 2011;32:1255–61.

82. Chen Z, Yu H, Shi Y, Zhu M, Wang Y, Hu X, et al. Vascular Remodelling Relates to an Elevated Oscillatory Shear Index and Relative Residence Time in Spontaneously Hypertensive Rats. Sci Rep. 2017;7(1):1–10.

83. Zhang Y, Jing L, Zhang Y, Liu J, Yang X. Low wall shear stress is associated with the rupture of intracranial aneurysm with known rupture point : case report and literature review. BMC Neurol [Internet]. 2016;10–3. Available from: http://dx.doi.org/10.1186/s12883-016-0759-0

84. Van Langenhove G, Wentzel JJ, Krams R, Slager CJ, Hamburger JN, Serruys PW. Helical Velocity Patterns in a Human Coronary Artery A Three-Dimensional Computational Fluid Dynamic Reconstruction Showing the Relation With Local Wall Thickness. Images Cardiovasc Med. 2000;102(3):22–4.

85. Soulis J V., Giannoglou GD, Chatzizisis YS, Farmakis TM, Giannakoulas GA, Parcharidis GE, et al. Spatial and phasic oscillation of non-Newtonian wall shear stress in human left coronary artery bifurcation: An insight to atherogenesis. Coron Artery Dis. 2006;17(4):351–8.

86. Krams R, Wentzel JJ, Oomen JAF, Vinke R, Schuurbiers JCH, De Feyter PJ, et al. Evaluation of endothelial shear stress and 3D geometry as factors determining the development of atherosclerosis and remodeling in human coronary arteries in vivo: Combining 3D reconstruction from angiography and IVUS (ANGUS) with computational fluid dyna. Arterioscler Thromb Vasc Biol. 1997;17(10):2061–5.

87. Le TB. Dynamic modes of inflow jet in brain aneurysms. J Biomech [Internet]. 2021;116:110238. Available from: https://doi.org/10.1016/j.jbiomech.2021.110238

88. Castro MA, Putman CM, Cebral JR. Patient-Specific Computational Modeling of Cerebral Aneurysms With Multiple Avenues of Flow From 3D Rotational Angiography Images 1. Acad Radiol. 2006;13(7):811–21.

89. Johnston BM, Johnston PR, Corney S, Kilpatrick D. Non-Newtonian blood flow in

human right coronary arteries: Steady state simulations. J Biomech. 2004;37(5):709–20.

90. Levitt MR, McGah PM, Aliseda A, Mourad PD, Nerva JD, Vaidya SS, et al. Cerebral aneurysms treated with flow-diverting stents: Computational models using intravascular blood flow measurements. AJNR Am J Neuroradiol. 2014;35(1):143–8.

91. Narracott A, Smith S, Lawford P, Liu H, Himeno R, Wilkinson I, et al. Development and validation of models for the investigation of blood clotting in idealized stenoses and cerebral aneurysms. J Artif Organs. 2005;8(1):56–62.

92. Steinman DA, Milner JS, Norley CJ, Lownie SP, Holdsworth DW. Image-based computational simulation of flow dynamics in a giant intracranial aneurysm. AJNR Am J Neuroradiol [Internet]. 2003;24(4):559–66. Available from: http://www.ajnr.org/content/24/4/559.abstract

93. Olcay AB, Amindari A, Kirkkopru K, Yalcin HC. Characterization of Disturbed Hemodynamics due to Stenosed Aortic Jets with a Lagrangian Coherent Structures Technique. J Appl Fluid Mech. 2018;11(2):375–84.

94. Kannojiya V, Das AK, Das PK. Effect of left ventricular assist device on the hemodynamics of a patient-specific left heart. Med Biol Eng Comput. 2022 Jun;60(6):1705–21.

95. Giannoglou GD, Soulis J V., Farmakis TM, Farmakis DM, Louridas GE. Haemodynamic factors and the important role of local low static pressure in coronary wall thickening. Int J Cardiol. 2002;86(1):27–40.

96. Fedorov A, Beichel R, Kalpathy-Cramer J, Finet J, Fillion-Robin JC, Pujol S, et al. 3D Slicer as an image computing platform for the Quantitative Imaging Network. Magn Reson Imaging [Internet]. 2012;30(9):1323–41. Available from: http://dx.doi.org/10.1016/j.mri.2012.05.001

97. Xu X, Kozar R, Zhang J, Dong J. Diverse activities of von Willebrand factor in traumatic brain injury and associated coagulopathy. J Thromb Haemost [Internet]. 2020;18(12):3154–62. Available from: https://doi.org/10.1111/jth.15096

98. Chandra A, Li WA, Stone CR, Geng X. The cerebral circulation and cerebrovascular

disease I : Anatomy. 2017;45–56.

99. Womersley JR. Oscillatory Flow in Arteries: the Constrained Elastic Tube as a Model of Arterial Flow and Pulse Transmission. Phys Med Biol. 1957;138:178–87.

100. Womersley JR. Flow in the larger arteries and its relation to the oscillating pressure. J Physiol. 1954 May;124(2):31-2P.

101. Womersley JR. Method for the calculation of velocity, rate of flow and viscous drag in arteries when the pressure gradient is known. J Physiol. 1955;127(3):553–563.

102. He X, Ku DN. Pulsatile flow in the human left coronary artery bifurcation: Average conditions. J Biomech Eng. 1996;118(1):74–82.

103. Redaelli A, Boschetti F, Inzoli F. The assignment of velocity profiles in finite element simulations of pulsatile flow in arteries a. Comput Biol Med. 1997;27(3):233–47.

104. Albayrak R, Degirmenci B. Letter to the Editor Diagnosis of Broncho-Pleural Fistula: Is There a Role for Sonography? J Clin Ultrasound. 2006;35:27–33.

105. Piskin S, Celebi MS. Analysis of the effects of different pulsatile inlet profiles on the hemodynamical properties of blood flow in patient specific carotid artery with stenosis. Comput Biol Med [Internet]. 2013;43(6):717–28. Available from: http://dx.doi.org/10.1016/j.compbiomed.2013.02.014

106. Mutlu O, Olcay AB, Bilgin C, Hakyemez B. Evaluating the Effectiveness of 2 Different Flow Diverter Stents Based on the Stagnation Region Formation in an Aneurysm Sac Using Lagrangian Coherent Structure. World Neurosurg [Internet]. 2019;127:e727–37. Available from: https://doi.org/10.1016/j.wneu.2019.03.255

107. Chiastra C. Numerical modeling of hemodynamics in stented coronary arteries. 2013;224.

108. Cho YI, Kensey KR. Effects of the non-Newtonian viscosity of blood on flows in a diseased arterial vessel. Part 1: Steady flows. Biorheology. 1991;28(3–4):241–62.

109. Malek AM, Alper SL. Hemodynamic Shear Stress and Its Role in Atherosclerosis. J Am Med Assoc. 1999;282(21):2035–42.

110. Stramba-Badiale M, Locati EH, Martinelli A, Courvillet J, Schwartz PJ. Gender and the relationship between ventricular repolarization and cardiac cycle length during 24-h Holter recordings. Eur Heart J. 1997;18:1000–6.

111. Hidekatsu F, Little WC. The Cardiac Cycle and the Physiological Basis of Left Ventricular Contraction, Ejection, Relaxation, and Filling. Hear Fail Clin. 2009;4(1):1–11.

112. Goodman DJ, Rossen RM, Rider AK, Harrison DC. The effect of cycle length on cardiac refractory periods in the denervated human heart. Am Heart J. 1976;91(3):332–8.

113. Liu B, Dalin T. Influence of non-Newtonian properties of blood on the wall shear stress in human atherosclerotic right coronary arteries. MCB Mol Cell Biomech. 2011;8(1):73–90.

114. Wonder AY. UNDERSTANDING BLOOD BEHAVIOR. Bloodstain Pattern Evid. 2007;23–32.

115. Okhota S, Melnikov I, Avtaeva Y, Kozlov S, Gabbasov Z. Shear stress-induced activation of vonwillebrand factor and cardiovascular pathology. Int J Mol Sci. 2020;21(20):1–18.

116. Westein E, Van Der Meer AD, Kuijpers MJE, Frimat JP, Van Den Berg A, Heemskerk JWM. Atherosclerotic geometries exacerbate pathological thrombus formation poststenosis in a von Willebrand factor-dependent manner. Proc Natl Acad Sci U S A. 2013;110(4):1357–62.

117. Sing CE, Alexander-Katz A. Elongational flow induces the unfolding of von willebrand factor at physiological flow rates. Biophys J [Internet]. 2010;98(9):L35–7. Available from: http://dx.doi.org/10.1016/j.bpj.2010.01.032

118. Ruggeri ZM, Zimmerman TS. Willebrand ' s Disease BY ANALYSIS OF MULTIMERIC COMPOSITION OF IN PLASMA AND PLATELETS. J Clin Invest. 2007;65(1980):1318–25.

119. Bryckaert M, Rosa JP, Denis C V., Lenting PJ. Of von Willebrand factor and platelets. Cell Mol Life Sci. 2015;72(2):307–26.

120. Fukuda S, Shimogonya Y, Yonemoto N. Differences in cerebral aneurysm rupture rate according to arterial anatomies depend on the hemodynamic environment. Am J Neuroradiol. 2019;40(5):834–9.

121. Chalouhi N, Tjoumakaris S, Starke RM, Gonzalez LF, Randazzo C, Hasan D, et al. Comparison of Flow Diversion and Coiling in Large Unruptured Intracranial Saccular Aneurysms. Stroke. 2013;44:2150–5.

APPENDIX A: ETHICAL APPROVAL FORM

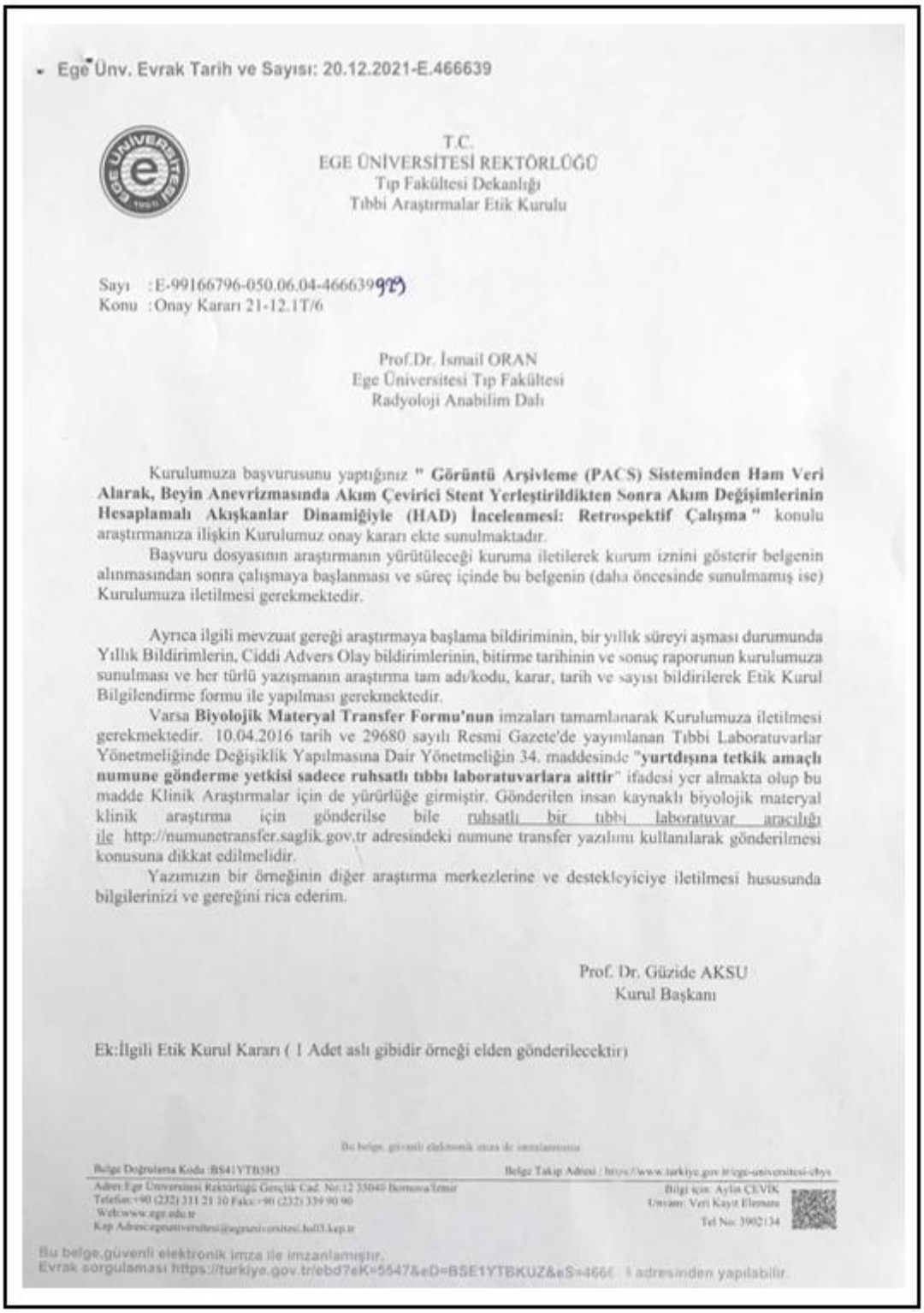

Ege Ünv. Evrak Tarih ve Sayısı: 20.12.2021-E.466639

T.C.
EGE ÜNİVERSİTESİ REKTÖRLÜĞÜ
Tıp Fakültesi Dekanlığı
Tıbbi Araştırmalar Etik Kurulu

Sayı : E-99166796-050.06.04-466639929
Konu : Onay Kararı 21-12.1T/6

Prof.Dr. İsmail ORAN
Ege Üniversitesi Tıp Fakültesi
Radyoloji Anabilim Dalı

Kurulumuza başvurusunu yaptığınız " **Görüntü Arşivleme (PACS) Sisteminden Ham Veri Alarak, Beyin Anevrizmasında Akım Çevirici Stent Yerleştirildikten Sonra Akım Değişimlerinin Hesaplamalı Akışkanlar Dinamiğiyle (HAD) İncelenmesi: Retrospektif Çalışma** " konulu araştırmanıza ilişkin Kurulumuz onay kararı ekte sunulmaktadır.

Başvuru dosyasının araştırmanın yürütüleceği kuruma iletilerek kurum iznini gösterir belgenin alınmasından sonra çalışmaya başlanması ve süreç içinde bu belgenin (daha öncesinde sunulmamış ise) Kurulumuza iletilmesi gerekmektedir.

Ayrıca ilgili mevzuat gereği araştırmaya başlama bildiriminin, bir yıllık süreyi aşması durumunda Yıllık Bildirimlerin, Ciddi Advers Olay bildirimlerinin, bitirme tarihinin ve sonuç raporunun kurulumuza sunulması ve her türlü yazışmanın araştırma tam adı/kodu, karar, tarih ve sayısı bildirilerek Etik Kurul Bilgilendirme formu ile yapılması gerekmektedir.

Varsa **Biyolojik Materyal Transfer Formu'nun** imzaları tamamlanarak Kurulumuza iletilmesi gerekmektedir. 10.04.2016 tarih ve 29680 sayılı Resmi Gazete'de yayımlanan Tıbbi Laboratuvarlar Yönetmeliğinde Değişiklik Yapılmasına Dair Yönetmeliğin 34. maddesinde "**yurtdışına tetkik amaçlı numune gönderme yetkisi sadece ruhsatlı tıbbi laboratuvarlara aittir**" ifadesi yer almakta olup bu madde Klinik Araştırmalar için de yürürlüğe girmiştir. Gönderilen insan kaynaklı biyolojik materyal klinik araştırma için gönderilse bile ruhsatlı bir tıbbi laboratuvar aracılığı ile http://numunetransfer.saglik.gov.tr adresindeki numune transfer yazılımı kullanılarak gönderilmesi konusuna dikkat edilmelidir.

Yazımızın bir örneğinin diğer araştırma merkezlerine ve destekleyiciye iletilmesi hususunda bilgilerinizi ve gereğini rica ederim.

Prof. Dr. Güzide AKSU
Kurul Başkanı

Ek:İlgili Etik Kurul Kararı (1 Adet aslı gibidir örneği elden gönderilecektir)

Bu belge güvenli elektronik imza ile imzalanmıştır

Belge Doğrulama Kodu :BS41YTB5IO — Belge Takip Adresi : https://www.turkiye.gov.tr/ege-universitesi-ebys

Adres:Ege Üniversitesi Rektörlüğü Gençlik Cad. No:12 35040 Bornova/İzmir
Telefon:+90 (232) 311 21 10 Faks:+90 (232) 339 90 90
Web:www.ege.edu.tr
Kep Adresi:egeuniversitesi@egeuniversitesi.hs03.kep.tr

Bilgi için: Aylin ÇEVİK
Unvanı: Veri Kayıt Elemanı
Tel No: 3902134

Bu belge,güvenli elektronik imza ile imzalanmıştır.
Evrak sorgulaması https://turkiye.gov.tr/ebd?eK=5547&eD=BSE1YTBKUZ&eS=466[illegible] adresinden yapılabilir.

Figure A.1. Ethical approval report first page

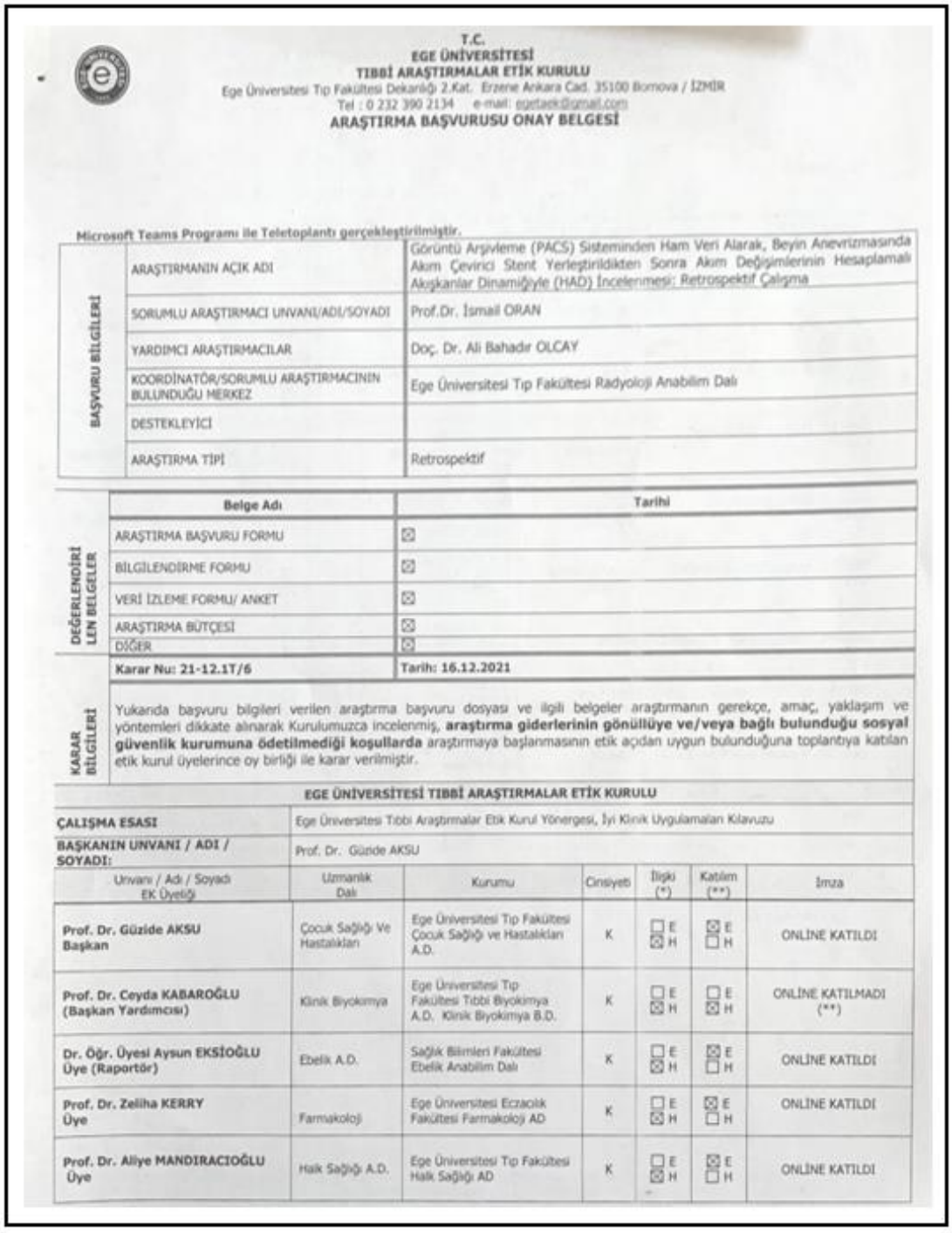

T.C.
EGE ÜNİVERSİTESİ
TIBBİ ARAŞTIRMALAR ETİK KURULU
Ege Üniversitesi Tıp Fakültesi Dekanlığı 2.Kat. Erzene Ankara Cad. 35100 Bornova / İZMİR
Tel : 0 232 390 2134 e-mail: egetaek@gmail.com

ARAŞTIRMA BAŞVURUSU ONAY BELGESİ

Microsoft Teams Programı ile Teletoplantı gerçekleştirilmiştir.

BAŞVURU BİLGİLERİ	
ARAŞTIRMANIN AÇIK ADI	Görüntü Arşivleme (PACS) Sisteminden Ham Veri Alarak, Beyin Anevrizmasında Akım Çevirici Stent Yerleştirildikten Sonra Akım Değişimlerinin Hesaplamalı Akışkanlar Dinamiğiyle (HAD) İncelenmesi: Retrospektif Çalışma
SORUMLU ARAŞTIRMACI UNVANI/ADI/SOYADI	Prof.Dr. İsmail ORAN
YARDIMCI ARAŞTIRMACILAR	Doç. Dr. Ali Bahadır OLCAY
KOORDİNATÖR/SORUMLU ARAŞTIRMACININ BULUNDUĞU MERKEZ	Ege Üniversitesi Tıp Fakültesi Radyoloji Anabilim Dalı
DESTEKLEYİCİ	
ARAŞTIRMA TİPİ	Retrospektif

DEĞERLENDİRİLEN BELGELER	Belge Adı	Tarihi
	ARAŞTIRMA BAŞVURU FORMU	☒
	BİLGİLENDİRME FORMU	☒
	VERİ İZLEME FORMU/ ANKET	☒
	ARAŞTIRMA BÜTÇESİ	☒
	DİĞER	☒
KARAR BİLGİLERİ	**Karar Nu: 21-12.1T/6**	**Tarih: 16.12.2021**
	Yukarıda başvuru bilgileri verilen araştırma başvuru dosyası ve ilgili belgeler araştırmanın gerekçe, amaç, yaklaşım ve yöntemleri dikkate alınarak Kurulumuzca incelenmiş, **araştırma giderlerinin gönüllüye ve/veya bağlı bulunduğu sosyal güvenlik kurumuna ödetilmediği koşullarda** araştırmaya başlanmasının etik açıdan uygun bulunduğuna toplantıya katılan etik kurul üyelerince oy birliği ile karar verilmiştir.	

EGE ÜNİVERSİTESİ TIBBİ ARAŞTIRMALAR ETİK KURULU

ÇALIŞMA ESASI	Ege Üniversitesi Tıbbi Araştırmalar Etik Kurul Yönergesi, İyi Klinik Uygulamaları Kılavuzu
BAŞKANIN UNVANI / ADI / SOYADI:	Prof. Dr. Güzide AKSU

Unvanı / Adı / Soyadı EK Üyeliği	Uzmanlık Dalı	Kurumu	Cinsiyeti	İlişki (*)	Katılım (**)	İmza
Prof. Dr. Güzide AKSU Başkan	Çocuk Sağlığı Ve Hastalıkları	Ege Üniversitesi Tıp Fakültesi Çocuk Sağlığı ve Hastalıkları A.D.	K	☐ E ☒ H	☒ E ☐ H	ONLİNE KATILDI
Prof. Dr. Ceyda KABAROĞLU (Başkan Yardımcısı)	Klinik Biyokimya	Ege Üniversitesi Tıp Fakültesi Tıbbi Biyokimya A.D. Klinik Biyokimya B.D.	K	☐ E ☒ H	☐ E ☒ H	ONLİNE KATILMADI (**)
Dr. Öğr. Üyesi Aysun EKSİOĞLU Üye (Raportör)	Ebelik A.D.	Sağlık Bilimleri Fakültesi Ebelik Anabilim Dalı	K	☐ E ☒ H	☒ E ☐ H	ONLİNE KATILDI
Prof. Dr. Zeliha KERRY Üye	Farmakoloji	Ege Üniversitesi Eczacılık Fakültesi Farmakoloji AD	K	☐ E ☒ H	☒ E ☐ H	ONLİNE KATILDI
Prof. Dr. Aliye MANDIRACIOĞLU Üye	Halk Sağlığı A.D.	Ege Üniversitesi Tıp Fakültesi Halk Sağlığı AD	K	☐ E ☒ H	☒ E ☐ H	ONLİNE KATILDI

Figure A.2. Ethical approval report second page

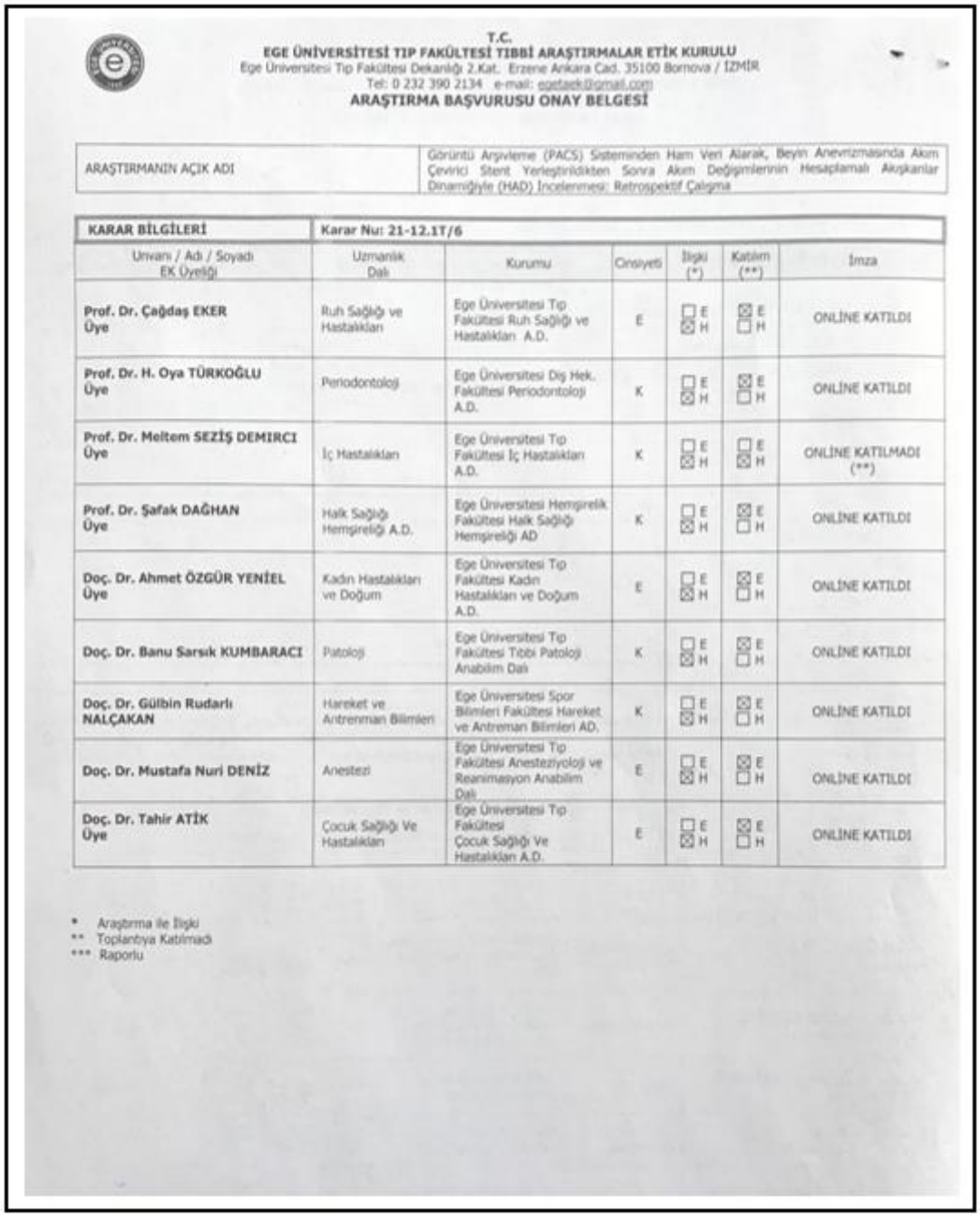

T.C.
EGE ÜNİVERSİTESİ TIP FAKÜLTESİ TIBBİ ARAŞTIRMALAR ETİK KURULU
Ege Üniversitesi Tıp Fakültesi Dekanlığı 2.Kat. Erzene Ankara Cad. 35100 Bornova / İZMİR
Tel: 0 232 390 2134 e-mail: egetaek@gmail.com
ARAŞTIRMA BAŞVURUSU ONAY BELGESİ

ARAŞTIRMANIN AÇIK ADI	Görüntü Arşivleme (PACS) Sisteminden Ham Veri Alarak, Beyin Anevrizmasında Akım Çevirici Stent Yerleştirildikten Sonra Akım Değişimlerinin Hesaplamalı Akışkanlar Dinamiğiyle (HAD) İncelenmesi: Retrospektif Çalışma

KARAR BİLGİLERİ	Karar Nu: 21-12.1T/6					
Unvanı / Adı / Soyadı EK Üyeliği	Uzmanlık Dalı	Kurumu	Cinsiyeti	İlişki (*)	Katılım (**)	İmza
Prof. Dr. Çağdaş EKER Üye	Ruh Sağlığı ve Hastalıkları	Ege Üniversitesi Tıp Fakültesi Ruh Sağlığı ve Hastalıkları A.D.	E	☐ E ☒ H	☒ E ☐ H	ONLİNE KATILDI
Prof. Dr. H. Oya TÜRKOĞLU Üye	Periodontoloji	Ege Üniversitesi Diş Hek. Fakültesi Periodontoloji A.D.	K	☐ E ☒ H	☒ E ☐ H	ONLİNE KATILDI
Prof. Dr. Meltem SEZİŞ DEMIRCI Üye	İç Hastalıkları	Ege Üniversitesi Tıp Fakültesi İç Hastalıkları A.D.	K	☐ E ☒ H	☐ E ☒ H	ONLİNE KATILMADI (**)
Prof. Dr. Şafak DAĞHAN Üye	Halk Sağlığı Hemşireliği A.D.	Ege Üniversitesi Hemşirelik Fakültesi Halk Sağlığı Hemşireliği AD	K	☐ E ☒ H	☒ E ☐ H	ONLİNE KATILDI
Doç. Dr. Ahmet ÖZGÜR YENİEL Üye	Kadın Hastalıkları ve Doğum	Ege Üniversitesi Tıp Fakültesi Kadın Hastalıkları ve Doğum A.D.	E	☐ E ☒ H	☒ E ☐ H	ONLİNE KATILDI
Doç. Dr. Banu Sarsık KUMBARACI	Patoloji	Ege Üniversitesi Tıp Fakültesi Tıbbi Patoloji Anabilim Dalı	K	☐ E ☒ H	☒ E ☐ H	ONLİNE KATILDI
Doç. Dr. Gülbin Rudarlı NALÇAKAN	Hareket ve Antreman Bilimleri	Ege Üniversitesi Spor Bilimleri Fakültesi Hareket ve Antreman Bilimleri AD.	K	☐ E ☒ H	☐ E ☒ H	ONLİNE KATILDI
Doç. Dr. Mustafa Nuri DENİZ	Anestezi	Ege Üniversitesi Tıp Fakültesi Anesteziyoloji ve Reanimasyon Anabilim Dalı	E	☐ E ☒ H	☒ E ☐ H	ONLİNE KATILDI
Doç. Dr. Tahir ATİK Üye	Çocuk Sağlığı Ve Hastalıkları	Ege Üniversitesi Tıp Fakültesi Çocuk Sağlığı Ve Hastalıkları A.D.	E	☐ E ☒ H	☒ E ☐ H	ONLİNE KATILDI

* Araştırma ile İlişki
** Toplantıya Katılmadı
*** Raporlu

Figure A.3. Ethical approval report third page